Draft version March 22, 2017
Preprint typeset using LaTeX style emulateapj v. 04/17/13

arXiv:1703.06948v1 [astro-ph.SR] 20 Mar 2017

NGC 1980 IS NOT A FOREGROUND POPULATION OF ORION: SPECTROSCOPIC SURVEY OF YOUNG STARS WITH LOW EXTINCTION IN ORION A

Min Fang[1], Jinyoung Serena Kim[1], Ilaria Pascucci[2], Dániel Apai[1, 2], Lan Zhang[3, 4], Aurora Sicilia-Aguilar[5], Miguel Alonso-Martínez[6], Carlos Eiroa[6], Hongchi Wang[7]

Draft version March 22, 2017

ABSTRACT

We perform a spectroscopic survey of the foreground population in Orion A with MMT/Hectospec. We use these data, along with archival spectroscopic data and photometric data, to derive spectral types, extinction values, and masses for 691 stars. Using the Spitzer Space Telescope data, we characterize the disk properties of these sources. We identify 37 new transition disk (TD) objects, one globally depleted disk candidate, and 7 probable young debris disks. We discover an object with a mass less than 0.018–0.030 $M_{\odot}$, which harbors a flaring disk. Using the Hα emission line, we characterize the accretion activity of the sources with disks, and confirm that fraction of accreting TDs is lower than that of optically thick disks (46±7% versus 73±9%, respectively). Using kinematic data from the Sloan Digital Sky Survey and APOGEE INfrared Spectroscopy of Young Nebulous Clusters program (IN-SYNC), we confirm that the foreground population shows similar kinematics to their local molecular clouds and other young stars in the same regions. Using the isochronal ages, we find that the foreground population has a median age around 1–2 Myr, which is similar to the one of other young stars in Orion A. Therefore, our results argue against the presence of a large and old foreground cluster in front of Orion A.

Keywords: accretion, accretion disks — planetary systems: protoplanetary disks — stars: pre-main sequence

1. INTRODUCTION

The Orion complex is the most active star-forming region in the solar neighborhood. The age range (<1–10 Myr), the diversity of local environments, and the distance (∼414 pc, Menten et al. 2007) of this complex make it an ideal laboratory to study challenging questions in star formation, e.g., star formation history, initial mass function, disk evolution (see e.g. Hillenbrand 1997; Hernández et al. 2007b,a; Fang et al. 2009; Lee & Chen 2009; Hernández et al. 2010; Hsu et al. 2012, 2013; Fang et al. 2013a; Hernández et al. 2014).

The entire Orion complex shows evidence for multiple star formation episodes, and the current, most active star formation is located in Orion A and B. Orion A, located in the southern part, consists of the most massive cluster in this region, the Orion nebula cluster, and several medium-size clusters, e.g., OMC 2, OMC 3, and Lynds 1641 (L1641). In L1641, about half of the young stellar objects (YSOs) are formed in isolation and others are formed in small aggregates (Fang et al. 2013a). Orion B is in the northern part of Orion and comprised of four clusters NGC 2023, 2024, 2068, and 2071. There is also a large population of off-cloud stellar groups aged 3-30 Myr, including the Orion OB1a and 1B associations (Briceño et al. 2005, 2007). The understanding of star formation in the Orion complex was further complicated by the discovery of a foreground population aged 4–5 Myr to Orion A (Alves & Bouy 2012; Bouy et al. 2014). This presumably older population is centered on NGC 1980 (ι Ori), and extends northward to Orion nebula cluster and NGC 1981, and eastward to L1641, thus contaminating the young populations in these regions.

In Alves & Bouy (2012), the foreground population was proposed by searching for the stars with low or no extinction in the field of Orion A. The surface densities of this population show a well-defined peak coinciding with NGC 1980, and several less distinct peaks around other star-forming regions in Orion A (Alves & Bouy 2012; Bouy et al. 2014). In $J-H$ vs. $H-K_{\rm s}$ color-color diagram, the stars in the population show near-infrared colors consistent with B- to M-type stars (Alves & Bouy 2012). Therefore, Alves & Bouy (2012) propose that the NGC 1980 cluster is a foreground population seen in projection against the Orion A cloud. Alves & Bouy (2012) estimate the age of the NGC 1980 cluster on the basis of the median spectral energy distribution (SED) and the age of a massive star, ι Ori, which is 4–5 Myr. However, the previous studies are all based only on photometric data, and lacks spectroscopic follow-up. In this work, we provide a spectroscopic study of the putative foreground population, and address the issue of its age and other properties. Our results suggest that NGC 1980 is actually associated with the Orion A cloud and has an age similar to other star-forming regions in Orion A. We organized the paper as follows: in §2 we will describe our observations and data reduction, in §3 we will delineate

[1] Department of Astronomy, University of Arizona, 933 North Cherry Avenue, Tucson, AZ 85721, USA
[2] Department of Planetary Sciences, University of Arizona, 1629 East University Boulevard, Tucson, AZ 85721, USA
[3] Key Lab of Optical Astronomy, National Astronomical Observatories, CAS, 20A Datun Road, Chaoyang District, 100012 Beijing, China
[4] CAS South America Center for Astronomy, Camino El observatorio #1515, Las Condes, Santiago, Chile
[5] SUPA, School of Physics and Astronomy, University of St Andrews, North Haugh, St Andrews KY16 9SS, UK
[6] Departamento de Fisica Teorica, Facultad de Ciencias, Universidad Autonoma de Madrid, 28049 Cantoblanco, Madrid, Spain
[7] Purple Mountain Observatory and Key Laboratory of Radio Astronomy, Chinese Academy of Sciences, 2 West Beijing Road, 210008 Nanjing, China

our data analysis, we will present our results in §4, followed by a discussion in §5, and we will summarize our results in §6.

2. OBSERVATIONS AND DATA REDUCTION

2.1. *Spectroscopic observations*

2.1.1. *Target selection*

Bouy et al. (2014) lists 1895 sources with probability more than 99% of being members of NGC 1980. These stars are distributed over several tens of square degrees with the stellar surface densities peaking around the Orion molecular cloud. Our targets for the spectroscopic study of NGC 1980 are selected from Bouy et al. (2014), and are limited to the vicinity of the Orion cloud. In Fig. 1, we show the regions we studied. In this area, there are 1,275 sources with probabilities more than 99% of being memebers of NGC 1980. Hereafter, these sources are considered to be high-confidence cluster members. We search for the available spectral types for these high-confidence cluster members in the literature (Hillenbrand 1997; Rebull et al. 2000; Rebull 2001; Hillenbrand et al. 2013; Fang et al. 2009, 2013a; Hsu et al. 2012), and in our unpublished data from our previously spectroscopic survey with MMT/Hectospec and WHT/AF2 (Fang, M., et al. 2017, in preparation). We obtain spectral types for 330 sources from published literature, and for 172 sources from our unpublished datasets. Due to limited observing time, we only selected a subsample of high-confidence cluster members for spectroscopic observations with MMT/Hectospec. In Fig. 2, we show the r *vs.* $r-i$ color-magnitude diagram for high-confidence cluster members, as well for sources with known spectral types and stars we selected for the MMT/Hectospec observations. We calculate the 3 Myr isochrone in the $r-i$ *vs.* r color-magnitude diagram for the pre-main-sequence (PMS) stellar evolutionary models of Baraffe et al. (2015), using the BT-Settl model atmospheres (Allard et al. 2011), with solar abundances from Asplund et al. (2009) [8]. As a comparison, we show the isochrone in Fig. 2, assuming a distance 414 pc (Menten et al. 2007). Most of our targets are located above this isochrone, indicating that they are younger than 3 Myr. However, the ages of our targets could be older, if they lie much closer than Orion A. If we assume an age of ∼4–5 Myr for our targets as suggested in Alves & Bouy (2012), they should be located at ∼210 pc to match their position in the color-magnitude diagram (see Fig. 2). However, Alves & Bouy (2012) argue that the distances of these sources would not be substantially different from the ones in Orion, and might be around 400 pc, since they show similar kinematics to the Orion A molecular cloud. Therefore, the ages and the distance for these sources assumed in Alves & Bouy (2012) are inconsistent.

2.1.2. *Spectroscopic observations and data reduction*

We performed a low-resolution spectroscopic survey of the stellar population in NGC 1980 with the Hectospec multi-object spectrograph, capable of taking a maximum of 300 spectra simultaneously. We used the 270 groove mm^{-1} grating and obtained spectra in the 3700–9000 $\mathring{A}$ range with a spectral resolution of ∼5 $\mathring{A}$. The targets are selected from Bouy et al. (2014), and have probabilities ≥99% as members of NGC 1980. Our ∼300 sources are distributed at 4 pointings. The data were taken in February, 2016. Table 1 lists the observational logs.

We use standard IRAF routines to reduce the Hectospec data according to standard procedures. We perform flat-field correction and extract the spectra using dome flats with the IRAF task ***dofibers*** in the package ***specred***. The wavelength solution for Hectospec is obtained with HeNeAr comparison spectra, using the IRAF task ***identify*** and ***reidentify*** in the package ***specred***. We calibrate the spectra with a wavelength solution constructed using the IRAF task ***dispcor*** under the package ***specred***. For each pointing, we took 3 exposures for the science targets, and one exposure for the sky by shifting the telescope by ∼5 arcseconds. We extracted the spectra for each exposure. Finally, we obtained the spectra for each target and the corresponding sky spectra close to this target. We subtracted the sky from the spectra of each target, and combined the sky-subtracted spectra into one final spectrum.

2.2. *Photometric data*

The photometric data used in this work are mainly from Bouy et al. (2014), in which they combine the photometric data from the Sloan Digital Sky Survey (SDSS, York et al. 2000), CTIO/DECam, the Two-Micron All Sky Survey (2MASS, Skrutskie et al. 2006), the UKIRT Infrared Deep Sky Survey (UKIDSS, Lawrence et al. 2007), and the AAVSO Photometric All-Sky Survey (APASS, Henden et al. 2016), and present a catalog with photometry in the $grizYJHKs$ bands. The photometric data from CTIO/DECam are in $grizY$ bands, and have been calibrated in flux by cross-matching the common stars in the SDSS DR9 catalog in $griz$ bands, and in the UKIDSS catalog in Y band (see Bouy et al. 2014). We complement them with the Spitzer data from Megeath et al. (2012), and Wide-field Infrared Survey Explorer (WISE, Wright et al. 2010). These infrared data is used to characterize the circumstellar disks.

2.3. *X-ray data*

Low-mass young stars usually present strong magnetic activity, and show two to three orders of magnitude brighter X-ray emission than the field population (Feigelson & Montmerle 1999; Feigelson et al. 2007). Thus X-ray data can be used to distinguish young stars from field stars in star-forming regions, particularly diskless (Class III) stellar population (Feigelson et al. 2007). Part of the region studied here has been observed by the X-ray space telescopes XMM-Newton and Chandra. The sky coverage of the XMM (Proposal IDs: 004956, 008994, 009300, 011259, 011266, 013453, 040657, 050356, 060590, and 069020) and Chandra (Proposal IDs: 01200704, 03200289, and 04200331) observations are shown in Fig. 1. The X-ray data will be used to characterize the youth of our sources.

3. DATA ANALYSIS

3.1. *Spectral classification*

[8] A discussion on the BT-Settl models with two types of solar abundances (Asplund et al. 2009; Caffau et al. 2011) can be found in Sect. 3.3.

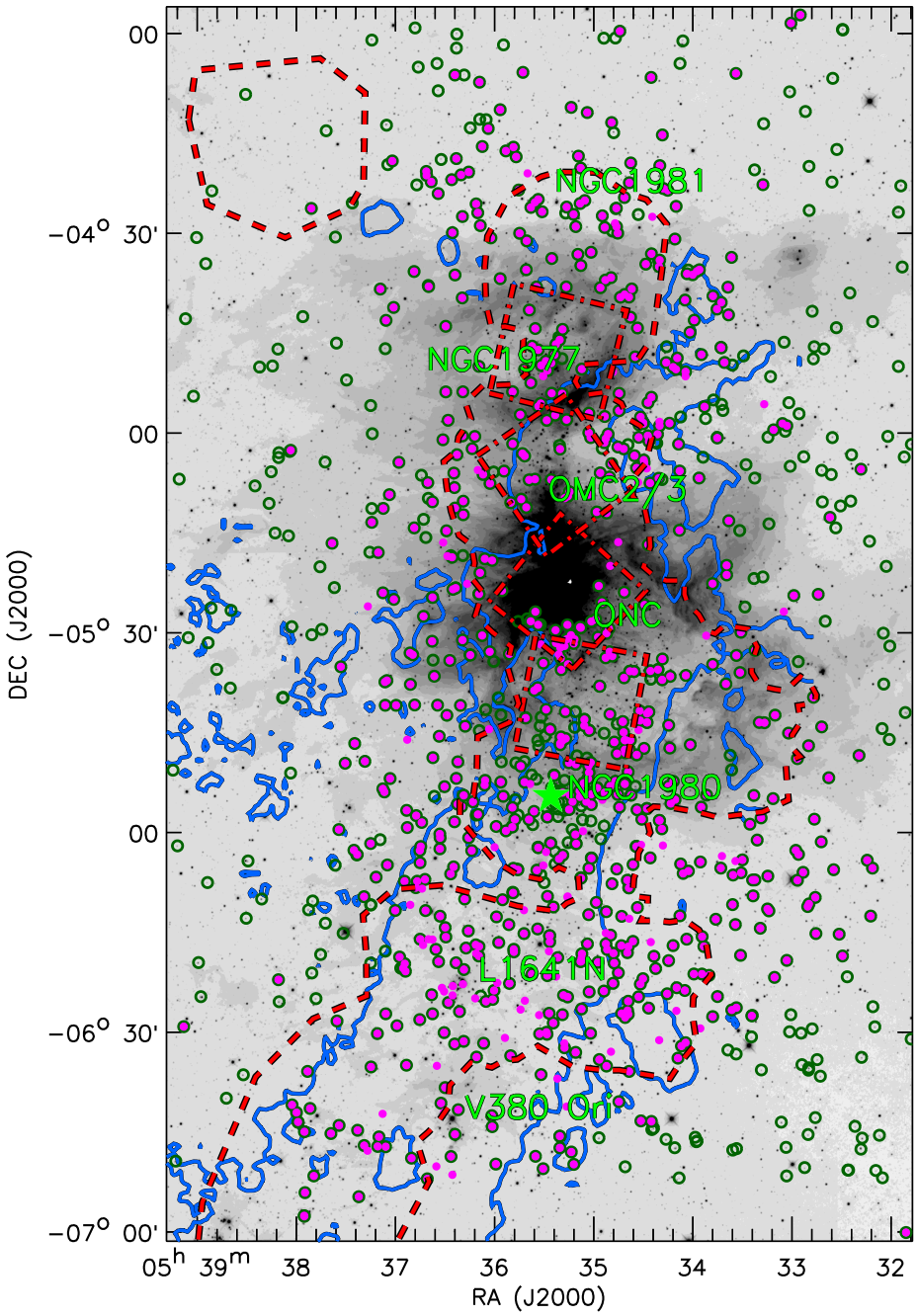

Figure 1. The WISE 3.4 micron image of Orion A. The circles (open dark green and magenta filled) show all the stars with probability more than 99% of being members of NGC 1980 and brighter than 19 mag in r band. The magenta filled circles mark the stars with spectroscopic data. The green filled star symbol mark the position of the massive star ι Ori. The blue solid-line contours are the ^{13}CO integrated intensity from Bally et al. (1987) with a contour level of 5 K km s^{-1}(5σ). The red dash lines enclose the field of view (FOV) of the XMM observations, and the red dash-dotted line boxes are for the FOVs of the Chandra observations.

Table 1
Hectospec observation logs.

		RA	DEC	Exposure	
		(J2000)	(J2000)	Obj	sky
Config.	Obs-date (UT)	(h:m:s)	(d:m:s)	(minutes)	(minutes)
1	2016 Feb 4	+05:33:54.6	−06:01:19	3×15	1×15
2	2016 Feb 4	+05:35:51.5	−05:48:52	3×15	1×15
3	2016 Feb 6	+05:35:15.9	−04:32:58	3×15	1×15
4	2016 Feb 8	+05:35:32.2	−05:22:39	3×15	1×15

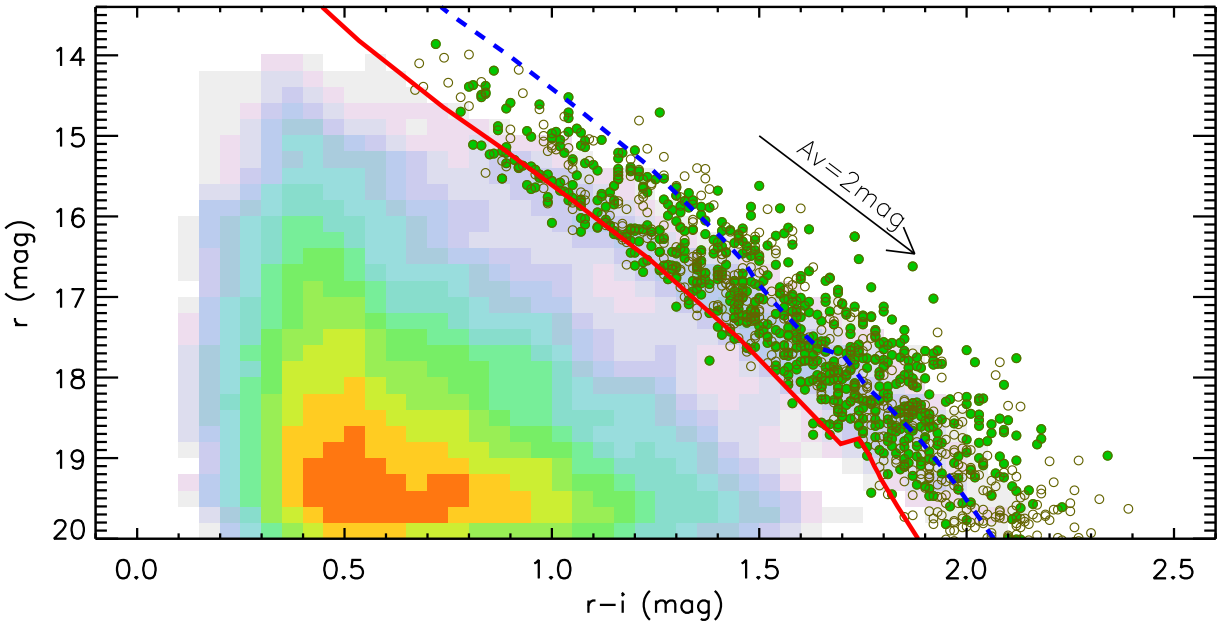

Figure 2. Hess $r - i$ vs. r color-magnitude diagram for all the stars in the field of Orion from Bouy et al. (2014). The circles (open and filled) show all the high-confidence members of NGC 1980 in the field shown in Fig. 1, and the filled circles are for those with spectroscopic data. The solid line shows the 3 Myr isochrone at an distance of 414 pc calculated for the PMS evolutionary models of Baraffe et al. (2015), using the BT-Settl model atmospheres (Allard et al. 2011), with the solar abundances from Asplund et al. (2009). The dashed line is similar to the solid line, but for a 4.5 Myr isochrone at a distance of 210 pc. The arrow show the extinction vector with visual extinction of 2 mag.

The spectral types of young stars are usually obtained by classifying their observed spectra. This is typically done by building a relation between the strength of spectral features and the spectral types of dwarf stars, and apply them to the young stars (Hillenbrand 1997; Hernández et al. 2004). Uncertainties on the spectral classification can be several subclasses depending on the spectral features and/or ranges used for the determination. One typical example is TW Hya, of which spectral type range from K6 to M2.5 (de la Reza et al. 1989; Torres et al. 2006; Pecaut & Mamajek 2013; Vacca & Sandell 2011; Herczeg & Hillenbrand 2014). Pecaut & Mamajek (2013) recently studied a sample of young stars in nearby groups: the η Cha cluster, the TW Hydra Association, the β Pic Moving Group, and the Tucana-Horologium Association. We found that the spectral types in Pecaut & Mamajek (2013) for the same stars are typically one subclass different from those in the literature. Though it is not clear which classification results are more accurate, we decide to classify our stars based on the same criteria as those in Pecaut & Mamajek (2013).

We select X-Shooter spectra for 85 young stars from ESO Phase 3 spectral data archive. Among them, 27 young stars in the η Cha cluster and the TW Hydra Association have been spectrally classified by Pecaut & Mamajek (2013). We use these spectra as the templates to classify the other sources with X-Shooter spectra. Using these X-Shooter spectra, we construct new relations between the strengths of spectral features and spectral types for young stars in the range of K2-M9.5 (See the detailed description in Appendix A). The new relations should be consistent with the classification criteria from Pecaut & Mamajek (2013). Thus, the conversion from spectral types to effective temperatures, intrinsic colors, and bolometric corrections for young populations in Pecaut & Mamajek (2013) can be used for other young stars with spectral types classified based on our relations. In this work, we use these relations to classify the spectra from Hectospec. In Fig. 3, we compare the spectral types from our relations and from the SPTCLASS code (Hernández et al. 2004). It can be noted that both spectral types are consistent with each other given the uncertanty within the range of M0–M6. When the spectral types are later than M6 or earlier than M0, our relations give about one subclass ealier spectral type than SPTCLASS.

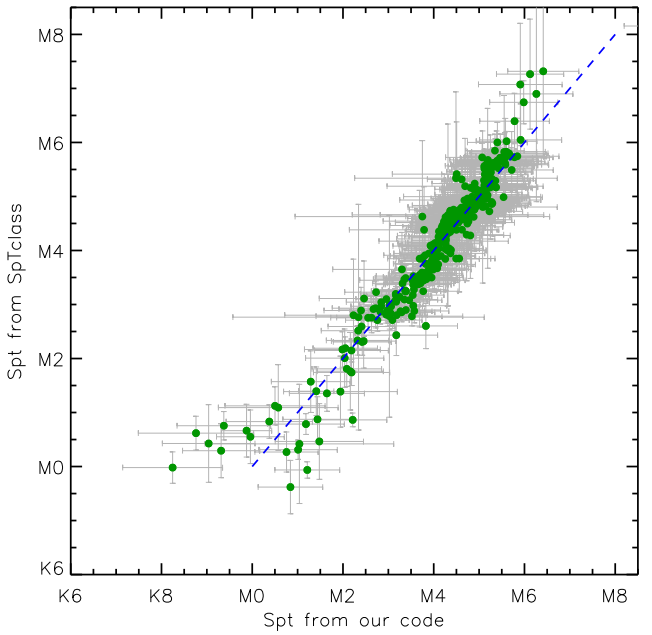

Figure 3. Comparison of spectral types from our code and from the SPTCLASS code (Hernández et al. 2004). The uncertainty for each spectral type are indicated. The dash line marks where the two spectral types are equal in M-type range.

3.2. *YSO selection criteria*

The targets in this work are obtained from a sample of candidate pre-main sequence (PMS) stars selected from different sets of color-magnitude diagrams by Bouy et al. (2014). Some of them could be interlopers from main-sequence (MS) stars or giants. In this section, we will clarify our criteria to remove the contaminators in our sample.

3.2.1. *Spectral features*

The youth of the stars can be characterized using several indicators. The typical one is the Li I absorption line at 6708 Å. In Fig. 4, we show the examples of Li I λ6708Å detections for 3 sources with MMT/Hectospec. Among the 752 sources in our sample, there are 444 sources for which we have obtained spectra. Among them, 295 stars show Li I λ6708Å absorption, 11 do not show clear Li I λ6708Å absorption, and others have spectra too noisy for Li I λ6708Å to be identified. An additional 152 stars are found to show Li I absorption in Hsu et al. (2012). In total, a group of 447 stars in our sample are identified as young stars based on the Li I λ6708Å absorption. In Table 6, we list the equivalent width (EW) of the Li I λ6708Å absorption for those stars. The typical uncertainty of the Li I λ6708Å EWs is around 0.1–0.2Å.

The strength of the Na I doublets at 8183 and 8195 Å has proved to be a good indicator for stellar surface gravitiy for M-type stars (Lawson et al. 2009). MS stars usually show strong Na I doublets, and giants present very weak ones. The PMS stars show the strengths of the Na I doublets between the main sequence stars and giants. In this work, we will use the $Index$(Na I) as a second indicator to select the PMS stars. We calculate the strength of the Na I doublets at 8183 and 8195 Å as $Index(\mathrm{Na\,I}) = F_{8135-8155}/F_{8180-8200}$, where $F_{8135-8155}$ and $F_{8180-8200}$ are fluxes between 8135 and 8155 Å, and between 8180 and 8200 Å, respectively. We also calculate the $Index$(Na I) for the MS stars and giants using the spectra for MS stars and giants from Danks & Dennefeld (1994) and Covey et al. (2007), respectively. To clarify the criteria for the selection of PMS stars, we use a well-studied sample of the PMS stars in L1641 (Fang et al. 2013a). In Fig. 5(a), we show the $Index$(Na I) for PMS stars and MS stars identified in L1641. In the figure, we also show the expected $Index$(Na I) values for MS stars and giants, which are derived from the spectra for MS stars and giants in the IRTF spectral library (Rayner et al. 2009), and the SDSS spectral templates for MS stars (Covey et al. 2007). We note that using

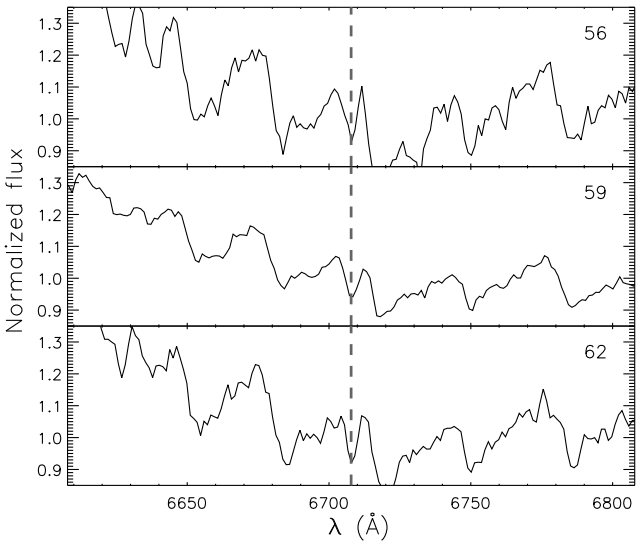

Figure 4. Examples of Li I λ6708Å detection with the MMT/Hectospec. The flux is in normalized in each panel.

Index(Na I) to separate the MS and PMS stars only works for the M-type stars, which is consistent with the findings of Lawson et al. (2009). According to the distribution of the MS stars, PMS stars, and giants in Fig. 5(a), we draw the boundaries for selecting PMS stars described as follows: For spectral types between M1 and M3.5, $1.03 < Index(\mathrm{Na\,I}) < 1.22$, and for spectral types between M3.5 and M7, $1.03 < Index(\mathrm{Na\,I}) < -3.61 + 0.0657 \times Sptnum$, where *Sptnum* is a number corresponding to a spectral type with 70 for M0, 75 for M5, and etc. As a comparison, in Fig. 5(b) we show the PMS stars, identified with the Li I λ6708Å absorption, in this work. As expected most sources are at the PMS boundary but six of them are not. We have checked their spectra. For three of those stars, which show the *Index*(Na I) values simiar to giants, the fringe patterns on their spectra can explain lower *Index*(Na I) values. The other three stars with large Index(NI) values show clear Li absorption as well as strong Na I doublets at 8183 and 8195 Å. A detailed discussion of these sources is presented in Sect. 4.1. In Fig. 5(c), we show the stars without estimated Li I λ6708Å EW due to their noisy spectra. For these stars, we characterize their youth using *Index*(Na I), in combination of X-ray emission and infrared excess emission.

3.2.2. *X-ray emission and Infrared excess emission*

In the field shown in Fig. 1, we extracted 3,688 XMM X-ray sources from the third XMM Serendipitous Source Catalogue (Rosen et al. 2015), and 1616 Chandra X-ray sources from Getman et al. (2005). We matched the X-ray sources to our sources using 1″ tolerance, and found 171 counterparts for our targets. We note that there are more than 100 targets with X-ray sources within radii of 1–3″. We visually check the 2MASS images, and consider those as conterparts to the X-ray sources if there is only one source within 1–3″ from X-ray source. In this way, we found 107 counterparts in our sample for the X-ray sources. In total, we have 267 sources with X-ray emission from the XMM observations, and an additional 11 sources with X-ray emission from Chandra observations. There are two main contaminators to the YSO catalog selected based on the X-ray data: extragalactic sources and nearby foreground stars. Since we have spectra for each source, extragalactic contaminators can be excluded.

The foreground nearby main-sequence stars can show detectable X-ray emission. We used the tool, Flux Limits from Images from XMM-Newton (FLIX)[9], to estimate the 5-σ upper limit of the 0.2–2 keV X-ray luminosity in the studied field. We note that the 5-σ upper limits vary from region to region with a typical value several $10^{29}\,\mathrm{erg\,s^{-1}}$ at the vicinity of Orion. The typical X-ray luminosity of field main-sequence stars is several$\times 10^{27}\,\mathrm{erg\,s^{-1}}$ for solar-type to M-type main sequence stars (Güdel 2004). According to the 5-σ upper limit of the 0.2–2 keV X-ray luminosity in the XMM survey of Orion estimated with FLIX, the XMM observations can detect the field main-sequence stars within the distance$\lesssim$50 pc. Based on the Besançon model of stellar population synthesis of the Galaxy (Robin et al. 2003), we expect only 4 ± 2 field main-sequence stars within a distance of 50 pc in the direction of Orion, suggesting that the fraction of contaminators from foreground stars in our YSO catalog, selected from X-ray emission, is negligible.

We also use infrared excess to identify the young stars. A detailed description of characterizing the disk properties of our sample is presented in Sect. 3.5.

3.3. *Intrinsic colors of young stars*

The extinction of young stars can be determined by comparing the observed colors with the intrinsic colors expected from their spectral types. In Fig. 6, we show the $g - r$ *vs.* $r - i$ color-color diagram for our sources. In the figure, we also show the young stars with low extinction ($A_\mathrm{V} < 0.3$) in Orion OB1, σ Ori, and L1641 (Briceño et al. 2005, 2007; Downes et al. 2014, 2015; Hernández et al. 2014; Fang et al. 2013a). Their colors are dereddend using the extinction law from Schlafly & Finkbeiner (2011), a total to selective extinction value typical of interstellar medium dust ($R_V = 3.1$), and the extinction values in the literature. These young stars in other regions show colors similar to our sources, indicating that the majority of our sources in this work have low or no extinction. As a comparison, in Fig. 6 we also show the empirical colors for dwarfs and giants (Covey et al. 2007). We note that there is a shift between the observed colors and the empirical colors for the dwarfs (thin dark dashed line) and giants (thin dark dash-dotted line). In order to derive the extinction properly, we need to construct intrinsic colors for our sources. We use the sources with negligible extinction shown in Fig. 6, and extract their *griz*-band photometric data from SDSS, JHK_s-band photometric data from 2MASS. The Y-band photometry is only available for the sources in Orion A, and come from Bouy et al. (2014). In Fig. 7, we show their colors vs. their spectral types. We fit the relations between them using 3-order polyno-

[9] FLIX is a on-line tool provided by the XMM-Newton Survey Science Center (see http://www.ledas.ac.uk/flix/flix3). It provides robust estimates of the X-ray upper limit to a given point in the sky where there are no sources detected in the 3XMMi catalog.

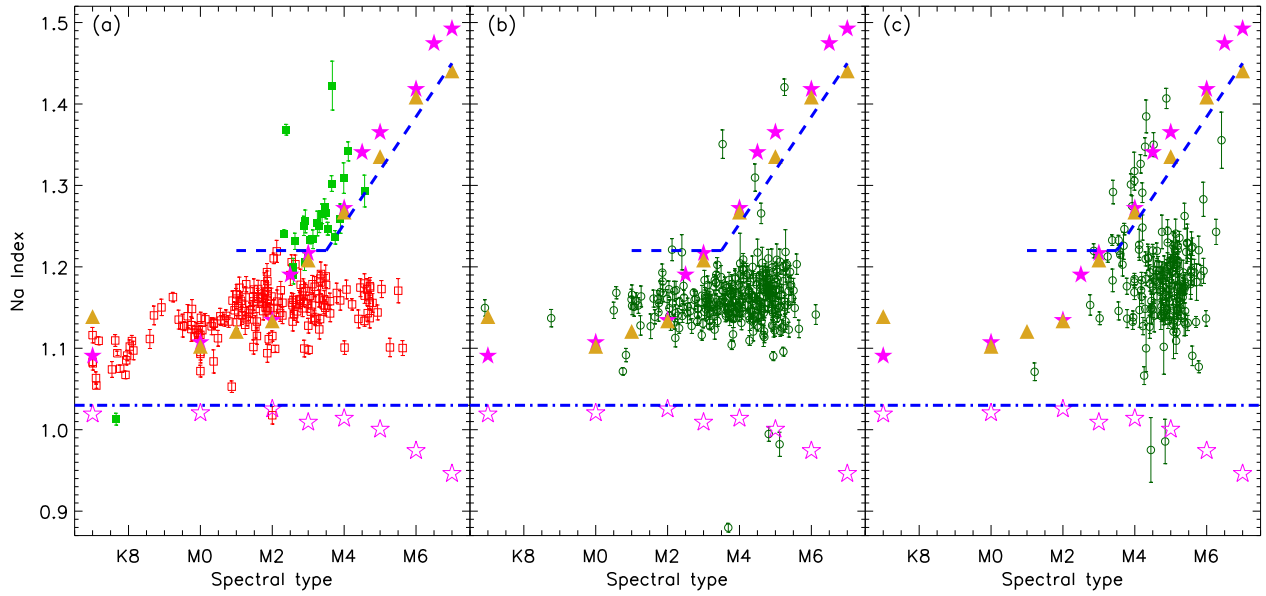

Figure 5. (a) *Index*(Na I) vs. spectral types for the stars in the field of L1641 (Fang et al. 2013a). The filled squares are for the identified field MS or giant stars in the field of L1641, and the open squares show the PMS stars. The dash and dash-dotted lines show the boundaries for MS stars and giants, respectively. The boundaries are defined according to the expected *Index*(Na I) of of MS stars and giants, which are derived using the spectra for MS (filled star symbols) and giants (open star symbols) in the IRTF spectral library (Rayner et al. 2009), and the SDSS spectral templates for MS stars (filled triangles) (Covey et al. 2007). (b) Similar to Panel (a), but for the PMS stars, which are identified using Li I λ6708Å absorption, in this work. (c) Similar to Panel (b), but for the stars in this work without knowledge of Li I λ6708Å absorption due to their noisy spectra.

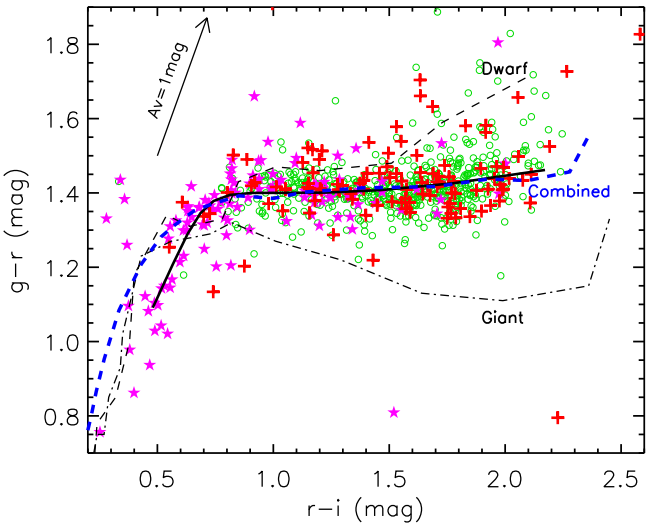

Figure 6. $g-r$ *vs.* $r-i$ color-color diagram. The open circles show the young stars in this work. The filled star symbols and pluses show the dereddened colors of young stars with low extinction ($A_V < 0.3$) in Orion OB1/σ Ori, and L1641, respectively. The thick dark solid line show the empirical colors for young stars used in this work (see Sect. 3.3). The thin dark dashed line and the dash-dotted line show the empirical colors for dwarfs and giants, respectively (Covey et al. 2007). The thick blue dashed line shows the synthetic colors using a set of the combined BT-Settl models with solar abundances from Asplund et al. (2009) (see Sect. 3.3).

mial functions. In Table 2, we list the empirical colors for young stars with spectral types ranged from K5 to M6 from the fitting.

We calculate the synthetic colors using two sets of BT-Settl atmospheric models (Allard et al. 2011, 2012): one with the solar abundances (AGSS2009) from Asplund et al. (2009), and the other with the solar abundances (CIFIST2011) from Caffau et al. (2011). Fig. 7 shows the synthetic $g-r$, $r-i$, $i-z$, $j-J$, $J-H$, and $H-K_s$ colors from these models with surface gravity log g=3.5, 4.0, and 5.0. While both sets of models are consistent with each other in $i-z$, $j-J$, $J-H$, and $H-K_s$ colors, the models with the AGSS2009 abundances show the $g-r$ and $r-i$ colors, which are more consistent with the observations than the ones with the CIFIST2011 abundances. To reproduce the observed colors, we construct a set of BT-Settl atmospheric models with the AGSS2009 abundances and using different log g values for different spectral types: log g=5.0 for the spectral types earlier than M1, log g=4.8 for spectral types between M1 and M3, log g=4.6 for spectral types between M3 and M6, and log g=4.5 for spectral types later than M6. The synthetic colors from this set of models are shown in Fig. 6 and 7, and can better fit the observations than using the atmospheric models with one log g value. Table 3 lists the synthetic colors and bolometric correction in J band from this set of models. In the table, the conversions from the spectral types to effective temperatures are from Pecaut & Mamajek (2013) for stars earlier than M4 and from Herczeg & Hillenbrand (2014) for stars later than M4. In Table 3, we also list the J-band bolometric correction Pecaut & Mamajek (2013, P13), and the ones from Herczeg & Hillenbrand (2015, H15). Our bolometric corrections are consistent with those in the literature.

3.4. *Determining stellar properties*

We derive the extinction for our sources using the empirical colors listed in Table 2 for the ones with spectral

Table 2
Emprical intrinsic colors for young stars

Spt	Teff (K)	$g-r$ (mag)	$r-i$ (mag)	$i-z$ (mag)	$i-Y$ (mag)	$i-J$ (mag)	$J-H$ (mag)	$H-Ks$ (mag)
K5	4140	1.09	0.48	0.30	···	1.45	0.62	0.15
K6	4020	1.21	0.57	0.40	···	1.65	0.66	0.17
K7	3970	1.29	0.63	0.46	···	1.78	0.68	0.19
K8	3940	1.35	0.69	0.50	···	1.85	0.70	0.20
K9	3880	1.38	0.74	0.52	···	1.88	0.71	0.20
M0	3770	1.39	0.81	0.54	···	1.90	0.72	0.20
M1	3630	1.40	0.91	0.57	1.54	1.93	0.71	0.21
M2	3490	1.40	1.04	0.61	1.57	2.00	0.70	0.21
M3	3360	1.40	1.22	0.69	1.64	2.11	0.68	0.23
M4	3160	1.41	1.46	0.82	1.79	2.31	0.65	0.25
M5	2980	1.43	1.78	1.00	2.06	2.60	0.62	0.28
M6	2860	1.46	2.17	1.25	2.48	3.02	0.58	0.32

Table 3
Synthetic colors for young stars

		This work							P03		H04, H05	
	Teff (K)	$g-r$ (mag)	$r-i$ (mag)	$i-z$ (mag)	$i-J$ (mag)	$J-H$ (mag)	$H-Ks$ (mag)	$BC_{\rm J}$ (mag)	Teff (K)	BCJ (mag)	Teff (K)	BCJ (mag)
F0	7280	0.15	-0.03	-0.08	0.57	0.15	0.02	0.60	7280	0.57	...	...
F1	6990	0.21	-0.01	-0.06	0.62	0.18	0.02	0.70	6990	0.68	...	...
F2	6710	0.26	0.02	-0.04	0.67	0.21	0.02	0.79	6710	0.75	...	...
F3	6660	0.27	0.02	-0.04	0.68	0.22	0.02	0.80	6660	0.76	...	...
F4	6590	0.29	0.03	-0.03	0.69	0.23	0.03	0.83	6590	0.79	...	...
F5	6420	0.33	0.05	-0.02	0.72	0.25	0.03	0.89	6420	0.85	6600	0.79
F6	6250	0.37	0.06	-0.01	0.76	0.27	0.03	0.94	6250	0.91	...	...
F7	6140	0.41	0.08	0.00	0.78	0.29	0.04	0.98	6140	0.95	...	...
F8	6100	0.42	0.08	0.01	0.79	0.29	0.04	1.00	6100	0.96	6130	0.95
F9	6090	0.42	0.08	0.01	0.79	0.30	0.04	1.00	6090	0.97	...	...
G0	6050	0.43	0.08	0.01	0.80	0.30	0.04	1.01	6050	0.98	5930	1.02
G1	5970	0.45	0.09	0.02	0.81	0.31	0.04	1.04	5970	1.00	...	...
G2	5870	0.49	0.10	0.03	0.84	0.33	0.04	1.08	5870	1.03	5690	1.10
G3	5740	0.53	0.12	0.04	0.87	0.35	0.05	1.12	5740	1.08	...	...
G4	5620	0.57	0.13	0.05	0.90	0.37	0.05	1.16	5620	1.12	...	...
G5	5500	0.61	0.15	0.06	0.94	0.40	0.05	1.20	5500	1.16	5430	1.18
G6	5390	0.65	0.16	0.07	0.97	0.42	0.06	1.23	5390	1.19	...	...
G7	5290	0.69	0.17	0.08	1.00	0.44	0.06	1.27	5290	1.23	...	...
G8	5210	0.72	0.18	0.09	1.02	0.46	0.06	1.29	5210	1.25	5180	1.26
G9	5120	0.76	0.20	0.10	1.05	0.48	0.07	1.32	5120	1.27	...	...
K0	5030	0.80	0.22	0.11	1.08	0.50	0.07	1.34	5030	1.30	4870	1.36
K1	4920	0.87	0.24	0.13	1.12	0.53	0.08	1.38	4920	1.34	...	...
K2	4760	0.95	0.27	0.15	1.18	0.58	0.08	1.42	4760	1.40	4710	1.41
K3	4550	1.08	0.33	0.19	1.26	0.63	0.10	1.48	4550	1.44	...	...
K4	4330	1.21	0.43	0.24	1.36	0.66	0.12	1.54	4330	1.52	...	...
K5	4140	1.28	0.51	0.30	1.44	0.67	0.15	1.58	4140	1.58	4210	1.56
K6	4020	1.31	0.58	0.33	1.50	0.66	0.17	1.61	4020	1.61	...	...
K7	3970	1.33	0.60	0.35	1.53	0.66	0.18	1.63	3970	1.63	4020	1.62
K8	3940	1.34	0.62	0.36	1.54	0.66	0.18	1.63	3940	1.63	...	...
K9	3880	1.35	0.66	0.38	1.58	0.65	0.19	1.65	3880	1.66	...	...
M0	3770	1.37	0.73	0.43	1.66	0.65	0.20	1.69	3770	1.69	3900	1.66
M1	3630	1.39	0.85	0.50	1.78	0.65	0.21	1.73	3630	1.74	3720	1.73
M2	3490	1.39	1.00	0.58	1.92	0.66	0.22	1.78	3490	1.80	3560	1.78
M3	3360	1.40	1.14	0.65	2.04	0.65	0.23	1.82	3360	1.84	3410	1.84
M4	3160	1.41	1.38	0.78	2.30	0.64	0.25	1.88	3160	1.91	3190	1.93
M5	2980	1.42	1.70	0.95	2.61	0.63	0.27	1.95	2880	2.01	2980	1.99
M6	2860	1.44	1.93	1.07	2.85	0.63	0.28	1.98	...	...	2860	2.03
M7	2770	1.43	2.10	1.19	3.08	0.62	0.30	2.02	...	...	2770	2.06
M8	2670	1.46	2.28	1.35	3.37	0.62	0.30	2.05	...	...	2670	...
M9	2570	1.55	2.36	1.60	3.77	0.57	0.33	2.11	...	...	2570	...

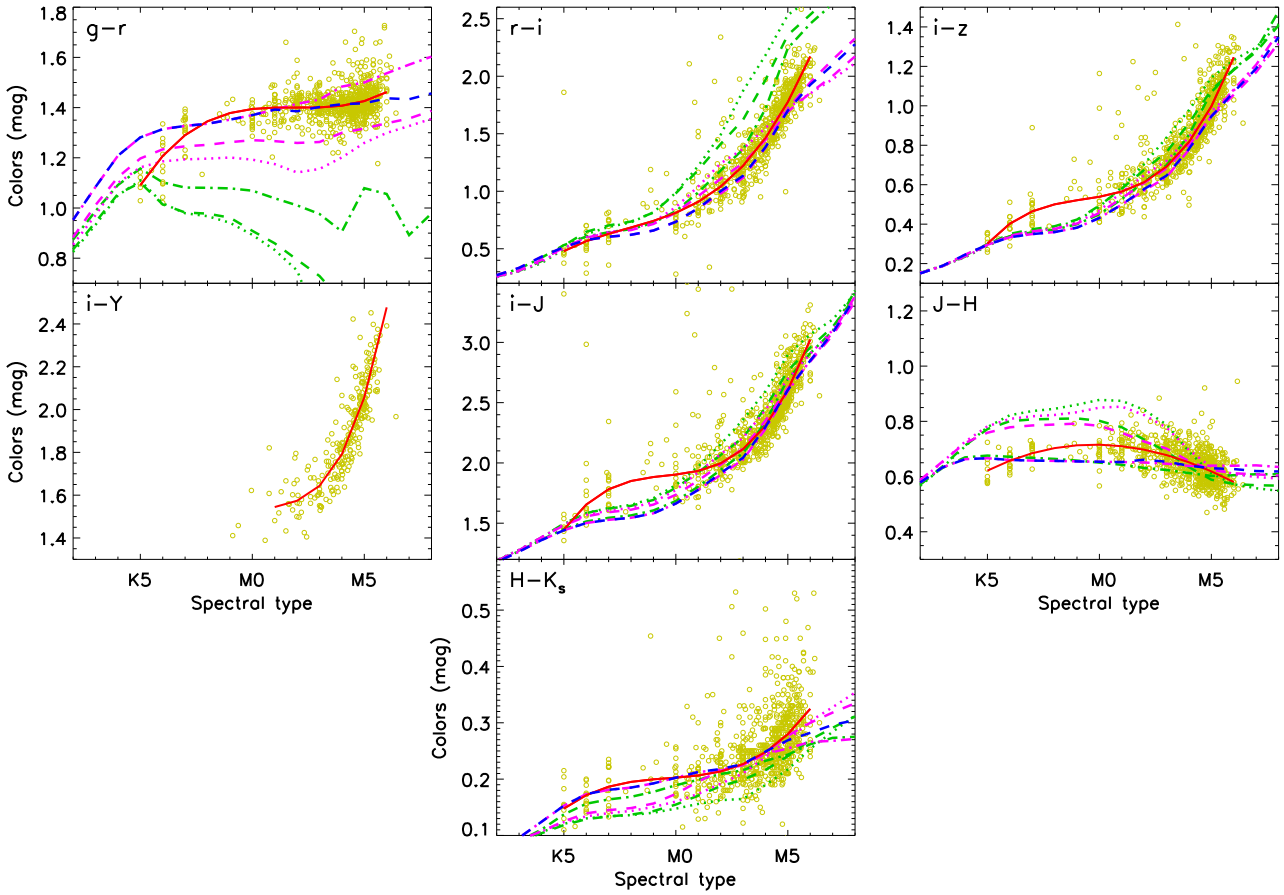

Figure 7. Intrinsic colors for young stars in this work and those in Orion OB1, σ Ori, and L1641. In each panel, The red solid line is the fit to the relation between the colors and the spectral types, the green lines show the synthetic colors from the BT-Settl atmospheric models with the AGSS2009 abundances with log g=3.5 (dotted line), 4.0 (dashed line), and 5.0 (dash-dotted line), and the magenta lines are similar to the green lines but for the models with the CIFIST2011 abundances. The blue dashed lines show the synthetic colors from the combined BT-Settl models.

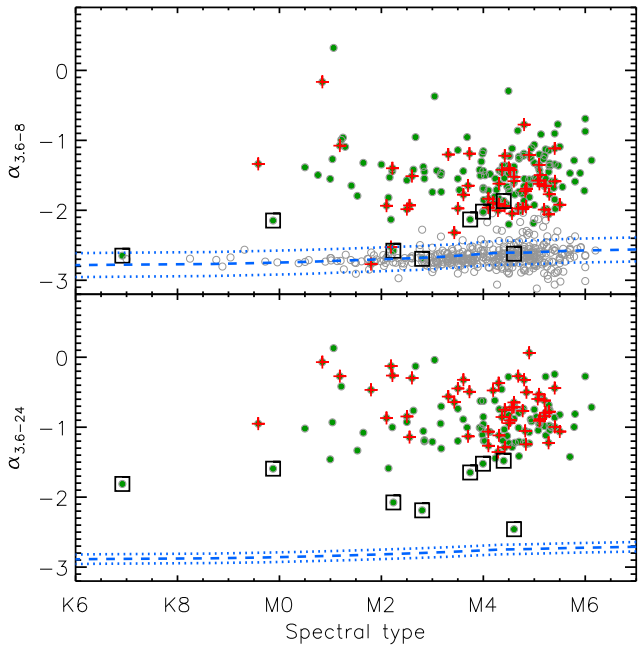

Figure 8. Dereddened Spitzer infrared spectral slopes, $\alpha_{3.6-8}$ and $\alpha_{3.6-24}$ vs. spectral type. In each panel, the open gray circles show the diskless stars, and the filled circles are for the sources with disks. The plus symbols mark the transition disks, and the open squares are for the other evolved disks in our sample (see Sect. 4.3.3 and Fig. 16). The dashed line show the infrared spectral slope of the photospheric emission calculated with the BT-Settl atmospheric models, and the dotted lines are the 1σ standard deviation, assuming a 10% uncertainty in Spitzer photometry.

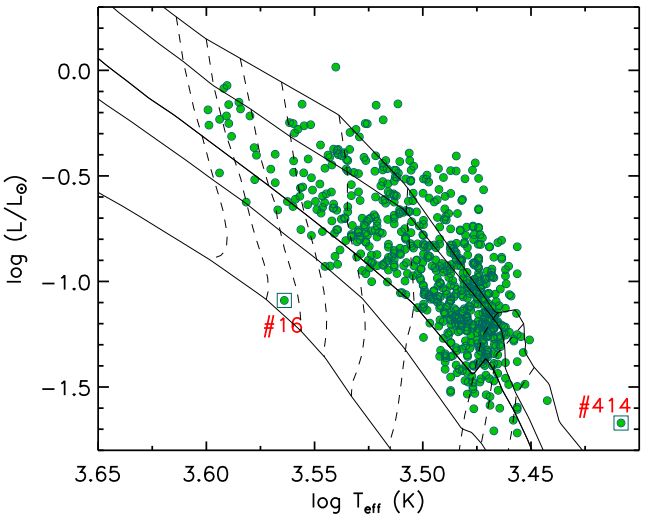

Figure 9. H-R diagram for the PMS stars (filled circles) in this work. The open squares mark the two interesting objects in our sample (see Sect. 4.3.1 and 4.3.2). The solid lines show the isochrones at ages of 0.5, 1, 3, 5, ,10, and 30 Myr, respectively, from Baraffe et al. (2015). The dash lines present the evolutionary tracks of young stellar/substellar objects with masses of 0.06, 0.08, 0.1, 0.2, 0.3, 0.4, 0.5, 0.6, and 0.7 $M_{\odot}$, respectively.

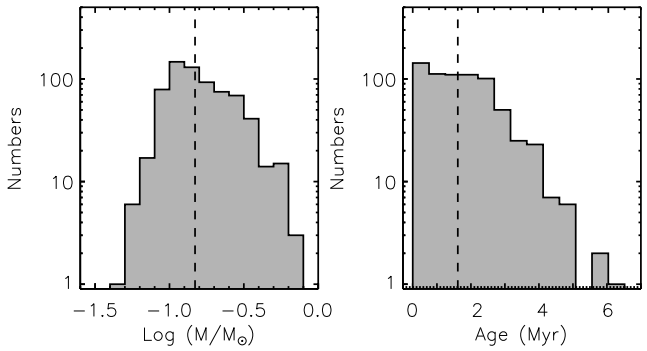

Figure 10. The mass (left) and age (right) distributions of the young stars. The dashed lines shows the median mass ($\sim$0.15 $M_{\odot}$) and age ($\sim$1.4 Myr) of our sample, respectively.

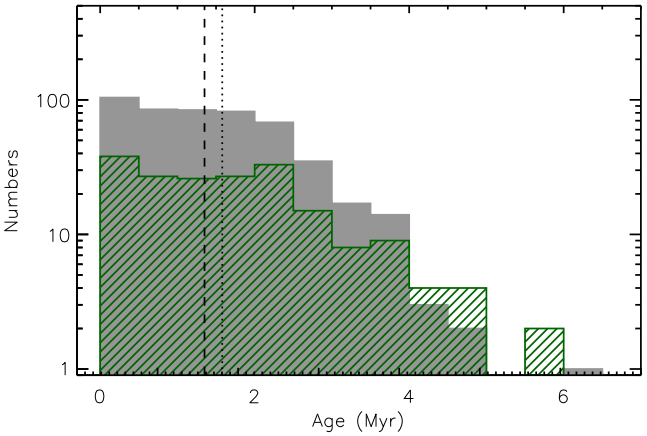

Figure 11. The age distributions of the young stars with disks (line-filled histogram) and without disks (gray-color filled histogram). The median ages of the two populations, 1.6 and 1.3 Myr, respectively, are shown with the dotted line and the dashed line.

types earlier than M6, and the synthetic colors in Table 3 for those with spectral types later than M6. Using the intrinsic colors of $g-r$, $r-i$, $i-z$, $i-j$, we derive mean visual extinctions (A_V) for individual sources employing the extinction law from Schlafly & Finkbeiner (2011) and a total to selective extinction ratio typical of interstellar medium dust ($R_V = 3.1$). We converted the spectral types to effective temperatures using the relation in Table 3, and derive the stellar luminosities for our sources using the J-band bolometric correction for the corresponding spectral types calculated in this work. The stellar luminosities ($L_\star$) are then calculated as follows:

$$M_{bol} = BC_J + m_J - 5 \times log(\frac{d}{10\ \mathrm{pc}})$$

$$\frac{L_\star}{L_\odot} = 10^{\frac{M_{\mathrm{bol},\odot} - M_{bol}}{2.5}}$$

where BC_J is the the bolometric correction in J band, m_J is the dereddened apparent magnitude in J band, d is the distance in the unit of pc, $M_{\mathrm{bol},\odot}$ is the bolometric magnitude of the Sun. Here we take $M_{\mathrm{bol},\odot} = 4.755$ (Mamajek 2012).

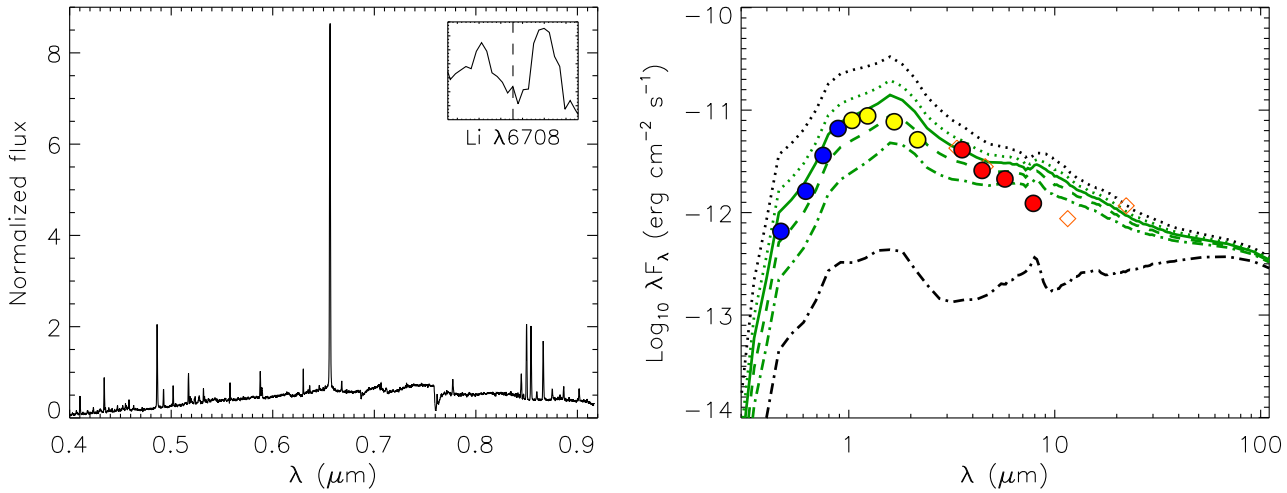

Figure 12. Left panel: the optical spectra of source 16. Right panel: the SED of source 16. The filled circles show the photometry from SDSS, 2MASS, and Spitzer. The open diamonds present the photometry from WISE. The model SEDs are calculated for a disk model with $M_{\rm d}$=5×10^{-4}$M_\star$, $R_{\rm in}$=0.2 AU, and $H_{out}/R_{\rm out}$ =0.1, and for disk inclinations of 78° (black doted line), 79° (green doted line), 79.5° (green solid line), 80° (green dash line), 80.5° (green dash-dotted line), and 82.5° (black dash-dotted line), respectively.

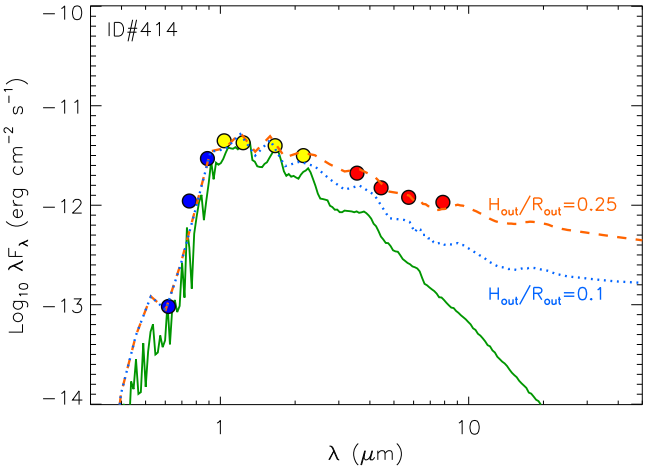

Figure 13. SED of an extremely low-mass object (Source 414). The filled circles show the photometry from SDSS, 2MASS, and Spitzer. The model SEDs are calculated for a disk model with $M_{\rm d}$=1×10^{-2}$M_\star$, $H_{out}/R_{\rm out}$ =0.25 (dashed line) and 0.1 (dotted line), and for a disk inclination of 40°.

3.5. *Characterizing disk properties*

We characterize the disk properties by comparing the model atmosperes from the BT-Settl models with the observed spectral energy distributions. The typical way is to compare the infrared spectral slopes with the expected slopes at the same wavelength ranges from purely photospheric emissions (Luhman et al. 2008). The infrared spectral slopes, defined as $\alpha = dlog(\lambda F_\lambda)/dlog(\lambda)$, are calculated with the dereddened photometry in each band. We compute two sets of infrared spectral slopes, $\alpha_{3.6-8}$ and $\alpha_{3.6-24}$, corresponding to the spectral range of [3.6] to [8.0] and [3.6] to [24], respectively. Table 6 lists the two infrared spectral slopes of the sources with detection in the corresponding infrared bands. In Fig. 8, we show the infrared spectral slopes, $\alpha_{3.6-8}$ and $\alpha_{3.6-24}$ versus the spectral types, for our sources. As a comparison, we calculate the spectral slopes (see Fig. 8) of the BT-Settl atmospheric models (Allard et al. 2012), assuming a 10% uncertainty in Spitzer photometry. Stars with the infrared spectral slopes steeper than the slopes of photospheric emissions are considered to be diskless. For sources with shallower infrared spectral slopes, we visually examine their SEDs. The sources that show infrared excess at more than 3σ confidence level are considered to have disks. A total of 185 sources belong to the disk population. In addition, there are 119 sources without detection in all the four IRAC bands. We visually compare their SEDs, constructed from the available Spitzer and WISE photometric data, to their photospheric emission. Among the 119 sources, 9 sources show infrared excess at more than 3σ confidence level, and are considered to have disks. In Table 6, we list the disk property of each source.

The young stars can be grouped into weak-line T Tauri stars (WTTS) or classical T Tauri stars (CTTS) based on their Hα *EW*. WTTSs have stopped accretion, and show weak and narrow Hα emission line in the spectra, while CTTSs are still accreting, and present strong and broad Hα emission lines. We divide the YSOs into WTTS or CTTS using the criteria described in Fang et al. (2009), in which a star is classified as a CTTS if EW(Hα)$\geq$ 3 Å for K0–K3 stars, EW(Hα)$\geq$5 Å for K4 stars, EW(Hα)$\geq$ 7 Å for K5–K7 stars, EW(Hα)$\geq$ 9 Å for M0–M1 stars, EW(Hα)$\geq$ 11 Å for M2 stars, EW(Hα)$\geq$ 15 Å for M3–M4 stars, EW(Hα)$\geq$ 18 Å for M5–M6 stars, and EW(Hα)$\geq$ 20 Å for M7–M8 stars. Table 6 list the Hα *EWs* of each source and its accretion property. However, we must stress that using EW(Hα) to distinguish WTTSs and CTTSs can fail to distinguish some stars that have low accretion rates, strong chromospheric activity, sky contamination, or self-absorptions of the Hα line.

4. RESULTS

4.1. *A census of PMS stars*

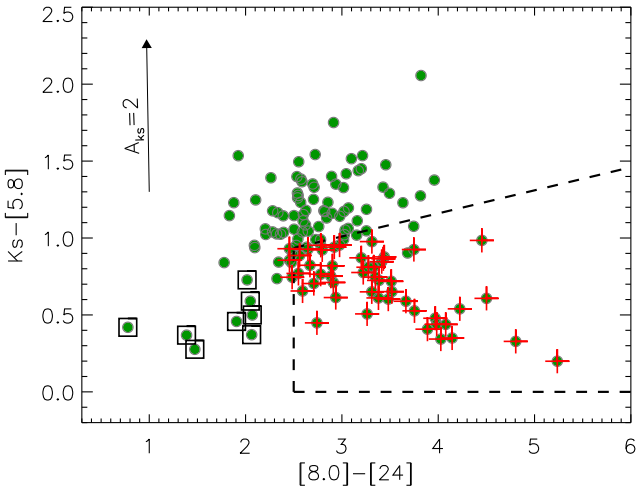

Figure 14. [8.0]−[24] vs. K_s−[5.8] color-color diagram. The dashed lines enclose the region for selecting transition disks. The pluses mark the transition disks, and the open squares show the other evolved disks in our sample (see Sect. 4.3.3 and Fig. 16) The large arrow show the reddening vector with K_s-band extinction of 2 mag.

We identify PMS stars mainly based on the Li I λ6708Å absorption. With this criterion, a sample of 447 stars are classified as PMS stars. For others without estimate of the EWs of Li I λ6708Å absorption line, we use the *Index*(Na I) to select the PMS stars as described in Sect. 3.2.1, which works for stars with spectral types later than M1. With this criterion, an additional 164 stars are classified as PMS stars. We also include 64 additional stars which show X-ray emission, and 27 additional stars with infrared excess emission. A total of 691 sources are classified as PMS stars according to the above criteria. Table 6 list these stars, as well as the criteria to classify them as the PMS stars.

We use the *Index*(Na I) to assess the contamination in our PMS sample from young field stars which may show weak Li I λ6708Å absorption line. In our sample, there are 447 sources with estimated EWs of Li I λ6708Å absorption line, and 63% of them (283/447) have the *Index*(Na I) in Table 6. As noted in Sect. 3.2.1, there are three sources, ID 156, 438, 572 in Table 6, that are located outside the PMS boundary in Fig. 5(b) and show *Index*(Na I) similar to the field dwarfs. However, for two sources, ID 156 and 438, the strengths of their Li I λ6708Å absorption lines are consistent with other young stars in Orion (see, e.g., Fang et al. 2013a). Hence, it is unclear why they show the strong Na I doublets. For the source 572, its Li I λ6708Å absorption line is weak (EW ∼0.2), and could be a young field dwarf. Therefore, we expect that the contamination in our sample from the field dwarfs is not significant.

4.2. *Stellar properties*

We derive the extinction of individual sources in the way described in Section 3.4. The typical uncertainty for our A_V measurements is around 0.3 mag, estimated from the sources without extinction in our sample. The resulting visual extinctions are listed in Table 6. With the derived effective temperatures and bolometric luminosities using the method described in Sect. 3.4, assuming a distance of 414 pc, we place the stars in the H-R diagram in Fig. 9. Most of our sources lie between the 0.1 and 3 Myr isochrones. We use a distinct symbol (open square symbols) for an "exotic" object that is apparently subluminous and a extremely low-mass object (see Section 4.3.1 and Section 4.3.2). We derive the masses and ages of the stars using the PMS evolutionary tracks from Baraffe et al. (2015). For the stars above the youngest isochrone (∼0.5 Myr) from the evolutionary models, their masses are estimated using the 0.5 Myr isochrone since the low-mass stars are evolving vertically in H-R diagram during the first several Mys. In Table 6, we list the stellar masses and ages of the stars. Seventeen objects in our sample have masses less than 0.075 $M_\odot$, and are brown dwarfs. Among them, the source 414 has the minimum mass (∼0.018 $M_\odot$). In Fig. 10, we show the mass and age distributions of our sample. The median mass and age of our sample is ∼0.15$M_\odot$ and ∼1.4 Myr, respectively. In Fig. 11, we show the age distributions of the young stars with and without disks. Both populations show a similar age distribution with most of stars younger than 2.5 Myr. The median ages of the two populations are 1.3, and 1.6 Myr for diskless and disk populations, respectively.

We must stress that the stellar ages derived from the H-R diagram are dependent on the distance that we use. Here, we assume that the foreground population is associated with the Orion molecular cloud, and use the same distance (414 pc) as Orion, which is supported by the fact that the foreground population and the Orion molecular cloud show similar kinematics (see Sect 5.1).

4.3. *Disk properties*

4.3.1. *A subluminous object*

In the H-R diagram (see Fig. 9), one source (ID 16 in Table 6) appears to be subluminous compared with others with the similar spectral type. In its spectrum, we detect Li I λ6708Å absorption line, indicating that it is a PMS star. The isochrone age of this object is ∼23 Myr. However, its optical spectrum show numerous strong emission lines. Among them (see the left panel in Fig. 12), the Hα are the strongest one with the EW of −134 Å. Such strong emission lines in the spectrum of Source 16 indicate that it should be much younger than its isochronal age (∼23 Myr). Its SED shows the strong infrared excess emission (see the right panel in Fig. 12), suggesting that it is surrounded by a disk. Similar young stars have been discovered in our previous spectroscopic surveys in Orion (Fang et al. 2009, 2013a), and also found in other regions, e.g., the Lupus 3 dark cloud, Taurus, and ϵ Cha (Comerón et al. 2003; White & Hillenbrand 2004; Fang et al. 2013b). One promising hypothesis for these exotic objects is that they are harboring disks with high inclinations, and the light seen mainly comes from photons scattered off the disk surface, and is therefore much reduced. The optical emission lines may arise in outflows or disk winds with emitting areas much larger than the central star, which allows at least part of the line fluxes to reach us relatively unattenuated. We employ the radiative transfer code RADMC-3D (Dullemond 2012) to model the SED of Source 16. We set the stellar effective temperature to 3,664 K (M0.8) and stellar radius 1.3 $R_\odot$, corresponding

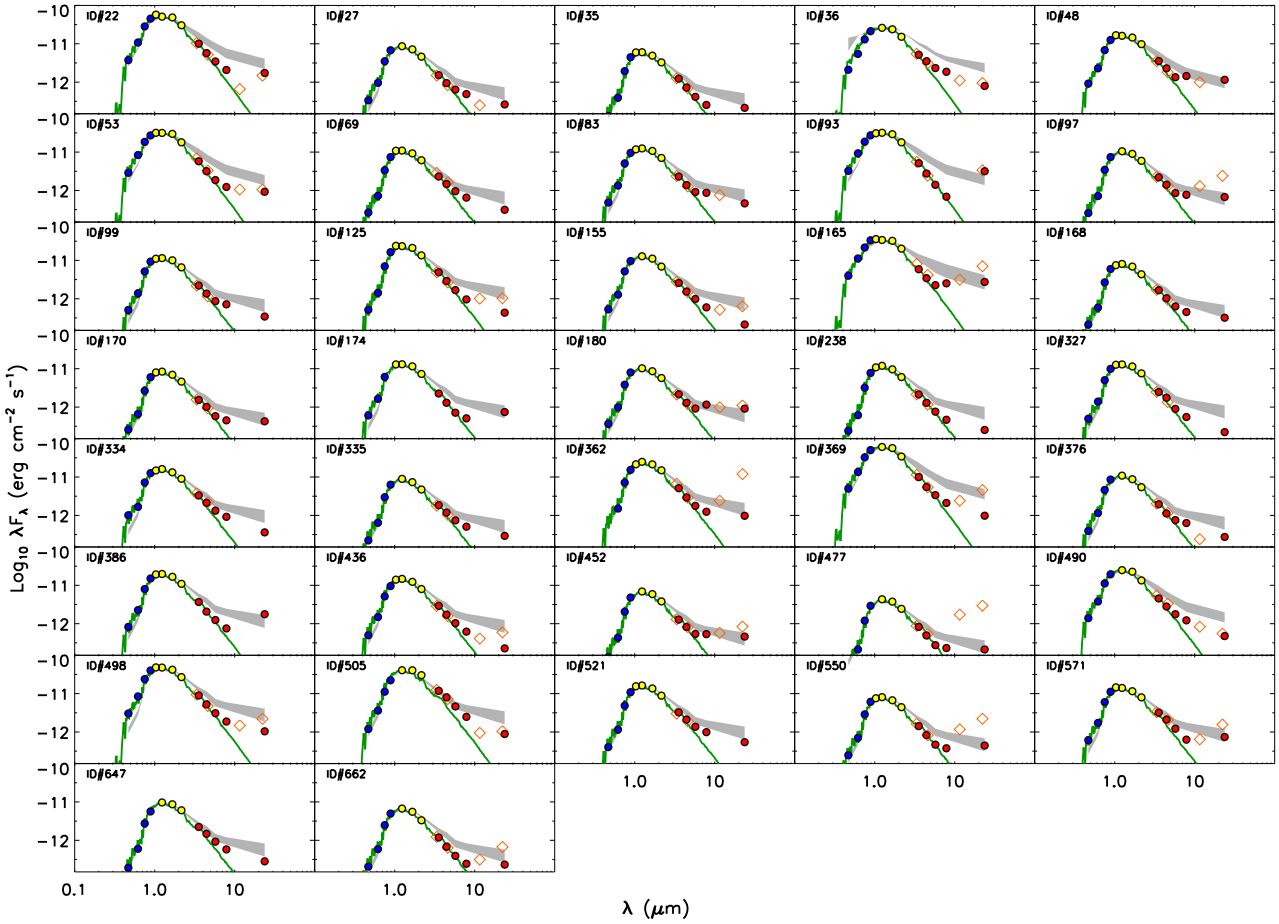

Figure 15. The SEDs of newly confirmed YSOs with transition disks. The circles show the photometry in different bands. The open diamonds are the photometry from WISE. In each panel, the green solid curve indicates the photospheric emission level, and the gray color filled region show the upper and lower quartiles of the median SEDs of L1641 CTTSs with the spectral types similar to our sources.

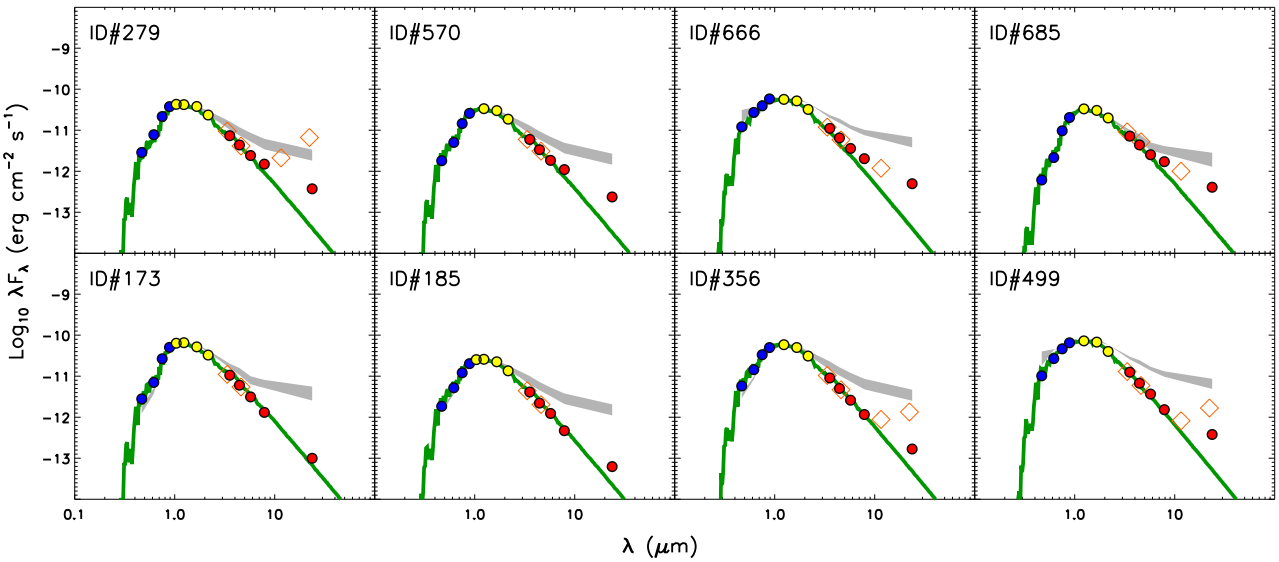

Figure 16. Same as in Fig. 15, but for the SEDs of other evolved disks.

to a PMS star with mass $\sim$0.4 $M_\odot$ and an age $\sim$2 Myr (Baraffe et al. 2015). We set the outer disk radius ($R_{\rm out}$) to 100 AU, and assume a pressure scale height ($H_{\rm P}$) that varies as a power law with the radius (R), $H_{\rm P}/R \propto R^{1/7}$. We vary the disk mass ($M_{\rm d}$) from $10^{-4}M_\star$, $5\times10^{-4}M_\star$, $1\times10^{-3}M_\star$, $5\times10^{-3}M_\star$, to $10^{-2}M_\star$, the inner disk radius ($R_{\rm in}$) from 0.1, 0.2, 0.3, to 0.4 AU, $H_{out}/R_{\rm out}$(H_{out}: the pressure scale height at $R_{\rm out}$) from 0.1, 0.2, to 0.3, and disk inclinations from 60° to 83°. We find that the SED of Source 16 can be reproduced by a model with parameters $H_{out}/R_{\rm out}$=0.1, $M_{\rm d}$=$10^{-4}M_\star$–$1\times10^{-3}M_\star$, and $R_{\rm in}$=0.1–0.4 AU, and an inclination $\sim$79–82° (see Fig. 12 for a representative model). A lower or higher disk inclination can lead to significantly over-predicted or under-predicted fluxes at short wavelengths, respectively (see Fig. 12).

The prominent emission lines in the spectrum of ID 16 include Balmer lines, He I lines at 5876 Å and 6678 Å, [O I] lines at 5577 Å and 6300 Å, Ca II infrared triplet (8498, 8542, 8662 Å), as well as many other lines. Such a spectrum rich in emission lines is similar to the one of EX Lup, an M0-type young star and the prototype of EXor variable star (Sicilia-Aguilar et al. 2015a). A detailed identification of all the lines and a comparison of ID 16 to EX Lup would require spectra with high spectral resolution. If the underluminosity of ID 16 is due to the occultation and scattering of photospheric emission by a highly inclined disk, we would expect that the EWs of the accretion-related lines are simialr to the ones typical to T Tauri stars since they are formed in the magnetospheric infall flows, which are close to the stellar surface and should be similarly occulted. We notice that the source shows the normal He I λ6678 Å line, but $\sim$4 times higher EWs of He I λ5876 Å line, and $\sim$10 times higher EWs of Ca II infrared triplet, compared with other CTTSs in Orion(see e.g. Fang et al. 2009). Both He I emission lines and Ca II infrared triplet are related to accretion activities. The large EWs of these lines could be explained if ID 16 is actively accreting. The spectrum of ID 16 also shows [O I] lines at 5577 Å and 6300 Å with *EWs* which are also $\sim$10 times higher than the ones typical to T Tauri stars (Simon et al. 2016). However, these [O I] lines could be contaminated by telluric [O I] emission lines since our spectral resolution is low. In the spectrum of ID 16 we did not clearly detect the the [S II] emission lines at 6716 Å and 6731 Å, but may see two peaks near them. The [S II] lines are thought to arise in jets emerging from accreting YSOs. New spectral data with high spectral resolution and signal-to-noise ratio is needed to identify them explicitly. Here, we must stress that the source ID 16 could be also a young star with a distance much larger than Orion. In this case, we do not need a highly inclined disk to reproduce its SED, and the distance of ID 16 could be $\sim$1 kpc, if its age is around 1 Myr.

4.3.2. *A disk around an extremely low-mass object*

In our sample, Source 414 has the latest spectral type. Its spectral type in this work is $\sim$M9$\pm$1, which is consistent with the one (M8) in Hillenbrand et al. (2013) given the uncertainties. In the H-R diagram, this object is above the youngest PMS isochrone ($\sim$0.5 Myr) from Baraffe et al. (2015). Assuming a 0.5 Myr isochrone, the mass of a source with a spectral type M8–M9 is around 0.018-0.030 $M_\odot$. However, the mass of 0.018-0.030 $M_\odot$ should be considered as the upper limit for Source 414, since the effective temperatures of young extremely low-mass objects decrease during their evolution (Baraffe et al. 2015). In Figure 13 we show the SED of this object. Its SED shows infrared excess emission in all four IRAC bands, suggesting that it possesses a disk. We employ the radiative transfer code RADMC-3D to model the SED of the source 414. We set the stellar effective temperature to 2,570 K (M9) and the stellar radius to 0.84 $R_\odot$, and a disk mass to $1\times10^{-2}M_\star$, and the inner edge to the dust sublimation radius, set $R_{\rm out}$ to 50 AU, and assume $H_{\rm P}/R \propto R^{1/7}$. We vary ($M_{\rm d}$) from $10^{-4}M_\star$, $5\times10^{-4}M_\star$, $1\times10^{-3}M_\star$, $5\times10^{-3}M_\star$, to $10^{-2}M_\star$, $H_{out}/R_{\rm out}$ from 0.1, 0.15, 0.2, 0.25,to 0.3, and and disk inclinations from 0° to 80°. We find that a flaring disk model with $H_{out}/R_{\rm out}$=0.25–0.3, $M_{\rm d}$=$5\times10^{-4}M_\star$–$1\times10^{-2}M_\star$ and an disk inclination $\lesssim$50° can reproduce the SED of Source 414. In Fig. 13, we compare the model SED with $H_{out}/R_{\rm out}$ =0.25 (a flaring disk model) with the one with $H_{out}/R_{\rm out}$ =0.1 (a flat disk model). Both flat and flared disks have been found around brown dwarfs (Apai et al. 2005; Pascucci et al. 2009).

4.3.3. *Evolved disks*

In our sample, 689 sources have infrared photometry in at least three IRAC or WISE bands and can be classified to be diskless or harboring disks. Among them, 72% (495/689) are diskless, and the rest are disk sources. Among the disk population, we select transition disk (TD) candidates based on colors as shown in Fig. 14: [8.0]−[24]≥2.5 and $K_{\rm s}$−[5.8]≤0.56+([8.0]−[24])×0.15. For individual candidates, we compare their SEDs with their model photospheric emissions, as well as the median SEDs of L1641 CTTSs (Fang et al. 2013a), corresponding to their spectral types. A total of 49 sources are confirmed as TD objects which show very weak or no infrared excess at near-infrared wavelengths and shorter IRAC bands, but strong excess emission at mid-infrared and longer wavelength. Among them, twelve TDs have already been described in the literarure (Fang et al. 2013a; Kim et al. 2013). In Fig. 15, we show the SEDs of the 37 new TDs in this work.

In our sample, we also found 8 sources which are detected in 24 μm, and show much weaker infrared excess emission than a typical TD. Their infrared spectral slopes and colors are smaller than other sources (see Fig. 8 and 14). In Fig. 16, we show the SEDs of those sources. Among these sources, one object (ID 666) shows the depleted infrared excess emission through the four IRAC band to 24 μm, and thus could be a globally depleted disk candidate, which can be produced when disks are deficient in small dust grains (Currie et al. 2009; Sicilia-Aguilar et al. 2011). In contrast to Source 666, the SEDs of the objects 279, 570, and 685 start to show the infrared excess emission from 8 μm, while the others show infrared excess only at 24 μm. The weak infrared excess emission of the seven sources indicate that their inner disks have been more strongly dissipated than a

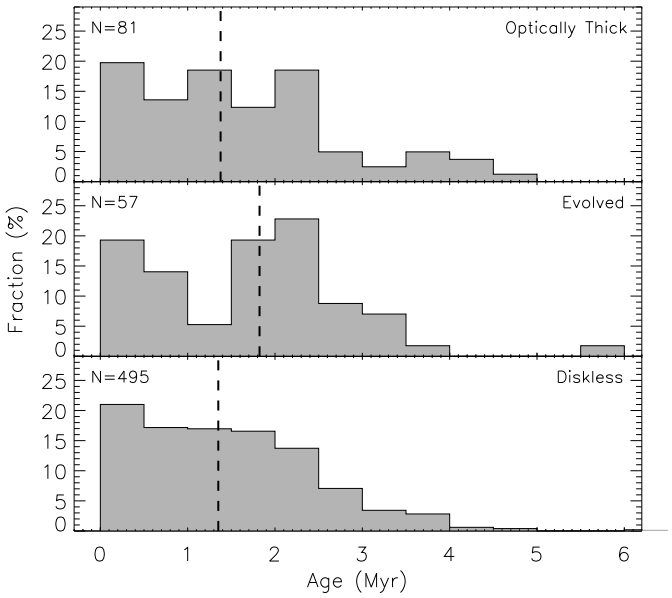

Figure 17. Histograms showing the age distribution for the young stars with optically thick disks, evolved disks, and without disks, respectively. The dashed line in each panel show the median age of each population.

typical TD in the same region. Without the data at far infrared bands, it is unknown if these sources are TDs with a big inner hole, or young debris disks. Actually, we also found two similar sources in L1641 (Fang et al. 2009, 2013a), one of which shows strong excess emission at 70 and 160 μm (Source 069001 in Stutz et al. 2013), suggesting that this object is a TD with a big inner hole. Similar objects have been found in the Tr 37 cluster (Sicilia-Aguilar et al. 2013, 2015b).

In Fig. 17, we show the age distributions of the three populations. The median ages of the sources with optically thick disks($\alpha_{3.6-8} \geq -1.8$), evolved disks, and without disks are ~1.4 Myr, 1.8 Myr, and 1.4 Myr, respectively. We note that the median age of the evolved disk systems is slightly larger than the other two populations. However, since each population shows a very broad distribution, the difference among their median ages is not significant.

4.3.4. *Accretion in disks at different evolutionary stages*

In Fig. 18(a), we compare the Hα *EW*s for sources with TDs, optically thick disks($\alpha_{3.6-8} \geq -1.8$), or without disks. It can be noted that the YSOs with optically thick disks usually present strong Hα emission, while diskless YSOs show weak Hα emission. However, for TDs, about half of TDs show no accretion, while a small fraction of them show strong accretion. In Fig. 18(b), we display the distribution of logarithmic ratio between the observed Hα *EW* and the *EW* threshold for the three populations shown in Fig. 18(a). Here, *EW* threshold is the one used to classify the YSOs into CTTSs or WTTSs, and is the spectral type dependent (see Sect. 3.5). According to these *EW* thresholds, 73±9% of YSOs with optically thick disks are accreting, while only 46±7% of TDs are accretors. If we define "strong accretion" sources to have Hα *EW*s greater than twice the *EW* thresholds, 25±7% of TDs belong to this group. For the YSOs with optically thick disks, this fraction is 45±10%. The accretion properties among the different types of disks are consistent with our previous studies (Fang et al. 2009, 2013a; Sicilia-Aguilar et al. 2010, 2013). For the eight evolved disks shown in Fig. 16, seven of them have estimates of Hα *EW*s. Six of them show no accretion, and one (499) shows Hα *EW* which is just above the threshold to be classified as a CTTS. Therefore, the fraction of accretors among these sources should be less than 14%, suggesting these objects are much more evolved than TDs.

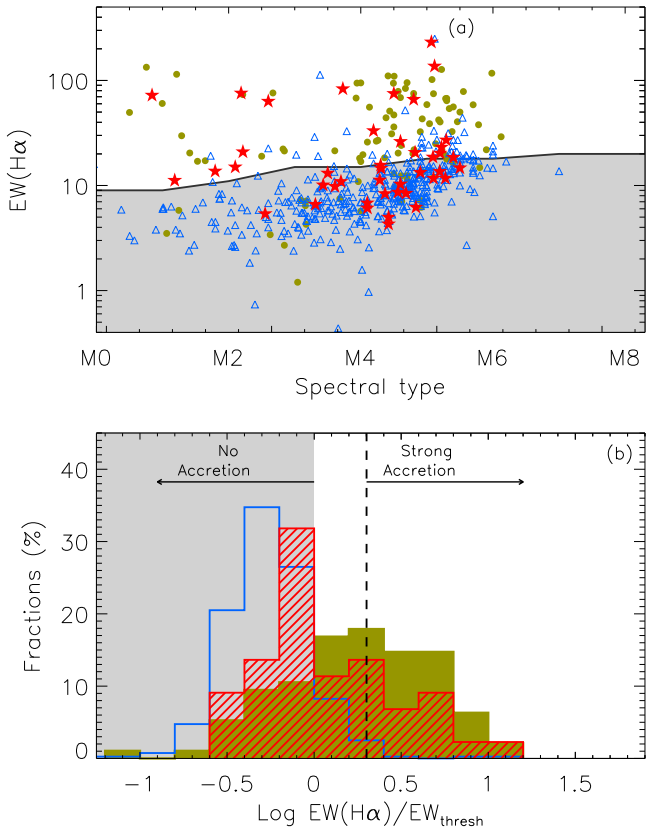

Figure 18. Hα *EW*s vs. spectral type for PMS stars in this work. The filled circles are for YSOs with optical thick disks($\alpha_{3.6-8} \geq -1.8$), and triangles for YSOs without disks. The star symbols show the transition disks in our sample. (b): the distribution of the ratio between the observed Hα *EW* and the *EW* threshold, separating CTTSs or WTTSs, for the three populations in the left panel: YSOs with optically thick disks (filled histogram), YSOs without disks (open histogram), and transition disks (line-filled histogram). The dash line marks $EW(\mathrm{H}\alpha)/EW_{thresh}$=2.

5. DISCUSSION

5.1. *Is the foreground population associated with the Orion A cloud?*

Tobin et al. (2009) performed a kinematic survey of 1,613 stars which span from NGC 1977 to L1641N. Their study suggests that the kinematics of young stars are consistent with the ones of their local clouds. Using the kinematic data from Tobin et al. (2009), Alves & Bouy (2012) show that the velocity dispersion of young stars near NGC 1980 is much smaller than those in other parts of Orion, though their kinematics are consistent with the gas. Therefore, they concluded that NGC 1980 is a distinct population from others. In this work, we use a

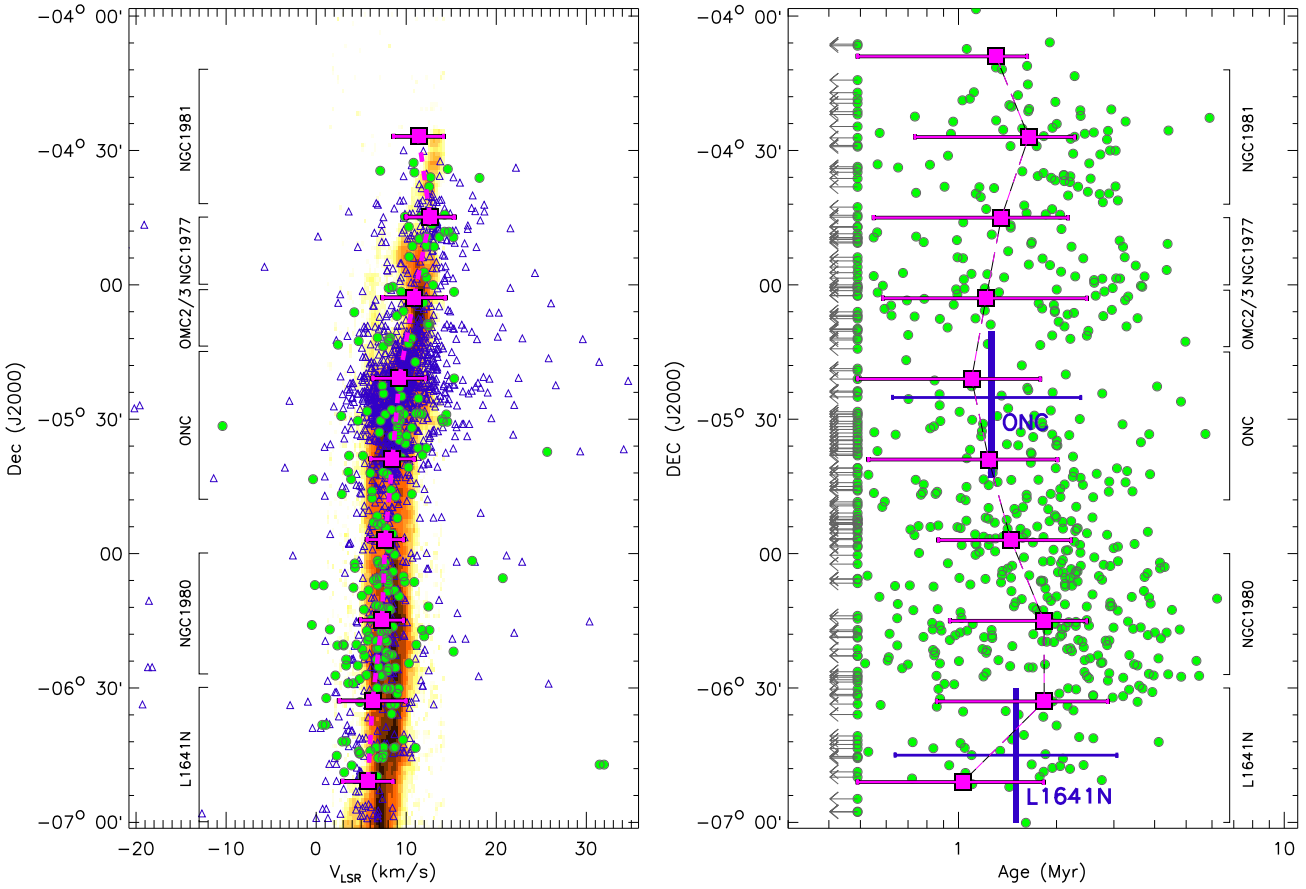

Figure 19. Left: Position-velocity (PV) of both stellar radial velocities and ^{13}CO (J=1–0) emission (background color map) along the Orion A cloud. The filled circles are for the foreground population in Bouy et al. (2014), and triangles for young stars in Orion. The ^{13}CO emission is from Bally et al. (1987). The PV plot for the ^{13}CO emission is summed over the range of R.A. shown in Fig. 1. The filled squares connected with the dashed line show the mean radial velocities for individual declination bins with the err-bars showing the standard deviations. Right: the ages of the young stars in this work vs. their Declination. The left pointing arrow indicates the up-limits of ages for the stars with ages above the youngest isochrone (∼0.5 Myr) in the PMS evolutionary models of Baraffe et al. (2015). The filled squares connected with the dashed line show the median ages for individual declination bins, and the err-bars show age ranges including 50% of the sources near the median ages. The median ages of ONC and L1641 are also shown in the figure as a comparison.

better dataset to re-visit this issue. Our data are collected from the SDSS APOGEE INfrared Spectroscopy of Young Nebulous Clusters program (IN-SYNC) survey of the Orion A molecular cloud (see detailed description in Da Rio et al. 2016). In the region studied here, we find more than 2,200 sources, which have been observed with SDSS and have velocity uncertainties less than 0.5 km s^{-1}. The size of this sample is much larger than the one (287 sources) with the same accuracy from Tobin et al. (2009). Among the APOGEE sample, more than 1,650 sources can be classified as young stars from the X-ray emission or infrared excess emission. In this dataset, we find 280 sources in the foreground population. In Fig. 19 (left), we show their radial velocity data as well as the ones of the other young stars in Orion A. As a comparison, we also show the PV diagrams for the gas emission in Orion A cloud. We do not find any significant difference between the kinematics of the foreground population, other young stars, and the gas material in Orion, which confirms the previous result in Tobin et al. (2009). Futhermore, we derive the velocity dispersions of all the young stars in Fig. 19 (left) as did in Tobin et al. (2009). However, we do not find significant difference between the the velocity dispersions of young stars at the different locations of Orion A. Therefore, our study suggests that the foreground population, as other young stars in this region, are associated with the Orion A cloud. Here, we must stress that the kinematic study is only based on the radial velocities of the stars, and can be improved in the future with their proper motions from *Gaia*

5.2. *Is the foreground population older than other regions in Orion A?*

As shown in Fig. 10 (right), the median age of the foreground population with spectroscopic data is around 1.4 Myr, which is younger than the age (4–5 Myr) proposed by Alves & Bouy (2012) for this population. In the previous work, the age is deduced based on two arguments: (1) the age of ι Ori, (2) the median SED of the disk population in NGC 1980. Gies & Bolton (1986) revealed that ι Ori is eccentric binary (O9 III+B1 III), and proposed that it could be formed as a result of binary-binary encounter that ejected the two runaways (AE Aur, μ Col), which is confirmed by Hoogerwerf et al. (2000) using the *Hipparcos* data supplemented with the available radial velocities. The trapezium cluster is the most

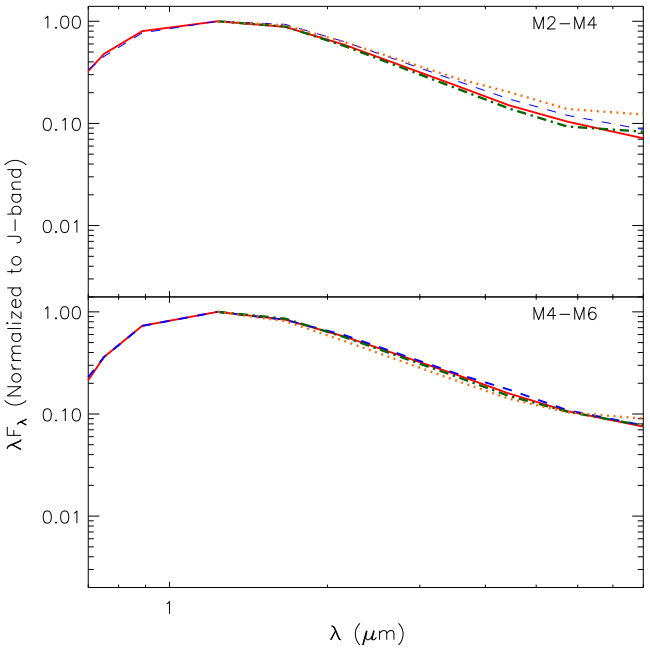

Figure 20. Median SEDs of class II sources with spectral type M2–M4 (upper) and M4–M6 (lower) in clusters of ONC (dotted line, 1 Myr), L1641 (dash line, 1.5 Myr), NGC 1980 (solid line), and σ Ori (dash-dotted line, 3 Myr).

likely parent for the three sources. Therefore it is still unclear if the ι Ori is related to the foreground population, and therefore uncertain to use the age of ι Ori as the one of the whole foreground population. When comparing the shapes of SEDs, Alves & Bouy (2012) normalized the SEDs of different regions to the J-band flux. We note there are systematic differences between the SEDs of these regions at wavelength shorter than J-band, which may suggest that the extinctions of different regions have not been corrected when they constructed the SEDs. We estimate how the extinction affects the spectral slopes. For $A_V = 5$, the dereddened spectral slope between J-band and Spitzer 8 μm band can be 0.5 less than the observed spectral slopes. In Fig. 20, we compare the median SED of class II sources in this work with those in Orion nebula cluster (ONC, 1 Myr), L1641 (1.5 Myr), and σ Ori (3 Myr), using the data from the literature (Hillenbrand 1997; Da Rio et al. 2010; Megeath et al. 2012; Fang et al. 2009, 2013a; Hernández et al. 2007a, 2014). These regions have been extensively surveyed with spectroscopy, which provides a reliable estimate of extinction for each source. In this work, most of sources are mid-M spectral types. Therefore, we only include the M-type stars for constructing the median SEDs. We divide the sources into two groups according to their spectral types: M2–M4 and M4–M6, since the luminosity of central stars can affect the infrared spectral slopes. For individual sources, their SEDs are first extinction-corrected before combination. The extinction law is from Schlafly & Finkbeiner (2011) for the SDSS bands adopting a total to selective extinction value typical of interstellar medium dust ($R_V = 3.1$), Rieke & Lebofsky (1985) for the 2MASS bands, and Flaherty et al. (2007) for the Spitzer bands. Figure 20 show the median SEDs of different clusters. After correcting the extinction, we do not see any significant difference between the foreground population and other regions in Orion, especially for the M4-M6 group. The low disk fraction (28%) of this population may indicate that this population may be older than its median isochronal age according to the relation between disk fractions and ages (Haisch et al. 2001; Sicilia-Aguilar et al. 2006; Hernández et al. 2007a; Fang et al. 2012, 2013b). However, this population is mostly likely biased against sources with hot inner disks, those showing K_s-band excess emission, since their sample selection criteria select stars with $i - K_s$ or $H - K_s$ colors similar to the intrinsic photospheric colors (Alves & Bouy 2012; Bouy et al. 2014). The typical fraction of sources with hot inner disks is ∼40%–50% for a young population with an age of 1–2 Myr (Hillenbrand 2005; Yasui et al. 2010). The low disk fraction (28%) of our sample is most likely due to the exclusion of sources with hot inner disks.

In Fig. 19 (right), we show the ages of sources in the foreground population vs. their declination. In different declinations, the ages of the stars all show large age spread with ages ranged from $\lesssim$0.5 Myr to ∼6 Myr. We divide the sources into different groups according to their declination, and derive the median ages. In the figure, we show these median ages as well as the bars which show the ranges including 50% of sources near the median ages. The median ages of the foreground population in the whole region are all around 1–2 Myr, and clearly younger than the age (4–5 Myr) proposed in Alves & Bouy (2012). Along the declination, though it is not statistically significant, the median ages of different regions seem to show a slight gradient, and the median ages of the stars around NGC 1980 are slightly older (1.8 Myr) than other regions, which is consistent with the result in Da Rio et al. (2016). As a comparison, we show the median ages of ONC (1.3 Myr) and L1641N (1.5 Myr). For both regions, we re-estimate their ages using the same PMS evolutionary tracks from Baraffe et al. (2015) as we did for the foreground population. The effective temperature and luminosity of each star in ONC is collected from Da Rio et al. (2010), and those in L1641N are from Fang et al. (2013a). In addition, we only include the sources with spectral types between K7–M6, which is range of spectral types for the foreground population in this work. As shown in Fig. 19 (right), the median ages (1–2 Myr) of the foreground population are consistent with the ones of ONC and L1641N.

5.3. *Is the foreground population from one cluster?*

In Alves & Bouy (2012) and Bouy et al. (2014), they proposed that the foreground population in Orion is from one cluster and centered on NGC 1980. However, as discussed in the above two sections, we can see that the kinematics of the foreground population are consistent with their local clouds and other young stars in the same regions. In Fig. 19 (left), the gradient in the kinematics of Orion A cloud can be clearly shown in the kinematics of the foreground population, which is a strong evidence that the foreground population is associated with the local clouds instead of being one cluster. Furthermore, we may see an age gradient along the declination, and the median age of the sources near NGC 1980 is slightly higher than others. Such age gradient should not be seen if the foreground population are from the

same cluster. Therefore, our results argue against the presence of an old, large foreground cluster in front of Orion A. We propose that the foreground population seen in Alves & Bouy (2012) and Bouy et al. (2014) is a combination of young stars with low or no extinction in NGC 1980 and other regions in Orion A.

6. SUMMARY

We performed a spectroscopic survey of the foreground population in Orion A with MMT/Hectospec. We combine the Hectospec data with optical and infrared photometric data to estimate the stellar effective temperatures, luminosities, and extinction values of individual sources, and derive masses and ages of individual sources by their placement in the H-R diagram. The disk properties of individual sources are characterized using Spitzer and WISE data, and their accretion properties are characterized using the Hα line. We also use archival APOGEE radial velocity data to study the kinematics of the foreground population and other young stars in the Orion A cloud. The main results are summarized as follows.

1. We present a catalog of 691 young stars including their spectral types, line of sight extinction, stellar masses and ages, disk properties, and accretion properties.

2. We find one new subluminous object in our spectroscopic sample, and explain it as a star with a nearly edge-on disk.

3. We discovered an object with extremely low mass ($<$0.018–0.030 $M_{\odot}$). The SED modeling indicates this object possesses a flaring disk.

4. We identify 37 new transition disk objects, one globally depleted disk candidate, and 7 young debris disk candidates. We investigate the accretion properties of YSOs with disks in our sample based on Hα EWs. We find that the fraction of accretors among transition disks is much lower than among the YSOs with optically-thick disks (46$\pm$7% versus 73$\pm$9%, respectively), which confirm our previous results in L1641.

5. We confirm that the kinematics of the foreground population is consistent with their local clouds and other young stars in the same regions in Orion A. The median age of the foreground population is also similar to those of other young stars in Orion A. Therefore, our results suggest that the foreground population is associated with Orion A, and prove that it is not a distinct large and old (4–5 Myr) cluster in front of Orion A.

Many thanks to the anonymous referee for comments that help to improve this paper. This material is based upon work supported by the National Aeronautics and Space Administration under Agreement No. NNX15AD94G for the program "Earths in Other Solar Systems". The results reported herein benefitted from collaborations and/or information exchange within NASAs Nexus for Exoplanet System Science (NExSS) research coordination network sponsored by NASA's Science Mission Directorate. L.Z. acknowledges supports from National Science Foundation of China (NSFC) grants 11303037 and 11390371/2 and support from the Chinese Academy of Sciences (CAS) through a CAS-CONICYT Postdoctoral Fellowship administered by the CAS South America Center for Astronomy (CASSACA) in Santiago, Chile. This research uses data obtained through the Telescope Access Program (TAP), which has been funded by the National Astronomical Observatories of China, the Chinese Academy of Sciences (the Strategic Priority Research Program "The Emergence of Cosmological Structures" Grant No. XDB09000000), and the Special Fund for Astronomy from the Ministry of Finance. Observations reported here were obtained at the MMT Observatory, a joint facility of the University of Arizona and the Smithsonian Institution.

REFERENCES

Alcalá, J. M., et al. 2014, A&A, 561, A2
Allard, F., Homeier, D., & Freytag, B. 2011, in Astronomical Society of the Pacific Conference Series, Vol. 448, 16th Cambridge Workshop on Cool Stars, Stellar Systems, and the Sun, ed. C. Johns-Krull, M. K. Browning, & A. A. West, 91
Allard, F., Homeier, D., & Freytag, B. 2012, Philosophical Transactions of the Royal Society of London Series A, 370, 2765
Alves, J., & Bouy, H. 2012, A&A, 547, A97
Apai, D., Pascucci, I., Bouwman, J., Natta, A., Henning, T., & Dullemond, C. P. 2005, Science, 310, 834
Asplund, M., Grevesse, N., Sauval, A. J., & Scott, P. 2009, ARA&A, 47, 481
Bally, J., Stark, A. A., Wilson, R. W., & Langer, W. D. 1987, ApJ, 312, L45
Baraffe, I., Homeier, D., Allard, F., & Chabrier, G. 2015, A&A, 577, A42
Bouy, H., Alves, J., Bertin, E., Sarro, L. M., & Barrado, D. 2014, A&A, 564, A29
Briceño, C., Calvet, N., Hernández, J., Vivas, A. K., Hartmann, L., Downes, J. J., & Berlind, P. 2005, AJ, 129, 907
Briceño, C., Hartmann, L., Hernández, J., Calvet, N., Vivas, A. K., Furesz, G., & Szentgyorgyi, A. 2007, ApJ, 661, 1119
Caffau, E., Ludwig, H.-G., Steffen, M., Freytag, B., & Bonifacio, P. 2011, Sol. Phys., 268, 255
Cieza, L., et al. 2007, ApJ, 667, 308
Cieza, L. A., et al. 2010, ApJ, 712, 925
Cohen, M., & Kuhi, L. V. 1979, ApJS, 41, 743
Comerón, F., Fernández, M., Baraffe, I., Neuhäuser, R., & Kaas, A. A. 2003, A&A, 406, 1001
Comerón, F., Neuhäuser, R., & Kaas, A. A. 2000, A&A, 359, 269
Comerón, F., Spezzi, L., & López Martí, B. 2009, A&A, 500, 1045
Covey, K. R., et al. 2007, AJ, 134, 2398
Covino, E., Alcala, J. M., Allain, S., Bouvier, J., Terranegra, L., & Krautter, J. 1997, A&A, 328, 187
Currie, T., Lada, C. J., Plavchan, P., Robitaille, T. P., Irwin, J., & Kenyon, S. J. 2009, ApJ, 698, 1
Da Rio, N., Robberto, M., Soderblom, D. R., Panagia, N., Hillenbrand, L. A., Palla, F., & Stassun, K. G. 2010, ApJ, 722, 1092
Da Rio, N., et al. 2016, ApJ, 818, 59
Danks, A. C., & Dennefeld, M. 1994, PASP, 106, 382
de la Reza, R., Torres, C. A. O., Quast, G., Castilho, B. V., & Vieira, G. L. 1989, ApJ, 343, L61
Donati, J.-F., et al. 2011, MNRAS, 417, 1747
Downes, J. J., et al. 2014, MNRAS, 444, 1793
—. 2015, MNRAS, 450, 3490
Dullemond, C. P. 2012, RADMC-3D: A multi-purpose radiative transfer tool, Astrophysics Source Code Library
Fang, M., Kim, J. S., van Boekel, R., Sicilia-Aguilar, A., Henning, T., & Flaherty, K. 2013a, ApJS, 207, 5
Fang, M., van Boekel, R., Bouwman, J., Henning, T., Lawson, W. A., & Sicilia-Aguilar, A. 2013b, A&A, 549, A15
Fang, M., van Boekel, R., Wang, W., Carmona, A., Sicilia-Aguilar, A., & Henning, T. 2009, A&A, 504, 461
Fang, M., et al. 2012, A&A, 539, A119
Feigelson, E., Townsley, L., Güdel, M., & Stassun, K. 2007, Protostars and Planets V, 313
Feigelson, E. D., & Montmerle, T. 1999, ARA&A, 37, 363
Fernández, D., Figueras, F., & Torra, J. 2008, A&A, 480, 735

Flaherty, K. M., Pipher, J. L., Megeath, S. T., Winston, E. M., Gutermuth, R. A., Muzerolle, J., Allen, L. E., & Fazio, G. G. 2007, ApJ, 663, 1069
Getman, K. V., et al. 2005, ApJS, 160, 319
Gies, D. R., & Bolton, C. T. 1986, ApJS, 61, 419
Güdel, M. 2004, A&A Rev., 12, 71
Haisch, Jr., K. E., Lada, E. A., & Lada, C. J. 2001, ApJ, 553, L153
Henden, A. A., Templeton, M., Terrell, D., Smith, T. C., Levine, S., & Welch, D. 2016, VizieR Online Data Catalog, 2336
Herbig, G. H., & Bell, K. R. 1988, Third Catalog of Emission-Line Stars of the Orion Population : 3 : 1988
Herczeg, G. J., & Hillenbrand, L. A. 2008, ApJ, 681, 594
—. 2014, ApJ, 786, 97
—. 2015, ApJ, 808, 23
Hernández, J., Calvet, N., Briceño, C., Hartmann, L., & Berlind, P. 2004, AJ, 127, 1682
Hernández, J., Morales-Calderon, M., Calvet, N., Hartmann, L., Muzerolle, J., Gutermuth, R., Luhman, K. L., & Stauffer, J. 2010, ApJ, 722, 1226
Hernández, J., et al. 2007a, ApJ, 662, 1067
—. 2007b, ApJ, 671, 1784
—. 2014, ApJ, 794, 36
Hillenbrand, L. A. 1997, AJ, 113, 1733
—. 2005, ArXiv Astrophysics e-prints
Hillenbrand, L. A., Hoffer, A. S., & Herczeg, G. J. 2013, AJ, 146, 85
Hoogerwerf, R., de Bruijne, J. H. J., & de Zeeuw, P. T. 2000, ApJ, 544, L133
Hsu, W.-H., Hartmann, L., Allen, L., Hernández, J., Megeath, S. T., Mosby, G., Tobin, J. J., & Espaillat, C. 2012, ApJ, 752, 59
Hsu, W.-H., Hartmann, L., Allen, L., Hernández, J., Megeath, S. T., Tobin, J. J., & Ingleby, L. 2013, ApJ, 764, 114
Hughes, J., Hartigan, P., Krautter, J., & Kelemen, J. 1994, AJ, 108, 1071
Ingleby, L., et al. 2013, ApJ, 767, 112
Kim, K. H., et al. 2013, ApJ, 769, 149
Krautter, J., Wichmann, R., Schmitt, J. H. M. M., Alcala, J. M., Neuhauser, R., & Terranegra, L. 1997, A&AS, 123, 329
Lawrence, A., et al. 2007, MNRAS, 379, 1599
Lawson, W. A., Lyo, A., & Bessell, M. S. 2009, MNRAS, 400, L29
Lee, H.-T., & Chen, W. P. 2009, ApJ, 694, 1423
Looper, D. L., Burgasser, A. J., Kirkpatrick, J. D., & Swift, B. J. 2007, ApJ, 669, L97
Looper, D. L., et al. 2010, ApJ, 714, 45
Luhman, K. L. 2004, ApJ, 602, 816
Luhman, K. L., & Steeghs, D. 2004, ApJ, 609, 917
Luhman, K. L., et al. 2008, ApJ, 675, 1375
Lyo, A.-R., Lawson, W. A., & Bessell, M. S. 2004, MNRAS, 355, 363
Mamajek, E. E. 2012, ApJ, 754, L20
Mamajek, E. E., Lawson, W. A., & Feigelson, E. D. 1999, ApJ, 516, L77
Manara, C. F., Testi, L., Natta, A., Rosotti, G., Benisty, M., Ercolano, B., & Ricci, L. 2014, ArXiv e-prints
Manara, C. F., et al. 2013, A&A, 551, A107
Megeath, S. T., et al. 2012, AJ, 144, 192
Menten, K. M., Reid, M. J., Forbrich, J., & Brunthaler, A. 2007, A&A, 474, 515
Mohanty, S., Jayawardhana, R., & Basri, G. 2005, ApJ, 626, 498
Muzerolle, J., Luhman, K. L., Briceño, C., Hartmann, L., & Calvet, N. 2005, ApJ, 625, 906
Nguyen, D. C., Brandeker, A., van Kerkwijk, M. H., & Jayawardhana, R. 2012, ApJ, 745, 119
Oliveira, I., et al. 2009, ApJ, 691, 672
Pascucci, I., Apai, D., Luhman, K., Henning, T., Bouwman, J., Meyer, M. R., Lahuis, F., & Natta, A. 2009, ApJ, 696, 143
Pecaut, M. J., & Mamajek, E. E. 2013, ApJS, 208, 9
Rayner, J. T., Cushing, M. C., & Vacca, W. D. 2009, ApJS, 185, 289
Rebull, L. M. 2001, AJ, 121, 1676
Rebull, L. M., Hillenbrand, L. A., Strom, S. E., Duncan, D. K., Patten, B. M., Pavlovsky, C. M., Makidon, R., & Adams, M. T. 2000, AJ, 119, 3026
Riaz, B., Gizis, J. E., & Harvin, J. 2006, AJ, 132, 866
Rieke, G. H., & Lebofsky, M. J. 1985, ApJ, 288, 618
Rigliaco, E., Natta, A., Testi, L., Randich, S., Alcalà, J. M., Covino, E., & Stelzer, B. 2012, A&A, 548, A56
Robin, A. C., Reylé, C., Derrière, S., & Picaud, S. 2003, A&A, 409, 523
Romero, G. A., Schreiber, M. R., Cieza, L. A., Rebassa-Mansergas, A., Merín, B., Smith Castelli, A. V., Allen, L. E., & Morrell, N. 2012, ApJ, 749, 79
Rosen, S. R., et al. 2015, ArXiv e-prints
Sacco, G. G., Franciosini, E., Randich, S., & Pallavicini, R. 2008, A&A, 488, 167
Schlafly, E. F., & Finkbeiner, D. P. 2011, ApJ, 737, 103
Sicilia-Aguilar, A., Fang, M., Roccatagliata, V., Collier Cameron, A., Kóspál, Á., Henning, T., Ábrahám, P., & Sipos, N. 2015a, A&A, 580, A82
Sicilia-Aguilar, A., Henning, T., Dullemond, C. P., Patel, N., Juhász, A., Bouwman, J., & Sturm, B. 2011, ApJ, 742, 39
Sicilia-Aguilar, A., Henning, T., & Hartmann, L. W. 2010, ApJ, 710, 597
Sicilia-Aguilar, A., Kim, J. S., Sobolev, A., Getman, K., Henning, T., & Fang, M. 2013, A&A, 559, A3
Sicilia-Aguilar, A., et al. 2006, ApJ, 638, 897
—. 2015b, A&A, 573, A19
Simon, M. N., Pascucci, I., Edwards, S., Feng, W., Gorti, U., Hollenbach, D., Rigliaco, E., & Keane, J. T. 2016, ApJ, 831, 169
Skrutskie, M. F., et al. 2006, AJ, 131, 1163
Stelzer, B., et al. 2013, A&A, 558, A141
Stutz, A. M., et al. 2013, ApJ, 767, 36
Teixeira, R., Ducourant, C., Chauvin, G., Krone-Martins, A., Song, I., & Zuckerman, B. 2008, A&A, 489, 825
Tobin, J. J., Hartmann, L., Furesz, G., Mateo, M., & Megeath, S. T. 2009, ApJ, 697, 1103
Torres, C. A. O., Quast, G. R., da Silva, L., de La Reza, R., Melo, C. H. F., & Sterzik, M. 2006, A&A, 460, 695
Torres, G., Guenther, E. W., Marschall, L. A., Neuhäuser, R., Latham, D. W., & Stefanik, R. P. 2003, AJ, 125, 825
Vacca, W. D., & Sandell, G. 2011, ApJ, 732, 8
Wahhaj, Z., et al. 2010, ApJ, 724, 835
Webb, R. A., Zuckerman, B., Platais, I., Patience, J., White, R. J., Schwartz, M. J., & McCarthy, C. 1999, ApJ, 512, L63
White, R. J., Gabor, J. M., & Hillenbrand, L. A. 2007, AJ, 133, 2524
White, R. J., & Ghez, A. M. 2001, ApJ, 556, 265
White, R. J., & Hillenbrand, L. A. 2004, ApJ, 616, 998
Wilking, B. A., Meyer, M. R., Robinson, J. G., & Greene, T. P. 2005, AJ, 130, 1733
Wright, E. L., et al. 2010, AJ, 140, 1868
Yasui, C., Kobayashi, N., Tokunaga, A. T., Saito, M., & Tokoku, C. 2010, ApJ, 723, L113
York, D. G., et al. 2000, AJ, 120, 1579

APPENDIX

A. SPECTRAL CLASSIFICATION OF YOUNG STARS

In Table 4, we list the young stars with X-Shooter spectra. These sources are mainly from the η Cha cluster, the TW Hydra Association, the Lupus star-forming region, the σ Ori cluster, and the Cha I star-forming region. We extract the spectra of these sources from the X-Shooter phase III data archive. In Fig 21, we show the example of spectra in our sample with spectral types from K2 to M9.5. In the figure, there is an obvious variation in the spectral type with the spectral type, which is mainly due to an change in the strength of molecular lines including the TiO, VO, and CaH bands. Thus these features can be used to do spectral classification.

We use the spectral features and define the indices of individual features in a similar way as do in the spectral classification code "SPTCLASS" (Hernández et al. 2004). The index of each spectral feature is calculated by defining the central wavelengths of the feature band (FB), blue continuum band (BCB), and red continuum band (RCB). The continuum flux ($F_{\rm FCB}$) at the central wavelengths ($\lambda_{\rm FB}$) of a FB is calculated as.

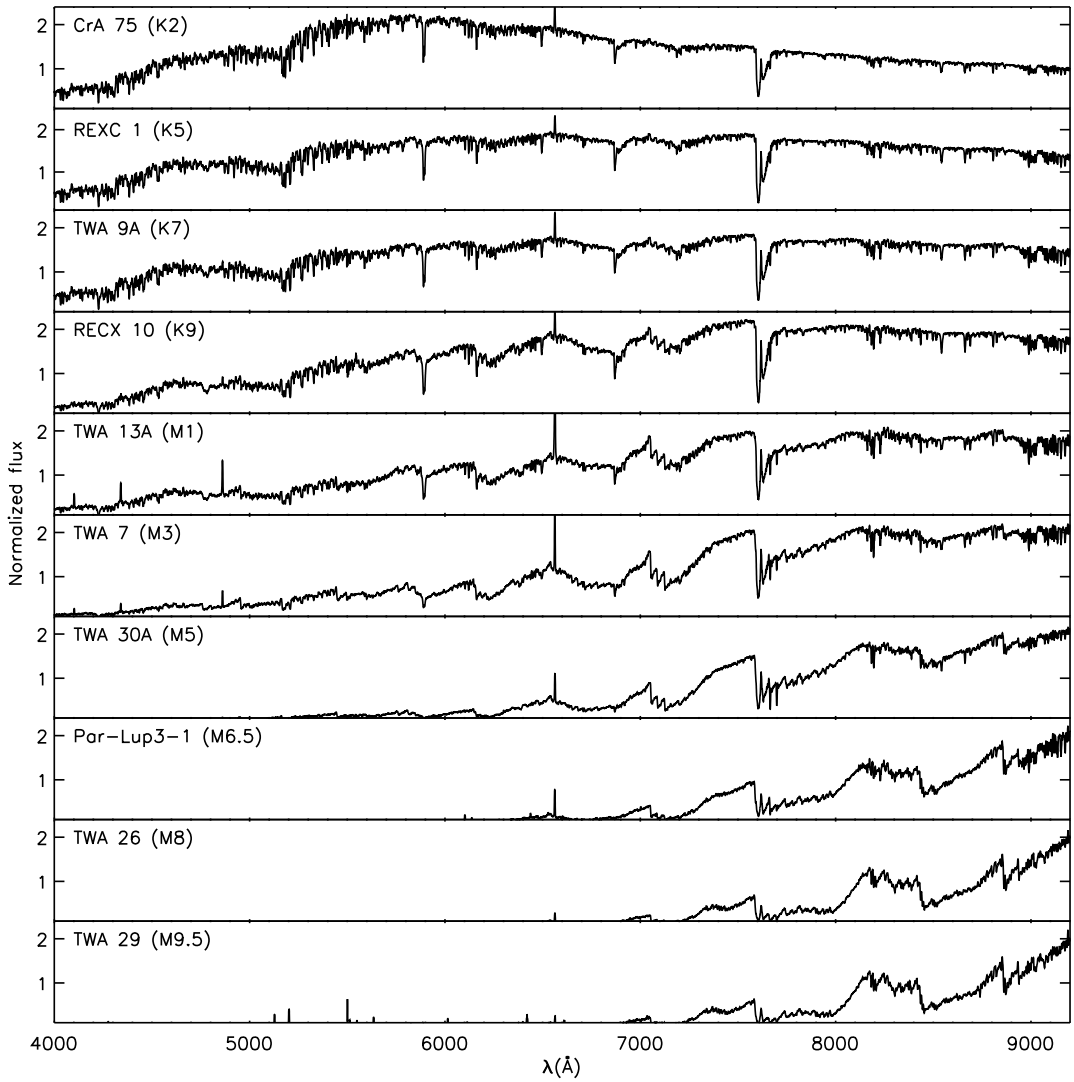

Figure 21. Examples of X-Shooter spectra which are used to refine our spectral classification scheme

$$F_{\rm FCB} = F_{\rm BCB} + \frac{\lambda_{\rm FB} - \lambda_{\rm BCB}}{\lambda_{\rm RCB} - \lambda_{\rm BCB}} \times (F_{\rm RCB} - F_{\rm BCB}) \tag{A1}$$

Where $\lambda_{\rm BCB}$ and $\lambda_{\rm RCB}$ are the central wavelengths of BCB and RCB, respectively, and $F_{\rm BCB}$ and $F_{\rm RCB}$ are the flux of BCB and RCB, respectively. $F_{\rm BCB}$ and $F_{\rm RCB}$ are the average fluxes over the widths of BCB and RCB. The index of a FB is calculated as:

$$Index(FB) = \Delta\lambda_{\rm FB} \times (1 - F_{\rm FB}/F_{\rm FCB}) \tag{A2}$$

Where $\Delta\lambda_{\rm FB}$ is the width of the FB, $F_{\rm FB}$ is the average flux over the width of the FB. We calculated the indices for 22 FBs. In Table 4, we list these features including $\lambda_{\rm FB}$, $\Delta\lambda_{\rm FB}$, $\lambda_{\rm BCB}$, $\lambda_{\rm RCB}$, and the widths of the BCBs and RCBs. In Fig. 22 and 23, we show the relations between the indices of individual spectral features and the spectral types. We fit these relations using polynomial functions, $Spt = C_0 + C_1 \times Index(FB) + C_2 \times (Index(FB))^2 + C_3 \times (Index(FB))^3 + C_4 \times (Index(FB))^4 + C_5 \times (Index(FB))^5$, where Spt is spectral-type number, and the numbers 0–19 are corresponding to K0 to M9. The results are listed in Table 4. To fully cover the range of spectral types, we have included some sources with low accretion rates. For these sources, their spectral features at wavelengths longer than 5500 Å are used for the fitting, to avoid the possible accretion-related veiling in the blue part of the optical spectra.

Table 4 The parameters for WTTSs

ID	Name	RA (J2000)	DEC (J2000)	Spt	Ref	Adopted Spt	Ref	$EW_{H\alpha}$ (Å)	$L_{acc}/L_\star$	Accreting	A_V (mag)	Ref
1	RECX 1	08 36 56.24	−78 56 45.7	K4, K5, K6, K7	1, 2, 3, 8	K5	3	−1.2	···	N	0	
2	RECX 5	08 42 27.088	−78 57 47.93	M3.8, M4	2, 3, 8	M4	3	−12.9	···	N	0	
3	RECX 6	08 42 38.770	−78 54 42.75	M2, M3	2, 3, 8, 9	M3	3	−4.8	···	N	0	
4	RECX 7	8 43 07.239	−79 04 52.49	K3, K4, K5, K6.9	2, 3, 8, 10	K5	3	−1.0	···	N	0	
5	RECX 9	08 44 16.41	−78 59 08.04	M4, M4.5	2, 3, 8	M4.5	3	−12.4	···	N	0	
6	RECX 10	08 44 31.90	−78 46 31.2	K7, K9, M0.3, M1	2, 3, 8, 9	K9	3	−1.7	···	N	0	
7	RECX 11	08 47 01.63	−78 59 34.37	K5, K5.5, K6.5	2, 3, 8	K5	3	−8.9	0.007	Y	0	28
8	RECX 12	08 47 56.766	−78 54 53.19	M2, M3.2, M3.25	2, 3, 8, 9	M3.25	3	−8.1	···	N	0	
9	RECX 17	08 38 51.50	−79 16 13.7	M5, M5.25, M5.75	2, 3, 8	M5.25	3	−12.1	···	N	0	
10	RECX 18	08 36 10.73	−79 08 18.4	M5.5	2, 3, 8	M5.5	3	−12.5	···	N	0	
11	TWA 2A	11 09 13.80	−30 01 39.9	M1.5, M2	3, 4, 5	M2	3	−2.5	···	N	0	
12	TWA 7	10 42 30.064	−33 40 16.62	M2, M3	3, 6	M3	3	−5.2	···	N	0	
13	TWA 8A	11 32 41.25	−26 51 55.9	M2, M3	3, 6, 7	M3	3	−8.8	···	N	0	
14	TWA 8B	11 32 41.16	−26 52 09.0	M5, M5.5	3, 7	M5.5	3	−17.2	···	N	0	
15	TWA 9A	11 48 24.223	−37 28 49.15	K5, K7	3, 7	K7	3	−1.7	···	N	0	
16	TWA 9B	11 48 23.73	−37 28 48.5	M1, M3.5	3, 4	M3.5	3	−5.4	···	N	0	
17	TWA 13A	11 21 17.24	−34 46 45.5	M1	3, 6	M1	3	−8.4	···	N	0	
18	TWA 13B	11 21 17.24	−34 46 45.5	M1	3, 6	M1	3	−2.0	···	N	0	
19	TWA 22	10 17 26.89	−53 54 26.5	M5	3	M5	3	−13.0	···	N	0	
20	TWA 25	12 15 30.72	−39 48 42.6	K9, M0	3, 4	K9	3	−3.0	···	N	0.4	
21	TWA 26	11 39 51.140	−31 59 21.50	M8	3, 6	M8	3	−12.3	···	N	0	
22	TWA 27	12 07 33.467	−39 32 54.00	M8	3, 6	M8	3	−194.4	0.003	Y	0	43
23	TWA 28	11 02 09.833	−34 30 35.53	M8.5	3, 13	M8.5	3	−101.4	0.0093	Y	0	43
24	TWA 29	12 45 14.16	−44 29 07.7	M9.5	3, 4, 12	M9.5	3	−10.6	···	N	0	
25	TWA 30A	11 32 18.314	−30 19 51.85	M5	3, 18	M5	3	−6.6	···	N	0	
26	V4046 sgr	18 14 10.466	−32 47 34.50	K4, K5	3, 17	K4	3	−44.0	0.096	Y	0	42
27	RECX 4	08 42 23.77	−79 04 03.0	M0, M1.3, M1.75	2, 3, 8	M1.3	2	−4.2	···	N	0	
28	TWA 3A	11 10 27.81	−37 31 53.2	M3, M4	5, 6	M4	5	−9.8	···	N	0	
29	TWA 3B	11 10 27.88	−37 31 52.0	M3.5, M4	5, 6	M4	5	−6.2	···	N	0	
30	TWA 6	10 18 28.700	−31 50 02.85	K7, M0	4, 11	K7	11	−4.5	···	N	0	
31	TWA 14	11 13 26.221	−45 23 42.74	M0, M0.5	4, 11	M0	11	−6.1	···	N	0	
32	TWA 15A	12 34 20.65	−48 15 13.50	M2	6	M3	this work	−12.8	···	N	0	
33	TWA 15B	12 34 20.47	−48 15 19.50	M2	6	M3	this work	−9.5	···	N	0	
34	Sz 74	15 48 05.228	−35 15 52.83	M1.5, M3.5	14, 15	M3.5	14	−22.8	0.030	Y	1.5	14
35	Sz 84	15 58 02.53	−37 36 02.7	M5, M5.5	14, 15	M4.5	this work	−113.2	0.021	Y	0.8	25
36	Sz 91	16 07 11.592	−39 03 47.54	M0.5, M1, M1.5	14, 15, 16	M1	14	−139.6	0.051	Y	1.2	14
37	Sz 94	16 07 49.596	−39 04 28.79	M4	4, 15	M3.5	this work	−6.4	···	N	0.0	
38	Sz 97	16 08 21.803	−39 04 21.48	M3, M4	14, 15	M4	14	−38.6	0.007	Y	0	14
39	Sz 100	16 08 25.764	−39 06 01.19	M5, M5.5	14, 15	M5.5	14	−45.1	0.006	Y	0	14
40	Sz 104	16 08 30.815	−39 05 48.87	M5,	14, 15	M5	14	−34.1	0.006	Y	0	14
41	Sz 107	16 08 41.799	−39 01 37.02	M5.5, M5.75	4, 19	M5.5	4	−12.8	···	N	0	
42	Sz 111	16 08 54.687	−39 37 43.11	M1, M1.5	14, 15	M0	this work	−79.7	0.019	Y	0.7	14
43	Sz 112	16 08 55.530	−39 02 33.95	M4, M5, M6	14, 15, 19	M5	14	−17.4	···	N	0	
44	Sz 114	16 09 01.850	−39 05 12.42	M4, M4.8, M5.5	14, 15, 20	M4.8	14	−94.4	0.010	Y	0	14
45	Sz 115	16 09 06.214	−39 08 51.86	M4, M4.5	14, 15	M4.5	14	−10.9	···	N	0	
46	Sz 121	16 10 12.199	−39 21 18.11	M3, M4	4, 15, 24	M4	24	−7.8	···	N	0	
47	Sz 122	16 10 16.424	−39 08 05.07	M2	4, 15, 24	M2	4	−6.9	···	N	0	
48	SO 587	05 38 34.04	−02 36 37.3	M3.5, M4.5	21, 22	M4.5	22	−16.3	···	N	0	
49	SO 641	05 38 38.57	−02 41 55.8	M5	4, 22	M5	22	−8.7	···	N	0	
50	SO 797	05 38 54.91	−02 28 58.19	M4, M4.5	4, 22	M4.5	22	−7.7	···	N	0	
51	SO 879	05 39 05.42	−02 32 30.34	K5, K7	4, 21, 24	K7	24	−2.2	···	N	0	
52	SO 925	05 39 11.41	−02 33 32.8	M5.5	4, 22	M5.5	22	−9.6	···	N	0	
53	SO 999	05 39 20.25	−02:38 25.8	M5.5	4, 22	M5.5	22	−11.0	···	N	0	
54	Par-Lup3-1	16 08 16.03	−39 03 04.29	M6.5, M7.5	23, 24	M6.5	24	−17.6	···	N	0	
55	Par-Lup3-2	16 08 35.78	−39 03 47.91	M5, M6	23, 24	M5	24	−5.5	···	N	0	
56	Par-Lup3-3	16 08 49.40	−39 05 39.2	M4, M4.5	14, 23	M3.5	this work	−28.2	···	N	3.5	
57	SST-Lup3-1	16 11 59.798	−38 23 38.34	M5	14	M5	14	−44.4	0.004	Y	0	14
58	Lup706	16 08 37.30	−39 23 10.8	M7.75	14	M7.75	14	−222.5	0.005	Y	0	14
59	Lup604s	16 08 00.20	−39 02 59.7	M5.25	14	M5.25	14	−16.7	···	N	0	
60	Lup818s	16 09 56.29	−38 59 51.7	M6	14	M6	14	−52.3	0.003	Y	0	14
61	CrA75	19 02 22.1	−36 55 40.9	K2	25	K2	25	−1.3	···	N	0.3	
62	ISO-217	11 09 52.15	−76 39 12.8	M6.25	26	M6.25	26	−125.2	0.007	Y	2.6	41
63	AKC2006-19	15 44 57.90	−34 23 39.5	M5	14	M5	14	−29.8	0.005	Y	0	14
64	2MASSJ16085953-3856275	16 08 59.53	−38 56 27.6	M8.5	14	M8.5	14	−111.5	0.003	Y	0	14
65	SSTc2d160901.4-392512	16 09 01.40	−39 25 11.9	M4	14, 19	M3	this work	−42.7	0.007	Y	0.8	14
66	Cha Hα 1	11 07 16.68	−77 35 53.2	M7.5, M7.75	26, 27	M7.75	26	−125.9	···	N	0	40
67	Ass-Cha-T-2-51	11 12 24.415	−76 37 06.41	K3.5, K4	10, 26	K3.5	26	−2.9	···	N	0	
68	LkCa 15	04 39 17.796	+22 21 03.48	K2, K5	25, 29, 30	K5	29	−28.3	0.066	Y	0.6	25

ID	Name	RA (J2000)	DEC (J2000)	Spt	Ref	Adopted Spt	Ref	$EW_{H\alpha}$ (Å)	$L_{acc}/L_\star$	Accreting	A_V (mag)	Ref
69	CS Cha	11 02 24.912	−77 33 35.72	K2, K4, K5, K6	6, 25, 26, 31	K5	31	−29.5	0.069	Y	0.3	25
70	CHXR 22E	11 07 13.300	−77 43 49.88	M3.5, M4	25, 26	M4	25	−6.4	···	N	3.4	
71	Sz 18	11 07 19.154	−76 03 04.85	M2, M2.5	25, 26	M2	25	−25.0	0.048	Y	0.6	25
72	Sz 27	11 08 39.051	−77 16 04.24	K7, K8	25, 26, 29	K7	25	−58.7	0.076	Y	2.8	25
73	RX J1615−3255	16 15 20.231	−32 55 05.10	K5, K7	25, 32, 33	K5	32	−35.6	0.056	Y	0	25
74	Oph 22	16 22 45.40	−24 31 23	M3	25, 34	M3	25	−5.0	···	N	1.4	
75	Oph 24	16 25 06.91	−23 50 50.3	M0, M3	25, 34	M2	this work	−5.1	···	N	0	
76	ISO-Oph196	16 28 16.51	−24 36 57.9	M4.5, M5.5	25, 35	M5	this work	−106.8	0.062	Y	2.0	25
77	Ser 29	18 29 11.50	00 20 38.6	M0, M2	25, 36	M2	25	−13.9	<0.004	Y	2.9	25
78	Ser 34	18 29 44.11	00 33 56.0	M0, M1	25, 36	M1.5	this work	−13.6	0.008	Y	2.3	25
79	RX J1842.9−3532	18 42 57.95	−35 32 42.7	K2	25, 37	K2	37	−32.9	0.056	Y	1.7	25
80	RX J1852.3−3700	18 52 17.29	−37 00 11.9	K2, K3	25, 37	K3	37	−44.8	0.051	Y	1.6	25
81	LkHα 330	03 45 48.	29 32 24 11.9	G3, G4	25, 38	G4	25	−15.8	0.024	Y	2.9	25
82	SR 21	16 27 10.28	−24 19 12.7	G4	25	G4	25	1.3	0.017	Y	5.2	25
83	T21	11 06 15.4	−77 21 56.9	G5	25, 26, 29	G5	25	−0.5	···	N	3.9	
84	IC348-127	03 45 07.9	32 04 01.8	G4	25, 39	G4	25	−2.8	···	N	6.2	
85	Cha Hα 9	11 07 18.608	−77 32 51.66	M5.5	30	M5.5	30	−20.1	···	N	5.0	40

[a] The reference for the available spectral types of individual sources, [b] The reference for the adopted spectral type, [c] The reference for the accretion luminosity.

References: 1. Covino et al. (1997), 2. Lyo et al. (2004), 3. Pecaut & Mamajek (2013), 4. Manara et al. (2013), 5. Riaz et al. (2006), 6. Torres et al. (2006), 7. Webb et al. (1999), 8. Luhman & Steeghs (2004), 9. Mamajek et al. (1999), 10. Covino et al. (1997), 11. Torres et al. (2003), 12. Looper et al. (2007), 13. Teixeira et al. (2008), 14. Alcalá et al. (2014), 15. Hughes et al. (1994), 16. Romero et al. (2012), 17. Fernández et al. (2008), 18. Looper et al. (2010), 19. Romero et al. (2012), 20. Comerón et al. (2009), 21. Sacco et al. (2008), 22. Rigliaco et al. (2012), 23. Comerón et al. (2003), 24. Stelzer et al. (2013), 25. Manara et al. (2014), 26.Luhman (2004), 27. Comerón et al. (2000), 28. Ingleby et al. (2013), 29. Nguyen et al. (2012), 30. White & Ghez (2001), 31. Herbig & Bell (1988), 32. Wahhaj et al. (2010), 33. Krautter et al. (1997), 34. Cieza et al. (2010), 35. Wilking et al. (2005), 36. Oliveira et al. (2009), 37. White et al. (2007), 38. Cohen & Kuhi (1979), 39. Cieza et al. (2007), 40. Mohanty et al. (2005), 41. Muzerolle et al. (2005), 42. Donati et al. (2011), 43. Herczeg & Hillenbrand (2008)

Table 5
Optical feature for spectral typing

Index	Feature	Center (Å)	Width (Å)	$C_{\rm left}$ (Å)	Width (Å)	$C_{\rm right}$ (Å)	Width (Å)	Spt Range	Index Range	C_0	C_1	C_2	C_3	C_4	C_5
1	VO	7810	110	7570	25	8140	20	M0–M8	11.51 to 66.23	5.44607	0.507010	-1.06971×10^{-2}	8.91401×10^{-5}	0	0
2	VO	7450	40	7540	20	7540	20	M3–M9.5	2.97 to 13.62	7.40348	2.63063	-0.284250	1.12802×10^{-2}	0	0
3	VO	7920	110	7562	20	8130	20	M2–M9.5	13.31 to 71.70	8.56015	0.310141	-3.77074×10^{-3}	-1.51972×10^{-5}	4.95808×10^{-7}	0
4	VO	8500	110	8408	10	8840	10	M3–M9	12.60 to 61.72	9.46791	0.377978	-8.78991×10^{-3}	8.24764×10^{-5}	0	0
5	VO	8675	150	8408	12	8840	10	M4–M9.5	13.54 to 58.77	10.0762	0.410874	-1.03032×10^{-2}	1.00317×10^{-4}	0	0
6	VO	8880	35	8850	10	9045	10	M3–M9	2.87 to 11.90	8.62001	2.16112	-0.256581	1.24604×10^{-2}	0	0
7	TiO	7108	30	7040	15	7326	15	K7–M6	2.37 to 18.62	3.61125	1.62902	-8.76069×10^{-2}	1.92530×10^{-3}	0	0
8	TiO	6255	45	6112	15	6525	15	K4–M5	4.52 to 25.74	-9.61363	4.82202	-0.522211	3.05772×10^{-2}	-8.68462×10^{-4}	9.40336×10^{-6}
9	TiO	4812	18	4742	10	4938	15	K7–M6	0.01 to 10.68	6.98046	2.31755	-0.250489	1.05380×10^{-2}	0	0
10	TiO	5225	75	4940	15	5415	15	K4–M5	8.65 to 20.53	-5.56706	0.852030	4.54304×10^{-2}	-1.85754×10^{-3}	0	0
11	CaH	6964	22	6533	10	7032	10	K6–M4	0.78 to 4.76	3.19107	3.86115	-0.334198	0	0	0
12	CaH	6840	30	6533	10	7032	10	K6–M5	3.04 to 15.68	1.23510	1.83375	-9.31380×10^{-2}	2.05201×10^{-3}	0	0
13	TiO	4975	40	4940	15	5385	15	K5–M6	2.53 to 20.70	-5.00123	5.58890	-0.783747	5.93566×10^{-2}	-2.27083×10^{-3}	3.46253×10^{-5}
14	TiO	7070	30	7045	10	7385	15	K4–M5	1.90 to 13.59	-8.50191	9.52190	-1.87384	0.188538	-9.13227×10^{-3}	1.69261×10^{-4}
15	TiO	5950	60	5810	20	6080	30	K6–M8.5	1.88 to 29.18	3.54680	1.43835	-7.45602×10^{-2}	1.44120×10^{-3}	0	0
16	TiO	6800	50	6530	15	7020	30	K4–M5	2.80 to 26.72	-2.75493	3.21562	-0.336413	1.91640×10^{-2}	-5.29676×10^{-4}	5.61103×10^{-6}
17	TiO	7150	50	7045	15	7400	20	K7–M5	7.14 to 33.44	2.22419	0.788315	-1.79554×10^{-2}	1.73645×10^{-4}	0	0
18	TiO	7220	50	7045	15	7315	15	K4–M5	3.53 to 23.97	-5.94651	3.86310	-0.351318	1.70392×10^{-2}	-4.04817×10^{-4}	3.68664×10^{-6}
19	TiO	6330	100	6080	15	6458	30	K4–M2	3.02 to 14.76	-6.93018	5.45853	-0.741166	4.67135×10^{-2}	-1.06148×10^{-3}	0
20	TiO	7250	150	7045	15	7531	50	K6–M5	16.44 to 72.03	-3.22166	0.716094	-1.03322×10^{-2}	5.41808×10^{-5}	0	0
21	TiO	6713	100	6530	20	6940	30	K8–M6	7.82 to 55.73	4.18776	0.573689	-1.17938×10^{-2}	9.51566×10^{-5}	0	0
22	TiO	5487	76	5385	10	5385	10	K4–M5	-1.90 to 24.91	6.28645	1.09733	-5.51680×10^{-2}	7.34970×10^{-4}	2.72954×10^{-5}	-6.52506×10^{-7}

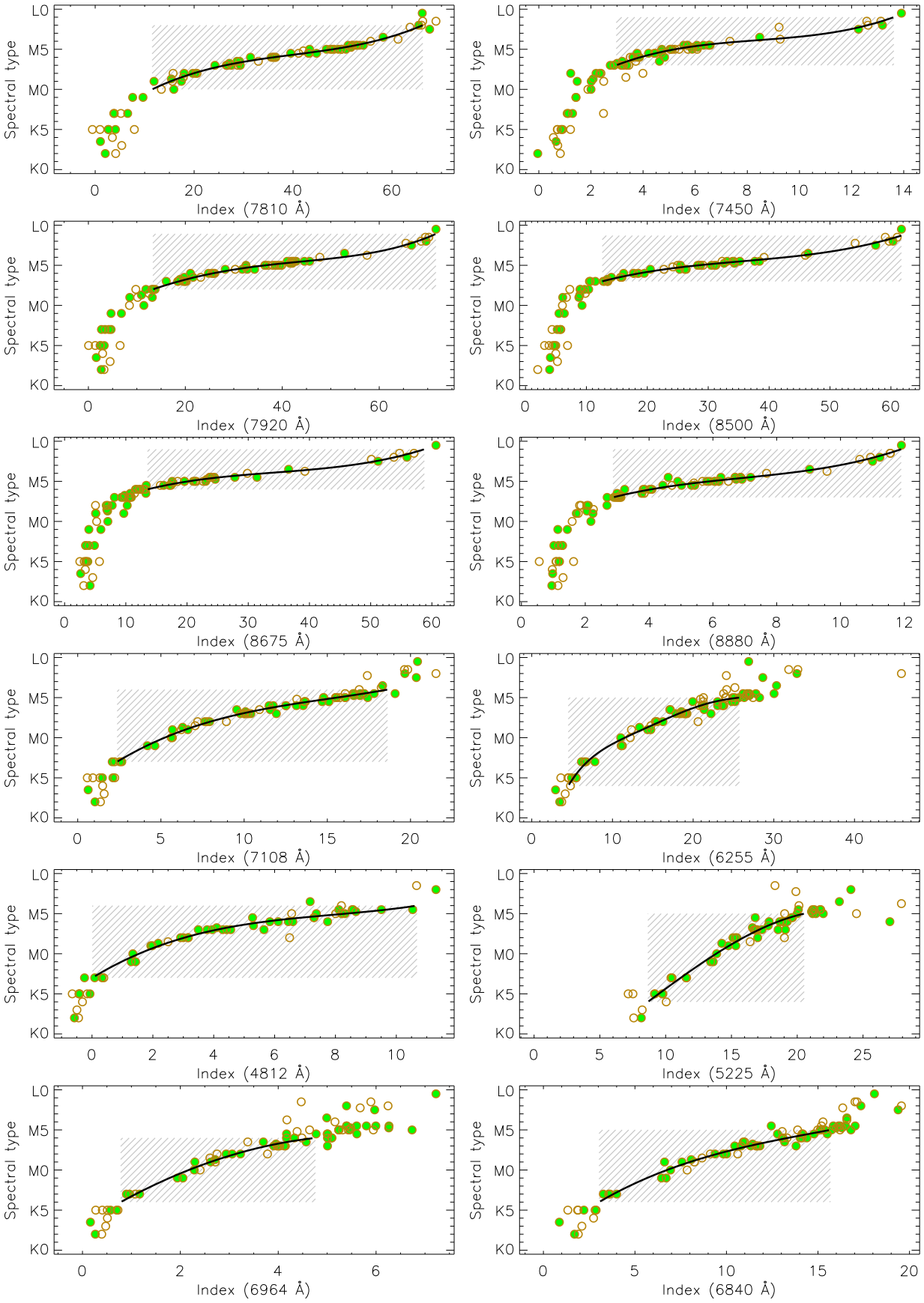

Figure 22. The relations between indices of individual spectral features and their spectral types for the young stars listed in Table 4. The filled circles show the sources without accretion activity, and the open circles show the ones with weak accretion activity. The solid lines show the fits to the relations. The line-shaded regions mark the ranges for the fitting.

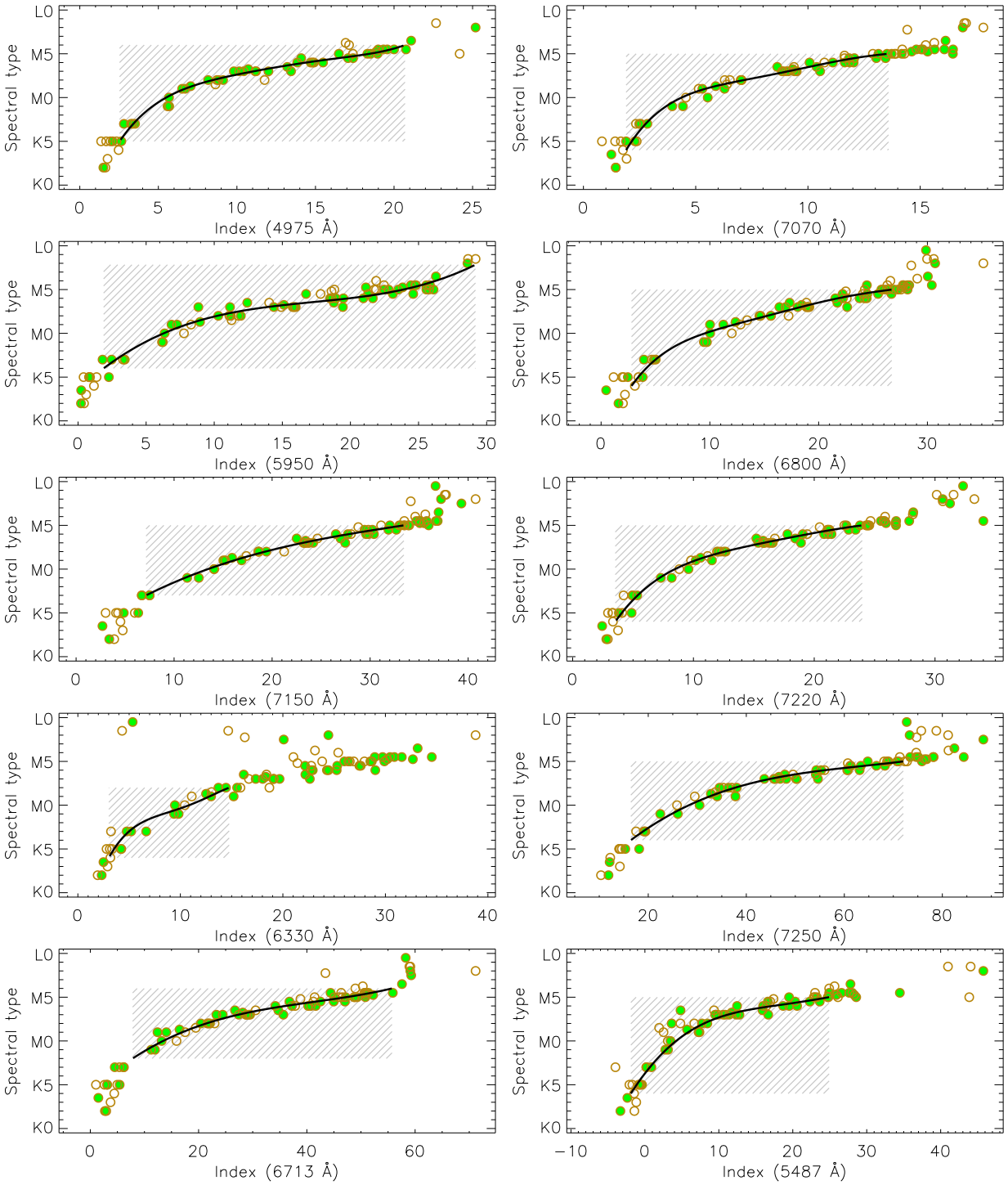

Figure 23. Same as in Fig. 22, but for different spectral features.

Table 6 Stellar properties for the YSOs

	RA (J2000)	DEC (J2000)	Spt	Lum ($L_\odot$)	Av (mag)	Mass ($M_\odot$)	Age Myr	$EW_{\rm Li\lambda6708\AA}$ (Å)	$EW_{\rm H\alpha}$ (Å)	$\alpha_{3.6-8.0}$	$\alpha_{3.6-24}$	TTS[a]	Disk[b]	Criteria[c]
1	05 31 50.98	−07 00 05.7	K8.7	0.610	0.2	0.58	1.5	0.71	−4.6	···	···	W	N	Li
2	05 32 11.59	−06 05 22.2	M4.8	0.076	0.0	0.12	1.4	...	−8.1	···	···	W	N	Na
3	05 32 12.63	−06 12 34.6	M5.3	0.059	0.0	0.096	1.5	...	−11.3	···	···	W	N	Na
4	05 32 14.78	−06 04 11.2	M4.0	0.096	0.0	0.18	2.0	...	−7.0	···	···	W	N	Na
5	05 32 19.82	−05 48 27.0	M4.1	0.320	0.0	0.18	< 0.5	0.33	−6.2	···	···	W	N	Li, Na
6	05 32 29.64	−06 18 34.8	M6.4	0.053	0.0	0.065	< 0.5	...	−61.3	···	···	C	?	Na
7	05 32 31.67	−06 15 18.5	M4.7	0.063	0.0	0.13	2.1	0.32	−6.4	···	···	W	N	Li, Na
8	05 32 35.04	−06 05 37.3	M3.6	0.696	0.0	0.21	< 0.5	...	−0.1	···	···	W	N	Na
9	05 32 37.49	−05 12 41.3	K8.2	0.327	0.1	0.67	4.8	0.84	−4.6	···	···	W	Y	Li, IRE
10	05 32 38.05	−05 51 48.4	M3.0	0.562	0.0	0.26	< 0.5	0.54	−2.4	···	···	W	N	Li, Na
11	05 32 42.38	−05 44 09.8	M5.0	0.119	0.0	0.12	< 0.5	0.59	−7.7	-2.71	···	W	N	Li, Na
12	05 32 42.55	−06 01 25.8	M3.8	0.107	0.0	0.20	2.0	0.22	−7.2	···	···	W	N	Li, Na
13	05 32 44.54	−05 24 15.2	M5.0	0.045	0.2	0.099	2.5	...	...	-1.55	···	...	Y	IRE
14	05 32 46.74	−05 58 02.0	M1.4	0.381	0.3	0.37	1.2	...	−20.4	-1.65	···	C	Y	IRE
15	05 32 47.31	−05 39 42.7	M1.3	0.328	0.2	0.39	1.5	0.62	−29.8	-1.09	···	C	Y	Li, X, IRE
16	05 32 49.93	−06 10 45.6	M0.8	0.082	0.9	0.55	22.9?	0.55	−133.7	-1.50	···	C	Y	Li, IRE
17	05 32 50.69	−06 11 09.3	M3.0	0.109	0.1	0.28	3.6	0.40	−4.3	-2.88	···	W	N	Li
18	05 32 53.52	−06 06 01.1	M3.6	0.144	0.2	0.21	1.6	0.40	−11.0	-2.73	···	W	N	Li
19	05 32 56.30	−06 03 18.9	M1.5	0.166	0.0	0.40	4.0	0.50	−6.0	-2.75	···	W	N	Li
20	05 32 57.01	−05 48 56.1	M5.4	0.087	0.1	0.10	< 0.5	0.43	−18.4	-2.89	···	W	N	Li, Na, X
21	05 32 57.92	−06 02 43.0	M2.6	0.167	0.0	0.30	2.3	0.30	−4.0	-2.68	···	W	N	Li
22	05 32 59.25	−05 24 26.1	M2.5	0.375	0.3	0.30	0.9	...	...	-1.98	-0.85	...	TD	IRE
23	05 33 01.36	−03 58 28.4	K9.4	0.658	0.0	0.53	1.1	0.57	−3.5	···	···	W	N	Li
24	05 33 02.38	−05 45 06.2	M4.0	0.167	0.0	0.18	1.0	...	−4.6	-2.72	···	W	N	Na, X
25	05 33 03.31	−06 19 15.1	M4.7	0.059	0.0	0.13	2.3	...	−8.1	···	···	W	N	Na
26	05 33 03.59	−04 58 55.9	M5.0	0.047	0.2	0.098	2.3	0.54	−38.8	-1.54	-0.86	C	Y	Li, Na, IRE
27	05 33 06.23	−04 58 35.9	M4.4	0.054	0.1	0.15	3.0	...	−8.4	-1.42	-0.85	W	TD	Na, IRE
28	05 33 10.52	−05 42 24.5	M2.8	0.485	0.0	0.27	0.5	0.40	−22.3	-1.38	-1.06	C	Y	Li, Na, X, IRE
29	05 33 10.73	−06 21 48.3	M4.9	0.056	0.0	0.11	2.2	...	−7.8	···	···	W	N	Na
30	05 33 11.59	−04 59 32.7	M0.5	0.294	0.0	0.47	2.6	0.35	−3.3	-2.74	···	W	N	Li
31	05 33 11.70	−05 54 57.0	M4.6	0.064	0.0	0.14	2.2	0.55	−7.7	···	···	W	N	Li, Na, X
32	05 33 14.16	−06 11 48.9	M2.6	0.163	0.0	0.30	2.4	0.30	−22.6	-2.66	···	W	N	Li
33	05 33 14.83	−06 06 35.8	M5.3	0.105	0.0	0.11	< 0.5	0.48	−14.1	-2.73	···	W	N	Li, Na
34	05 33 16.95	−05 43 33.1	M5.4	0.060	0.0	0.095	1.3	0.24	−19.7	···	···	W	N	Li, Na, X
35	05 33 17.28	−04 55 41.8	M5.2	0.036	0.1	0.087	3.4	...	−13.6	-1.99	-0.84	W	TD	Na, IRE
36	05 33 18.14	−04 22 43.3	K9.6	0.238	0.7	0.60	5.8	...	−30.0	-1.34	-0.95	C	TD	IRE
37	05 33 18.92	−05 57 50.7	M4.7	0.039	0.0	0.12	3.4	0.65	−9.2	-2.58	···	W	N	Li, Na
38	05 33 19.34	−06 14 25.6	M4.6	0.127	0.0	0.14	0.6	0.30	−7.9	-2.63	···	W	N	Li
39	05 33 20.04	−05 43 30.7	M4.4	0.087	0.0	0.15	1.7	...	−6.8	···	···	W	N	Na, X
40	05 33 22.58	−05 32 40.1	M4.0	0.149	0.0	0.18	1.1	0.35	−9.6	···	···	W	N	Li, Na
41	05 33 22.64	−06 07 09.8	M1.8	0.225	0.1	0.35	2.1	0.40	−4.5	-2.60	···	W	N	Li
42	05 33 23.30	−05 54 28.2	M4.0	0.123	0.0	0.18	1.5	...	−4.8	-2.57	···	W	N	Na, X
43	05 33 23.71	−06 09 33.6	K9.0	0.488	0.0	0.58	2.0	0.50	−4.7	-2.67	···	W	N	Li
44	05 33 24.42	−06 27 35.3	M3.2	0.686	0.0	0.24	< 0.5	0.40	−4.6	···	···	W	N	Li, Na
45	05 33 25.65	−05 58 47.5	M4.6	0.047	0.1	0.13	2.9	...	−10.9	···	···	W	N	Na
46	05 33 30.21	−06 04 09.6	M0	0.397	0.4	0.51	2.0	0.47	−16.0	-2.74	···	W	N	Li
47	05 33 31.00	−06 06 05.6	M3.4	0.151	0.1	0.23	1.7	0.50	−6.1	-2.66	···	W	N	Li
48	05 33 31.20	−05 29 57.7	M3.7	0.109	0.3	0.21	2.1	0.46	−83.2	-1.19	-0.49	C	TD	Li, Na, IRE
49	05 33 31.25	−06 18 29.6	M4.7	0.066	0.0	0.12	2.0	...	−9.9	-2.89	···	W	N	Na
50	05 33 33.78	−06 26 22.1	M4.2	0.239	0.0	0.17	< 0.5	0.30	−10.9	-2.64	···	W	N	Li
51	05 33 33.90	−05 33 26.4	M3.2	0.334	0.0	0.25	0.7	0.41	−6.4	-1.50	-0.95	W	Y	Li, Na, X, IRE
52	05 33 34.37	−06 04 20.0	M5.9	0.022	0.0	0.060	3.6	...	−21.9	-1.47	···	C	Y	IRE
53	05 33 34.40	−06 13 52.7	M2.1	0.223	0.1	0.33	1.9	0.50	−15.0	-1.94	-0.87	C	TD	Li, IRE
54	05 33 35.81	−06 06 25.8	M3.9	0.151	0.1	0.19	1.3	0.50	−11.7	-2.54	···	W	N	Li
55	05 33 36.10	−06 10 52.4	M5.6	0.050	0.1	0.084	1.4	...	−18.1	-2.63	···	W	N	Na
56	05 33 36.52	−06 26 42.4	M3.1	0.123	0.0	0.27	2.8	0.30	−3.4	-2.73	···	W	N	Li
57	05 33 37.02	−04 33 38.3	M3.8	0.338	0.0	0.19	< 0.5	0.45	−5.2	-2.71	···	W	N	Li, Na
58	05 33 38.56	−05 13 12.5	M3.5	0.200	0.0	0.22	1.2	...	...	-1.14	-0.74	...	Y	IRE
59	05 33 38.81	−04 42 16.8	M5.4	0.060	0.1	0.096	1.3	...	−7.0	-2.74	···	W	N	Na
60	05 33 39.17	−04 38 07.3	M5.0	0.100	0.0	0.12	< 0.5	0.66	−7.1	-2.79	···	W	N	Li, Na
61	05 33 39.81	−05 21 20.7	M5.4	0.070	0.0	0.10	0.6	...	...	···	···	...	N	Na
62	05 33 40.21	−05 37 43.4	M4.7	0.075	0.0	0.13	1.6	...	−15.0	···	···	W	N	Na, X
63	05 33 41.28	−04 49 25.8	M3.5	0.313	0.0	0.21	0.5	0.39	−6.3	-2.66	···	W	N	Li, Na
64	05 33 43.19	−04 47 14.3	M4.2	0.113	0.0	0.16	1.4	0.25	−26.4	-1.55	-1.44	C	Y	Li, Na, IRE
65	05 33 43.19	−04 40 24.6	M4.3	0.122	0.0	0.16	1.1	0.60	−8.2	-2.65	···	W	N	Li, Na
66	05 33 43.25	−06 05 23.5	M3.4	0.130	0.0	0.24	2.1	0.60	−7.1	-2.70	···	W	N	Li
67	05 33 43.35	−04 47 09.2	M4.5	0.262	0.0	0.15	< 0.5	0.43	−7.5	-2.62	···	W	N	Li, Na
68	05 33 45.18	−06 24 41.2	M4.6	0.040	0.3	0.13	3.3	0.30	−9.2	-2.49	···	W	N	Li
69	05 33 45.58	−05 00 46.1	M5.4	0.064	0.0	0.097	1.1	...	...	-1.59	-1.00	...	TD	Na, IRE
70	05 33 46.25	−06 13 04.8	M4.9	0.090	0.0	0.12	0.9	0.80	−17.2	-2.65	···	W	N	Li
71	05 33 48.07	−06 27 42.4	M3.7	0.087	0.2	0.21	2.9	0.60	−5.6	-2.63	···	W	N	Li
72	05 33 48.18	−04 39 27.4	M3.0	0.389	0.2	0.26	0.7	0.53	−6.5	-2.73	···	W	N	Li, Na
73	05 33 48.23	−05 34 47.2	M4.0	0.102	0.0	0.19	1.9	...	...	-2.42	···	...	N	Na, X
74	05 33 48.34	−05 22 39.4	M3.4	0.236	0.0	0.23	1.1	0.45	−6.4	···	···	W	N	Li, Na
75	05 33 50.32	−06 21 30.9	M1.0	0.562	0.0	0.39	0.8	0.40	−6.0	-2.68	···	W	N	Li, X
76	05 33 51.88	−05 54 25.8	M2.3	0.198	0.0	0.31	2.0	0.32	−1.8	-2.68	···	W	N	Li, Na, X
77	05 33 52.11	−05 30 28.5	M3.8	0.300	0.0	0.19	< 0.5	0.57	−7.1	-2.73	···	W	N	Li, Na, X

TABLE 6 – continued

	RA (J2000)	DEC (J2000)	Spt	Lum ($L_\odot$)	Av (mag)	Mass ($M_\odot$)	Age Myr	$EW_{\rm Li\lambda6708\AA}$ (Å)	$EW_{\rm H\alpha}$ (Å)	$\alpha_{3.6-8.0}$	$\alpha_{3.6-24}$	TTS[a]	Disk[b]	Criteria[c]
78	05 33 53.41	−06 17 10.2	M3.4	0.146	0.0	0.23	1.8	0.40	−9.6	-2.71	···	W	N	Li, X
79	05 33 54.50	−06 15 41.3	M4.6	0.073	0.0	0.14	1.9	0.60	−7.3	-2.74	···	W	N	Li
80	05 33 54.59	−06 21 18.7	M4.8	0.094	0.2	0.13	1.0	0.50	−12.7	-1.86	···	W	Y	Li, IRE
81	05 33 55.10	−05 56 13.8	M5.2	0.071	0.1	0.11	1.1	...	−12.5	-2.90	···	W	N	Na, X
82	05 33 55.54	−06 29 28.6	M4.7	0.038	0.2	0.12	3.3	...	−8.6	-2.75	···	W	N	Na
83	05 33 56.39	−04 35 30.0	M4.4	0.076	0.0	0.15	2.0	...	−4.3	-1.22	-0.75	W	TD	Na, IRE
84	05 33 56.54	−05 06 47.7	M3.0	0.560	0.0	0.26	< 0.5	0.47	−5.8	-2.84	···	W	N	Li, Na
85	05 33 57.90	−04 35 43.8	M5.0	0.063	0.1	0.11	1.6	0.59	−13.9	-2.75	···	W	N	Li, Na
86	05 33 59.45	−06 21 18.2	M4.1	0.087	0.3	0.17	2.1	0.30	−25.9	-1.72	···	C	Y	Li, IRE
87	05 33 59.46	−04 43 04.6	M1.0	0.330	0.1	0.41	1.7	0.57	−6.2	-2.68	···	W	N	Li, Na
88	05 34 00.42	−04 36 15.0	M4.9	0.184	0.0	0.13	< 0.5	0.27	−18.6	-2.63	···	W	N	Li, Na
89	05 34 01.72	−05 46 51.4	M1.5	0.311	0.1	0.37	1.5	...	...	-2.91	···	...	N	X
90	05 34 02.03	−04 44 53.7	M4.6	0.140	0.0	0.15	< 0.5	0.39	−20.4	-1.46	-1.28	C	Y	Li, Na, IRE
91	05 34 02.85	−06 05 50.9	M4.7	0.048	0.0	0.12	2.7	0.70	−10.6	-2.44	···	W	N	Li
92	05 34 03.83	−06 16 04.5	M2.2	0.407	0.0	0.31	0.8	0.40	−6.2	-2.69	···	W	N	Li, X
93	05 34 03.84	−04 36 06.2	M2.2	0.218	0.0	0.32	1.9	0.45	−75.7	-2.53	-0.13	C	TD	Li, Na, IRE
94	05 34 04.40	−05 36 26.4	M5.3	0.088	0.1	0.11	< 0.5	...	−13.5	-2.93	···	W	N	Na, X
95	05 34 04.47	−06 31 37.9	M4.0	0.078	0.6	0.18	2.6	...	−10.0	-2.03	···	W	Y	IRE
96	05 34 04.70	−04 51 31.0	M4.9	0.040	1.6	0.10	2.8	0.49	−8.6	-1.81	···	W	Y	Li, Na, IRE
97	05 34 04.71	−04 50 49.6	M5.1	0.062	0.0	0.10	1.5	0.50	−18.6	-1.35	-0.53	C	TD	Li, Na, IRE
98	05 34 04.95	−06 23 47.0	M4.0	0.146	0.2	0.18	1.2	0.20	−5.7	-1.70	···	W	Y	Li, IRE
99	05 34 05.02	−04 40 03.4	M4.5	0.069	0.0	0.14	2.1	...	...	-1.42	-0.90	...	TD	Na, IRE
100	05 34 05.99	−06 06 11.7	M4.6	0.062	0.0	0.13	2.2	0.60	−68.7	-1.37	-0.88	C	Y	Li, IRE
101	05 34 06.96	−06 32 07.9	M3.0	0.126	0.1	0.27	2.8	0.32	−1.2	-0.37	-0.04	W	Y	Li, Na, X, IRE
102	05 34 07.52	−06 04 46.4	M2.6	0.256	0.0	0.29	1.3	0.70	−6.8	-2.75	···	W	N	Li
103	05 34 07.94	−06 12 34.0	M4.0	0.054	0.5	0.18	3.9	0.50	−16.9	-1.44	-0.96	C	Y	Li, IRE
104	05 34 08.22	−05 05 44.5	M5.0	0.083	0.3	0.12	1.0	0.47	−12.9	-2.47	···	W	N	Li, Na
105	05 34 08.89	−05 01 42.1	M3.4	0.343	0.0	0.23	0.5	0.34	−5.4	-2.78	···	W	N	Li, Na
106	05 34 09.07	−06 33 56.7	M4.6	0.068	0.0	0.14	2.1	0.55	−9.8	-2.59	···	W	N	Li, Na
107	05 34 09.71	−04 48 46.4	M4.5	0.101	0.0	0.14	1.2	0.53	−10.0	-2.64	···	W	N	Li, Na
108	05 34 09.85	−06 23 22.0	M3.1	0.134	0.0	0.27	2.5	...	−6.9	-2.74	···	W	N	X
109	05 34 10.06	−06 26 50.6	M4.9	0.031	0.4	0.097	3.7	0.30	−5.1	-2.64	···	W	N	Li
110	05 34 10.44	−04 25 58.9	M4.3	0.066	0.0	0.16	2.5	...	−7.0	-2.57	···	W	N	Na
111	05 34 10.47	−04 50 27.5	M4.4	0.093	0.0	0.16	1.6	0.43	−18.4	-1.46	-0.46	C	Y	Li, Na, IRE
112	05 34 11.15	−04 30 53.7	M4.8	0.044	0.2	0.11	2.7	...	−21.9	-1.55	···	C	Y	Na, IRE
113	05 34 11.95	−05 52 22.0	M5.6	0.092	0.0	0.098	< 0.5	...	−32.2	-2.55	···	W	N	Na, X
114	05 34 12.06	−06 17 02.4	M5.0	0.110	0.2	0.12	< 0.5	...	−9.7	-2.66	···	W	N	X
115	05 34 12.21	−04 50 07.3	M0.8	0.240	2.7	0.45	3.1	0.29	−72.3	-0.16	-0.07	C	TD	Li, IRE
116	05 34 13.46	−05 55 41.8	M3.2	0.252	0.1	0.25	1.1	0.38	−7.1	-1.74	-1.31	W	Y	Li, Na, IRE
117	05 34 13.87	−05 36 35.4	M4.7	0.176	0.1	0.14	< 0.5	0.46	−52.1	-2.58	···	W	N	Li, Na
118	05 34 14.09	−05 47 21.9	M3.5	0.127	0.0	0.23	2.0	...	...	···	···	...	N	X
119	05 34 14.38	−04 58 33.7	M3.6	0.089	0.0	0.22	3.0	0.44	−5.2	-2.85	···	W	N	Li, Na
120	05 34 14.75	−06 19 18.2	M2.8	0.325	0.0	0.28	0.9	0.40	−4.7	-2.68	···	W	N	Li, X
121	05 34 14.79	−05 43 56.0	M4.3	0.062	0.1	0.16	2.7	0.48	−13.2	···	···	W	N	Li, Na, X
122	05 34 14.71	−05 53 07.6	M4.5	0.105	0.0	0.15	1.2	...	−31.0	-1.66	-1.12	C	Y	Na, X, IRE
123	05 34 15.50	−04 23 34.1	M5.7	0.057	0.0	0.088	0.9	...	−17.8	-2.60	···	W	N	Na
124	05 34 15.62	−06 24 16.8	M4.0	0.076	0.7	0.18	2.7	...	−5.7	-2.68	···	W	N	X
125	05 34 16.35	−04 49 27.2	M5.3	0.147	0.3	0.11	< 0.5	0.27	−11.7	-2.06	-1.22	W	TD	Li, Na, IRE
126	05 34 18.12	−04 23 18.4	M5.2	0.068	0.0	0.11	1.2	...	−9.5	-2.61	···	W	N	Na
127	05 34 18.22	−06 02 00.2	M4.9	0.032	0.4	0.098	3.6	...	−32.5	-1.56	-1.07	C	Y	IRE
128	05 34 18.53	−05 34 00.2	K8.2	0.587	0.4	0.61	1.7	...	...	-2.69	···	...	N	X
129	05 34 18.67	−05 37 08.2	M4.7	0.125	0.6	0.14	< 0.5	0.33	−162.4	-1.94	-1.01	C	Y	Li, Na, X, IRE
130	05 34 18.73	−04 15 15.9	M5.0	0.065	0.0	0.11	1.5	0.69	−7.7	-2.69	···	W	N	Li, Na
131	05 34 18.89	−05 59 29.9	M4.8	0.084	0.0	0.13	1.2	0.45	−10.6	-2.65	···	W	N	Li, Na
132	05 34 20.26	−05 58 15.6	M4.4	0.204	0.0	0.16	< 0.5	0.40	−4.4	-2.66	···	W	N	Li, Na
133	05 34 20.27	−04 19 52.0	M3.8	0.152	0.0	0.20	1.4	...	−9.6	-2.72	···	W	N	Na
134	05 34 20.32	−04 34 03.4	M4.3	0.245	0.0	0.17	< 0.5	0.40	−5.1	-2.74	···	W	N	Li, Na
135	05 34 20.39	−04 58 20.4	M4.7	0.085	0.0	0.13	1.3	...	−9.6	-2.17	···	W	N	Na
136	05 34 20.43	−06 31 15.1	M5.1	0.056	0.6	0.10	1.9	...	−74.8	-1.20	-0.96	C	Y	IRE
137	05 34 20.69	−04 35 01.9	M3.5	0.141	0.0	0.22	1.8	...	...	-1.55	-1.20	...	Y	IRE
138	05 34 20.88	−05 06 50.1	M4.9	0.100	0.0	0.13	0.5	0.39	−6.4	-2.63	···	W	N	Li, Na
139	05 34 21.24	−05 35 34.8	M4.7	0.129	0.0	0.14	< 0.5	0.49	−5.8	-2.57	···	W	N	Li, Na
140	05 34 21.56	−05 00 13.0	M5.1	0.035	0.0	0.092	3.5	...	...	···	···	...	N	Na
141	05 34 22.57	−06 20 29.3	M4.5	0.138	0.0	0.15	0.6	0.30	−7.9	-2.75	···	W	N	Li, X
142	05 34 23.61	−06 18 38.9	M2.6	0.288	0.1	0.29	1.1	0.50	−4.8	-2.69	···	W	N	Li, X
143	05 34 24.77	−04 27 33.2	M5.1	0.047	0.3	0.097	2.4	...	−102.0	-1.38	-1.04	C	Y	Na, IRE
144	05 34 25.11	−06 43 27.5	M0.9	0.567	0.0	0.40	0.8	0.40	−3.8	-2.73	···	W	N	Li
145	05 34 25.26	−04 54 39.8	M4.9	0.366	0.0	0.12	< 0.5	0.33	−8.5	-2.60	···	W	N	Li, Na
146	05 34 25.28	−04 33 06.1	M3.5	0.314	0.0	0.22	0.5	0.40	−5.8	-2.76	···	W	N	Li, Na, X
147	05 34 25.53	−06 16 31.0	M4.9	0.040	0.7	0.10	2.8	...	−7.2	-1.64	-1.23	W	Y	IRE
148	05 34 25.53	−04 06 37.7	M2.7	0.527	0.0	0.27	< 0.5	0.40	−5.5	-2.68	···	W	N	Li, Na
149	05 34 25.79	−05 35 46.6	M4.8	0.065	0.0	0.12	1.9	0.60	−5.1	···	···	W	N	Li, Na, X
150	05 34 25.89	−06 03 52.0	M4.7	0.087	0.0	0.13	1.3	0.40	−16.5	-2.56	···	W	N	Li
151	05 34 26.07	−05 07 33.3	M4.9	0.167	0.0	0.12	< 0.5	0.52	−16.0	-2.72	···	W	N	Li, Na
152	05 34 26.51	−05 01 00.9	M2.0	0.387	0.0	0.33	1.0	0.39	−3.7	-2.73	···	W	N	Li, Na, X
153	05 34 26.76	−05 41 57.4	M3.7	0.178	0.0	0.20	1.2	0.51	−7.5	-0.95	-1.01	W	Y	Li, Na, IRE
154	05 34 26.76	−05 01 17.8	M4.1	0.306	0.0	0.18	< 0.5	0.40	−7.0	-2.70	···	W	N	Li, Na
155	05 34 26.84	−06 26 25.8	M4.1	0.085	0.3	0.17	2.2	0.30	−6.1	-1.83	-1.27	W	TD	Li, IRE

TABLE 6 – continued

	RA	DEC		Lum	Av	Mass	Age	$EW_{\mathrm{Li\lambda6708\AA}}$	$EW_{\mathrm{H}\alpha}$					
	(J2000)	(J2000)	Spt	($L_\odot$)	(mag)	($M_\odot$)	Myr	(Å)	(Å)	$\alpha_{3.6-8.0}$	$\alpha_{3.6-24}$	TTS[a]	Disk[b]	Criteria[c]
156	05 34 27.12	−05 16 48.8	M5.3	0.079	0.0	0.11	0.5	0.57	−13.6	···	···	W	N	Li
157	05 34 27.31	−04 55 28.6	K8.9	0.561	0.5	0.58	1.6	0.36	−2.6	-2.80	···	W	N	Li
158	05 34 27.43	−05 00 26.3	M4.4	0.044	0.3	0.14	3.6	...	−110.5	-1.54	-1.03	C	Y	Na, IRE
159	05 34 27.81	−05 42 10.1	M2.2	0.176	0.0	0.33	2.6	0.36	−7.5	-2.13	···	W	Y	Li, Na, X
160	05 34 27.84	−05 43 31.5	M3.9	0.214	0.0	0.19	0.7	0.32	−7.8	-2.77	···	W	N	Li, Na, X
161	05 34 27.86	−05 56 28.2	M4.3	0.104	0.0	0.16	1.5	0.28	...	-2.85	···	...	N	Li, Na
162	05 34 28.08	−05 05 21.9	M6.1	0.055	0.3	0.076	0.6	0.73	−29.1	-1.29	-0.71	C	Y	Li, Na, IRE
163	05 34 28.68	−04 34 39.6	M3.1	0.198	0.0	0.26	1.5	0.46	−4.0	-2.66	···	W	N	Li, Na, X
164	05 34 29.60	−05 04 28.9	M5.1	0.058	0.3	0.100	1.7	...	...	-2.53	···	...	N	Na
165	05 34 29.60	−05 47 24.7	M1.2	0.254	0.2	0.41	2.4	0.49	−11.2	-1.08	-0.27	C	TD	Li, Na, IRE
166	05 34 29.86	−05 04 05.4	M3.0	0.186	0.0	0.27	1.7	0.30	−7.7	-2.66	···	W	N	Li, Na, X
167	05 34 30.21	−04 58 30.4	M3.8	0.263	0.0	0.19	< 0.5	0.37	−5.6	-2.63	···	W	N	Li, Na
168	05 34 30.23	−04 58 37.9	M5.2	0.047	0.0	0.092	2.5	0.66	−23.1	-1.65	-0.79	C	TD	Li, Na, IRE
169	05 34 30.25	−06 22 01.1	M3.3	0.298	0.2	0.24	0.8	0.40	−6.5	-2.73	···	W	N	Li, X
170	05 34 30.96	−05 58 03.7	M5.1	0.049	0.0	0.098	2.2	...	−232.0	-1.57	-0.60	C	TD	Na, IRE
171	05 34 31.45	−06 43 22.6	M3.7	0.217	0.1	0.20	1.0	0.40	−10.8	-2.69	···	W	N	Li
172	05 34 31.79	−04 57 37.4	M5.5	0.063	0.1	0.095	1.0	...	−27.1	-2.87	···	W	N	Na
173	05 34 31.81	−06 22 49.8	M4.6	0.394	0.0	0.14	< 0.5	0.10	−12.3	-2.62	-2.46	W	DB	Li, Na, X, IRE
174	05 34 32.23	−05 41 48.5	M4.2	0.082	0.1	0.17	2.1	0.46, 0.42	−33.2	-1.89	-0.48	C	TD	Li, Na, IRE
175	05 34 32.76	−04 58 46.8	M5.3	0.072	0.0	0.10	0.9	0.51	−67.2	-1.14	-0.68	C	Y	Li, Na, IRE
176	05 34 32.87	−06 24 44.0	M4.8	0.068	0.0	0.12	1.7	0.60	−10.6	-2.58	···	W	N	Li, X
177	05 34 32.91	−05 00 40.4	M3.8	0.375	0.0	0.20	< 0.5	0.44	−5.9	-2.75	···	W	N	Li, Na, X
178	05 34 33.02	−05 44 39.7	M4.3	0.080	1.9	0.16	2.1	...	−26.9	-1.71	···	C	Y	Na, IRE
179	05 34 33.26	−05 07 26.7	M4.8	0.033	0.6	0.10	3.4	0.68	−8.6	···	···	W	N	Li
180	05 34 33.61	−06 11 19.5	M4.8	0.061	0.0	0.12	2.1	0.70	−66.0	-0.78	-0.32	C	TD	Li, IRE
181	05 34 33.70	−04 44 15.0	M4.8	0.068	0.0	0.12	1.7	0.39	−7.6	···	···	W	N	Li, Na
182	05 34 33.87	−05 56 38.1	M4.3	0.202	0.0	0.16	< 0.5	0.56	−7.1	-2.70	···	W	N	Li, Na, X
183	05 34 33.96	−05 48 25.0	M4.8	0.111	0.0	0.13	< 0.5	0.37	−68.4	-1.19	···	C	Y	Na, X, IRE
184	05 34 34.17	−05 05 17.0	M4.0	0.115	0.1	0.18	1.7	0.38	−10.9	-1.30	-1.02	W	Y	Li, Na, X, IRE
185	05 34 34.26	−06 02 09.7	M2.8	0.176	0.1	0.28	2.0	0.40	−6.9	-2.69	-2.19	W	DB	Li, IRE
186	05 34 35.12	−04 48 35.9	M5.4	0.105	0.0	0.10	< 0.5	...	−13.9	-1.85	···	W	Y	Na, IRE
187	05 34 35.46	−05 03 26.8	M5.1	0.043	0.2	0.092	2.9	...	−21.2	-2.63	···	W	N	Na, X
188	05 34 35.68	−05 35 52.1	M3.7	0.119	0.0	0.21	2.0	0.39, 0.53	−7.1	-2.70	···	W	N	Li, Na, X
189	05 34 36.25	−06 04 51.5	M3.2	0.184	0.1	0.25	1.5	0.30	−7.4	-2.58	···	W	N	Li, X
190	05 34 36.31	−06 16 24.4	M4.8	0.059	0.4	0.12	2.1	...	−75.2	-1.66	-1.22	C	Y	IRE
191	05 34 37.45	−05 54 26.9	M5.6	0.049	0.0	0.082	1.3	...	...	-2.88	···	...	N	Na
192	05 34 37.78	−04 19 28.1	M5.0	0.095	0.0	0.12	< 0.5	...	−15.0	-2.67	···	W	N	Na
193	05 34 37.87	−04 42 38.5	M5.7	0.098	0.0	0.095	< 0.5	...	−8.7	···	···	W	N	Na
194	05 34 37.95	−05 46 10.6	M4.6	0.049	0.0	0.13	2.8	0.30	...	···	···	...	N	Na
195	05 34 38.19	−05 35 49.6	M4.9	0.073	0.0	0.12	1.4	0.37	...	-2.35	···	...	N	Na, X
196	05 34 38.56	−05 47 35.1	K9.3	0.708	0.4	0.53	1.0	1.08	−5.3	-2.56	···	W	N	Li, X
197	05 34 38.59	−06 35 56.4	M3.2	0.193	0.1	0.25	1.4	0.30	−6.9	-2.71	···	W	N	Li
198	05 34 38.61	−04 22 26.2	M5.9	0.052	0.0	0.079	0.7	...	−14.8	-2.53	···	W	N	Na
199	05 34 38.75	−06 08 22.9	M3.7	0.162	0.1	0.20	1.4	0.50	−7.7	-2.70	···	W	N	Li
200	05 34 38.79	−04 39 37.1	M4.4	0.057	0.2	0.14	2.7	...	...	-1.91	···	...	Y	IRE
201	05 34 39.09	−06 27 21.2	M1.8	0.211	0.0	0.36	2.4	0.15	−10.8	-2.85	···	W	N	Li, Na, X
202	05 34 39.12	−06 17 11.7	M3.8	0.192	0.0	0.19	1.0	...	−8.7	-2.69	···	W	N	X
203	05 34 39.20	−06 25 24.2	M3.9	0.127	0.0	0.19	1.6	0.51	−6.2	-2.81	···	W	N	Li, Na
204	05 34 39.24	−05 50 56.6	M5.2	0.103	0.0	0.11	< 0.5	0.36	...	···	···	...	N	Na
205	05 34 39.68	−06 18 06.3	M4.6	0.070	0.0	0.14	2.0	0.60	−13.1	-2.75	···	W	N	Li, X
206	05 34 39.71	−06 07 13.3	M3.5	0.299	0.0	0.22	0.6	0.40	−9.0	-2.67	···	W	N	Li
207	05 34 41.00	−05 48 04.9	M5.0	0.084	0.0	0.12	0.9	0.33	...	···	···	...	N	Na
208	05 34 41.03	−06 27 50.7	M1.4	0.232	0.0	0.39	2.5	0.30	−2.4	-2.71	···	W	N	Li, X
209	05 34 41.11	−05 47 39.4	M4.3	0.099	0.0	0.16	1.6	0.35	...	-1.83	···	...	Y	Na, X
210	05 34 41.18	−05 46 11.6	M2.7	0.329	0.0	0.29	0.9	0.47	−76.0	-0.95	-0.13	C	Y	Li, Na, X, IRE
211	05 34 41.26	−05 52 45.6	M4.8	0.059	0.0	0.12	2.1	0.35	−10.4	···	···	W	N	Li, Na
212	05 34 41.43	−04 39 13.8	M3.0	0.154	0.3	0.27	2.2	...	...	-1.74	-1.21	...	Y	IRE
213	05 34 41.60	−04 24 39.3	M5.6	0.128	0.0	0.097	< 0.5	...	−18.9	-2.73	···	W	N	Na
214	05 34 41.63	−05 23 57.5	M5.0	0.126	0.3	0.12	< 0.5	0.34	...	···	···	...	N	X
215	05 34 41.73	−05 36 48.8	M5.5	0.064	0.0	0.096	1.0	...	...	-1.36	···	...	Y	Na, X, IRE
216	05 34 41.99	−05 45 00.6	M5.2	0.112	0.2	0.11	< 0.5	0.17	−127.2	-1.13	-0.28	C	Y	Li, Na, IRE
217	05 34 42.04	−05 02 24.9	M4.4	0.065	0.1	0.15	2.5	0.16	−11.3	-2.29	···	W	N	Li, Na, X
218	05 34 42.44	−05 43 25.5	M4.2	0.127	0.8	0.16	1.2	...	−87.1	-1.80	-0.62	C	Y	Na, IRE
219	05 34 43.12	−06 12 38.9	M1.8	0.254	0.0	0.35	1.8	0.50	−3.9	-2.76	···	W	N	Li, X
220	05 34 43.16	−06 27 14.6	M4.8	0.182	0.0	0.13	< 0.5	0.40	−20.1	-1.22	-0.74	C	Y	Li, Na, X, IRE
221	05 34 43.29	−06 17 03.6	M1.9	0.345	0.2	0.34	1.2	0.41	−7.5	-2.74	···	W	N	Li, Na, X
222	05 34 43.98	−04 39 38.5	M5.2	0.071	0.0	0.11	1.0	0.22	−22.0	-1.55	-1.12	C	Y	Li, Na, IRE
223	05 34 44.45	−05 56 14.9	M4.0	0.135	0.0	0.18	1.3	...	...	-2.67	···	...	N	X
224	05 34 44.75	−06 40 29.4	M4.8	0.074	0.3	0.12	1.5	0.50	−10.2	-2.68	···	W	N	Li
225	05 34 44.77	−04 56 40.8	M2.2	0.121	0.5	0.35	4.8	0.07	−73.3	-1.44	-1.00	C	Y	Li, Na, IRE
226	05 34 44.78	−04 54 05.1	M5.3	0.056	0.3	0.095	1.9	...	−30.6	···	···	C	Y	Na, IRE
227	05 34 45.15	−06 21 07.3	M1.6	0.240	0.1	0.37	2.1	0.45	−6.9	-2.73	···	W	N	Li, Na, X
228	05 34 45.46	−05 02 07.9	M2.5	0.342	0.0	0.30	1.0	0.47	−5.9	-2.68	···	W	N	Li, Na, X
229	05 34 45.51	−05 54 20.4	M4.0	0.091	0.2	0.18	2.1	0.46	−8.7	-2.58	···	W	N	Li, Na, X
230	05 34 45.61	−04 30 00.7	M4.5	0.051	0.0	0.14	2.8	...	−9.3	···	···	W	N	Na
231	05 34 45.90	−05 48 12.3	M3.8	0.119	0.0	0.19	1.8	0.54	...	···	···	...	N	Li, Na, X
232	05 34 46.34	−04 29 02.9	M4.0	0.115	0.0	0.18	1.7	0.29	−3.1	-2.57	···	W	N	Li, Na
233	05 34 46.45	−04 26 15.9	M3.5	0.109	0.0	0.22	2.4	...	−2.9	-2.80	···	W	N	Na

TABLE 6 – continued

	RA	DEC		Lum	Av	Mass	Age	$EW_{\mathrm{Li}\lambda 6708\mathrm{\AA}}$	$EW_{\mathrm{H}\alpha}$					
	(J2000)	(J2000)	Spt	($L_\odot$)	(mag)	($M_\odot$)	Myr	(Å)	(Å)	$\alpha_{3.6-8.0}$	$\alpha_{3.6-24}$	TTS[a]	Disk[b]	Criteria[c]
234	05 34 46.96	−05 52 20.4	M5.1	0.093	0.0	0.12	< 0.5	0.28	...	···	···	...	N	Li, Na
235	05 34 47.52	−05 46 30.1	M3.2	0.395	0.0	0.24	0.5	0.51, 0.51	−4.6	-2.77	···	W	N	Li, Na, X
236	05 34 47.66	−06 19 40.1	M2.5	0.227	0.4	0.30	1.6	0.60	−19.0	-1.57	-0.93	C	Y	Li, IRE
237	05 34 48.11	−06 18 11.6	M2.9	0.113	0.0	0.29	3.7	0.30	−3.5	-2.79	···	W	N	Li, X
238	05 34 48.32	−06 22 42.8	M5.5	0.071	0.1	0.099	< 0.5	0.30	−14.7	-1.92	-1.06	W	TD	Li, X, IRE
239	05 34 48.44	−04 50 51.4	M1.2	0.177	1.3	0.43	4.3	...	−114.5	-0.99	-0.42	C	Y	Na, IRE
240	05 34 48.82	−05 33 33.1	M3.9	0.104	0.3	0.19	1.9	0.44	−94.4	-1.50	-0.63	C	Y	Na, X, IRE
241	05 34 48.97	−06 07 45.0	M2.1	0.233	0.0	0.33	1.8	0.50	−2.6	-2.68	···	W	N	Li, X
242	05 34 49.22	−05 04 38.1	M3.8	0.242	0.0	0.19	0.6	0.40	−5.5	-2.88	···	W	N	Li, Na, X
243	05 34 49.30	−04 13 24.1	M3.1	0.147	0.0	0.27	2.2	0.28	−4.0	-2.64	···	W	N	Li, Na
244	05 34 49.59	−06 32 59.4	M4.9	0.063	0.7	0.11	1.8	0.40	−13.1	-2.65	···	W	N	Li, X
245	05 34 49.64	−04 36 41.6	M4.9	0.062	0.0	0.11	1.8	0.28	−7.8	···	···	W	N	Li, Na
246	05 34 49.80	−06 15 28.5	M5.0	0.090	0.0	0.12	0.7	...	−7.1	-2.73	···	W	N	Na, X
247	05 34 50.01	−05 53 04.1	M5.1	0.150	0.0	0.12	< 0.5	0.56	...	-2.64	···	...	N	Li, Na, X
248	05 34 50.14	−05 19 59.9	M6.0	0.025	0.0	0.058	1.8	0.16	...	···	···	...	?	X
249	05 34 50.24	−05 42 16.5	M4.3	0.047	0.2	0.15	3.5	...	...	···	···	...	N	X
250	05 34 50.47	−05 32 53.9	M5.5	0.055	0.1	0.088	1.4	0.26	...	···	···	...	N	X
251	05 34 50.55	−05 06 38.3	M5.1	0.053	0.0	0.098	2.1	0.68	...	···	···	...	N	Li, Na
252	05 34 50.86	−05 29 25.1	M4.5	0.178	0.0	0.15	< 0.5	0.39	...	···	···	...	N	X
253	05 34 51.41	−05 00 11.4	M4.6	0.135	0.0	0.15	0.5	0.67	−9.4	-2.63	···	W	N	Li, Na, X
254	05 34 51.90	−06 17 38.1	M3.1	0.100	0.3	0.27	3.8	0.34	−5.5	-2.63	···	W	N	Li, Na, X
255	05 34 52.26	−05 12 03.2	M3.0	0.155	0.0	0.27	2.1	0.54	...	···	···	...	N	X
256	05 34 52.31	−06 35 08.7	M4.2	0.117	0.0	0.17	1.3	...	−9.5	-2.67	···	W	N	Na, X
257	05 34 52.34	−05 30 08.0	M4.1	0.149	0.0	0.17	1.1	0.21, 0.55	...	···	···	...	Y	Li, Na, X, IRE
258	05 34 52.40	−06 11 57.0	M1.9	0.261	0.4	0.34	1.6	0.30	−8.3	-2.70	···	W	N	Li, X
259	05 34 52.63	−06 16 47.3	M2.8	0.131	0.1	0.30	3.1	0.22	−8.9	-2.56	···	W	N	Li, Na, X
260	05 34 52.74	−06 15 09.8	M5.4	0.034	0.6	0.079	3.2	...	−14.4	-2.54	···	W	N	X
261	05 34 52.76	−05 00 50.9	M4.2	0.145	0.1	0.16	1.0	0.31	−8.2	-2.72	···	W	N	Li, Na, X
262	05 34 52.84	−05 33 48.3	M4.5	0.109	0.0	0.15	1.1	0.40	...	-2.83	···	...	N	X
263	05 34 53.07	−04 37 03.6	M4.3	0.077	0.4	0.16	2.1	...	...	-1.43	-0.74	...	Y	Na, IRE
264	05 34 53.31	−05 54 05.3	M3.8	0.215	0.1	0.19	0.9	0.21	−6.8	-2.75	···	W	N	Li, Na, X
265	05 34 53.44	−04 57 32.8	M4.5	0.121	0.2	0.15	0.9	0.43	−9.6	-1.23	-0.90	W	Y	Li, Na, IRE
266	05 34 53.45	−04 29 09.5	M5.3	0.115	0.0	0.10	< 0.5	...	−12.8	-2.73	···	W	N	Na
267	05 34 53.63	−05 01 29.1	M5.2	0.046	0.0	0.090	2.7	...	...	-2.52	···	...	N	Na, X
268	05 34 53.87	−06 23 52.6	M1.2	0.693	0.6	0.37	0.6	0.50	−5.8	-0.96	···	W	Y	Li, Na, IRE
269	05 34 54.80	−05 55 08.3	M5.6	0.025	0.0	0.071	3.7	...	−78.4	-1.67	···	C	Y	Na, IRE
270	05 34 54.90	−04 27 24.5	M4.1	0.086	0.0	0.17	2.1	...	−2.6	-2.67	···	W	N	Na, X
271	05 34 55.06	−05 25 29.5	M3.0	0.375	0.8	0.26	0.7	0.53	...	-2.53	···	...	N	X
272	05 34 56.04	−04 38 12.0	M4.1	0.146	0.0	0.17	1.1	0.55	−4.2	···	···	W	N	Li, Na
273	05 34 56.13	−05 06 01.8	M4.1	0.249	0.0	0.17	< 0.5	0.25	−10.0	-2.81	···	W	N	Li, Na, X
274	05 34 56.40	−05 38 05.2	M5.0	0.180	0.0	0.12	< 0.5	0.51	...	-2.35	···	...	N	X
275	05 34 56.62	−06 34 10.2	M5.0	0.087	0.3	0.12	0.7	0.30	−11.8	-2.64	···	W	N	Li, X
276	05 34 57.01	−05 23 00.0	M3.7	0.142	0.6	0.21	1.6	0.55, 0.45	...	···	···	...	N	Li, X
277	05 34 57.45	−05 30 42.0	M2.5	0.214	0.1	0.30	1.7	0.64	...	···	···	...	N	X
278	05 34 57.45	−06 19 33.1	M3.6	0.135	0.0	0.21	1.8	0.36	−9.8	-1.78	-0.32	W	TD	Li, Na, X, IRE
279	05 34 57.94	−05 53 21.6	M4.0	0.263	0.0	0.18	< 0.5	0.43, 0.31	...	-2.02	-1.52	...	Y	Li, Na, X, IRE
280	05 34 58.19	−05 11 53.7	M5.0	0.219	0.0	0.12	< 0.5	0.53	...	-2.12	···	...	N	X
281	05 34 58.47	−06 10 33.7	M4.7	0.071	0.0	0.13	1.8	0.40	−9.2	-2.55	···	W	N	Li, X
282	05 34 58.90	−05 28 03.3	M3.0	0.171	0.0	0.27	1.9	0.46	...	···	···	...	N	X
283	05 35 01.37	−06 03 55.7	M4.5	0.066	0.0	0.14	2.2	0.30	−47.0	-1.22	-0.83	C	Y	Li, IRE
284	05 35 01.36	−05 55 54.8	M1.5	0.554	0.0	0.36	0.7	0.42, 0.49	−2.7	-2.75	···	W	N	Li, X
285	05 35 01.49	−05 28 20.8	M2.5	0.334	0.9	0.30	1.0	0.55	...	···	···	...	N	X
286	05 35 01.60	−05 54 18.8	M5.6	0.062	0.1	0.092	0.9	0.43	−19.5	-2.63	···	W	N	Li, Na, X
287	05 35 01.67	−04 32 52.9	M1.6	0.220	0.1	0.37	2.4	0.37	−17.2	-1.32	-1.08	C	Y	Li, Na, X, IRE
288	05 35 01.84	−05 49 32.6	M5.1	0.051	0.0	0.097	2.2	0.29, 0.26	...	···	···	...	N	Li, Na
289	05 35 01.94	−05 00 43.3	M4.9	0.040	0.1	0.10	2.8	...	−25.6	-2.72	···	W	N	Na, X
290	05 35 01.94	−06 30 12.8	M1.1	0.527	0.0	0.39	0.8	0.51	−6.3	-2.73	···	W	N	Li, Na, X
291	05 35 02.79	−05 44 43.0	M5.1	0.071	0.0	0.11	1.1	...	−249.8	···	···	W	N	Na
292	05 35 02.79	−06 23 59.9	M4.8	0.098	0.0	0.13	0.9	0.50	−11.7	-2.55	···	W	N	Li, X
293	05 35 02.84	−05 51 03.2	M3.1	0.201	0.0	0.26	1.5	0.38, 0.42	−7.2	-1.43	···	W	Y	Li, Na, X, IRE
294	05 35 02.93	−06 05 25.2	M0.4	0.341	0.1	0.47	2.1	0.50, 0.51	−5.9	-2.76	···	W	N	Li, X
295	05 35 03.00	−04 57 04.0	M5.0	0.057	0.0	0.11	2.0	...	...	···	···	...	N	Na
296	05 35 03.04	−04 59 59.8	M4.6	0.211	0.0	0.14	< 0.5	0.37	−9.0	-2.61	···	W	N	Li, Na
297	05 35 03.09	−06 12 23.4	M4.3	0.151	0.1	0.16	0.7	0.80	−14.4	-2.64	···	W	N	Li, X
298	05 35 03.12	−05 09 17.0	M2.6	0.185	0.8	0.29	2.0	0.66, 0.35	−3.4	-1.42	-0.76	W	Y	Li, Na, X, IRE
299	05 35 03.14	−05 50 01.5	M5.2	0.063	0.0	0.10	1.4	0.30	...	···	···	...	N	Na
300	05 35 03.51	−05 51 59.0	M5.6	0.056	0.0	0.088	1.2	0.12	...	···	···	...	N	Na
301	05 35 03.81	−06 16 47.5	M2.8	0.172	0.0	0.28	2.0	0.46	−5.5	-2.65	···	W	N	Li, Na, X
302	05 35 03.98	−04 11 53.8	M3.6	0.173	0.0	0.21	1.3	0.35	−3.8	-2.72	···	W	N	Li, Na
303	05 35 04.52	−05 55 25.6	M5.2	0.103	0.0	0.11	< 0.5	0.27	−10.2	-2.77	···	W	N	Na
304	05 35 05.45	−04 25 06.7	M2.0	0.266	0.0	0.33	1.5	0.54	−5.5	-2.64	···	W	N	Li, Na, X
305	05 35 05.67	−05 43 04.7	M5.0	0.049	0.0	0.099	2.3	0.24	...	···	···	...	N	Na, X
306	05 35 05.76	−05 44 00.1	M3.4	0.197	0.0	0.23	1.3	0.32	−6.9	-2.74	···	W	N	Li, Na, X
307	05 35 06.08	−05 52 39.3	M3.6	0.220	0.0	0.21	1.0	0.54	−15.3	-2.43	···	W	N	Li, Na, X
308	05 35 06.58	−05 59 51.4	M4.9	0.095	0.0	0.12	0.6	...	−23.0	-2.66	···	W	N	Na, X
309	05 35 07.16	−06 18 16.3	M4.3	0.118	0.0	0.16	1.2	0.20	−13.0	-2.71	···	W	N	Li, X
310	05 35 07.24	−04 50 25.5	M4.8	0.308	0.0	0.13	< 0.5	...	−17.3	-2.57	···	W	N	Na, X
311	05 35 07.34	−06 18 55.2	M4.4	0.038	0.5	0.14	4.1	0.60	−13.6	-2.54	···	W	N	Li, X

TABLE 6 – continued

	RA	DEC		Lum	Av	Mass	Age	$EW_{\rm Li\lambda6708\AA}$	$EW_{\rm H\alpha}$					
	(J2000)	(J2000)	Spt	($L_\odot$)	(mag)	($M_\odot$)	Myr	(Å)	(Å)	$\alpha_{3.6-8.0}$	$\alpha_{3.6-24}$	TTS[a]	Disk[b]	Criteria[c]
312	05 35 07.38	−06 26 34.1	M5.4	0.063	0.0	0.097	1.1	0.30	−13.7	-2.57	···	W	N	Li, X
313	05 35 07.51	−06 19 23.3	M3.1	0.124	0.1	0.27	2.7	0.14	−5.5	-2.76	···	W	N	Li, Na, X
314	05 35 07.66	−06 06 54.1	M3.6	0.214	0.0	0.21	1.1	0.42	−13.5	-2.70	···	W	N	X
315	05 35 07.84	−04 34 52.3	M5.1	0.100	0.0	0.12	< 0.5	...	−14.5	···	···	W	N	Na
316	05 35 07.84	−05 29 17.4	M3.5	0.188	1.0	0.22	1.3	...	...	···	···	...	N	X
317	05 35 07.92	−04 20 14.1	M3.8	0.144	0.0	0.19	1.4	0.54	−3.7	-2.69	···	W	N	Li, Na
318	05 35 08.05	−05 53 43.5	M2.3	0.395	0.0	0.31	0.8	0.50, 0.48	−4.2	-2.97	···	W	N	Li, Na, X
319	05 35 08.25	−05 29 12.1	M4.5	0.085	0.8	0.14	1.6	0.23	...	···	···	...	N	X
320	05 35 08.25	−04 25 33.3	M0.6	0.219	0.1	0.49	4.2	0.54	−3.0	-2.71	···	W	N	Li, X
321	05 35 08.38	−05 54 41.7	M4.8	0.154	0.0	0.13	< 0.5	0.32, 0.45	−8.5	-2.68	···	W	N	Li, Na, X
322	05 35 08.56	−05 53 51.4	M5.1	0.084	0.0	0.11	0.6	...	−6.9	···	···	W	N	Na
323	05 35 09.29	−04 18 26.8	M4.7	0.097	0.0	0.13	1.0	...	−10.6	-2.63	···	W	N	Na
324	05 35 09.61	−04 33 11.0	M2.4	0.408	0.0	0.30	0.8	0.17	−0.7	-2.76	···	W	N	Li, Na
325	05 35 10.62	−06 01 44.8	M3.2	0.163	0.0	0.25	1.8	0.40, 0.44	−11.4	-2.74	···	W	N	Li, X
326	05 35 10.88	−05 49 48.6	M5.6	0.054	0.0	0.086	1.2	0.21	...	···	···	...	N	Na
327	05 35 10.89	−04 29 01.5	M4.8	0.077	0.0	0.12	1.4	0.58	−6.2	-1.95	-1.24	W	TD	Li, Na, IRE
328	05 35 10.94	−06 33 05.3	M4.4	0.046	0.4	0.14	3.4	0.40	−20.1	-2.57	···	W	N	Li, X
329	05 35 11.11	−06 00 21.6	M4.3	0.182	0.0	0.16	< 0.5	0.50, 0.46	−7.6	···	···	W	N	Li, X
330	05 35 11.66	−05 31 01.1	M6.0	0.147	0.0	0.088	< 0.5	...	...	-0.69	-0.27	...	Y	X, IRE
331	05 35 12.05	−06 49 54.5	M4.6	0.138	0.0	0.14	< 0.5	0.50	−10.3	-1.52	-0.65	W	TD	Li, IRE
332	05 35 12.15	−05 31 38.8	M4.5	0.336	0.2	0.15	< 0.5	0.43	...	-2.20	···	...	Y	X
333	05 35 12.22	−04 27 11.6	M3.8	0.353	0.0	0.19	< 0.5	0.49	−12.7	-2.70	···	W	N	Li, Na, X
334	05 35 12.83	−05 55 26.3	M4.3	0.099	0.0	0.16	1.6	0.23	−14.6	-1.62	-1.12	W	TD	Li, Na, IRE
335	05 35 13.56	−06 48 03.2	M5.1	0.053	0.0	0.098	2.1	0.30	−11.7	-1.62	-0.91	W	TD	Li, IRE
336	05 35 13.65	−04 11 07.4	M4.3	0.098	0.0	0.16	1.6	0.60	−4.8	-2.70	···	W	N	Li, Na
337	05 35 13.81	−05 30 24.4	M3.5	0.256	0.0	0.22	0.8	0.59	...	-2.90	···	...	N	X
338	05 35 14.44	−05 54 26.6	M4.0	0.087	0.0	0.18	2.2	0.30	−19.6	-1.50	-1.19	C	Y	Li, Na, X, IRE
339	05 35 14.67	−05 08 52.1	M3.5	0.207	0.2	0.22	1.2	...	...	···	···	...	N	X
340	05 35 14.93	−05 56 36.2	M4.1	0.133	0.0	0.17	1.3	0.33, 0.43	−7.8	-2.73	···	W	N	Li, Na, X
341	05 35 14.94	−05 49 34.8	M3.3	0.351	0.0	0.23	0.6	0.41, 0.37	−4.8	···	···	W	N	Li, Na, X
342	05 35 15.59	−05 34 46.7	M5.0	0.222	0.6	0.12	< 0.5	0.36	...	···	···	...	N	X
343	05 35 15.60	−05 09 31.8	M5.7	0.061	0.0	0.090	0.9	0.65	−9.3	···	···	W	N	Li, Na, X
344	05 35 15.79	−06 09 39.8	M4.5	0.044	0.6	0.13	3.3	0.40, 0.16	−7.7	-2.74	···	W	N	Li
345	05 35 15.83	−06 24 45.7	M4.9	0.098	0.0	0.12	0.6	0.50	−12.6	-2.51	···	W	N	Li, X
346	05 35 15.85	−06 09 46.7	M5.3	0.029	0.3	0.080	3.8	...	−67.5	-1.36	-1.04	C	Y	IRE
347	05 35 15.86	−05 28 52.9	M2.2	1.039	1.4	0.30	< 0.5	0.55	...	-1.53	···	...	Y	X, IRE
348	05 35 16.26	−05 31 00.7	M4.5	0.115	0.2	0.15	1.0	0.43	...	···	···	...	N	X
349	05 35 16.38	−06 41 13.4	M5.4	0.046	0.2	0.084	2.3	0.50	−19.2	-2.90	···	W	N	Li
350	05 35 16.41	−04 58 02.0	M4.7	0.125	0.0	0.14	< 0.5	0.67	−10.3	···	···	W	N	Li, Na, X
351	05 35 16.42	−04 26 05.5	M5.4	0.077	0.0	0.10	< 0.5	...	−17.4	-2.56	···	W	N	Na, X
352	05 35 16.66	−04 38 05.7	M5.0	0.088	0.0	0.12	0.7	...	−6.9	···	···	W	N	Na
353	05 35 16.95	−05 45 55.8	M5.1	0.273	0.1	0.11	< 0.5	0.32	−25.0	-0.91	-0.59	C	Y	Li, Na, X, IRE
354	05 35 17.16	−05 41 53.9	M5.0	0.129	0.0	0.12	< 0.5	...	...	-1.32	···	...	Y	X, IRE
355	05 35 17.48	−05 09 49.1	M5.4	0.106	0.0	0.10	< 0.5	0.21, 0.44	−21.0	···	···	W	N	Li, Na, X
356	05 35 17.68	−06 32 23.9	M2.2	0.400	0.0	0.31	0.9	0.44	−5.4	-2.58	-2.08	W	DB	Li, Na, X, IRE
357	05 35 17.68	−05 32 02.4	M4.0	0.187	0.0	0.18	0.8	...	...	···	···	...	N	X
358	05 35 17.78	−06 31 44.2	M4.7	0.246	0.1	0.14	< 0.5	0.37	−9.1	-2.64	···	W	N	Li, Na, X
359	05 35 18.26	−06 24 30.3	M5.7	0.075	0.0	0.095	< 0.5	0.50	−13.8	-2.43	···	W	N	Li
360	05 35 18.70	−06 03 27.6	M4.7	0.062	0.0	0.13	2.1	0.60	−13.4	-2.60	···	W	N	Li
361	05 35 18.68	−05 54 06.4	M2.2	0.424	0.0	0.31	0.8	0.52	...	-2.74	···	...	N	X
362	05 35 18.87	−04 44 27.7	M5.3	0.146	0.0	0.11	< 0.5	...	−27.1	-1.77	-0.78	C	TD	Na, X, IRE
363	05 35 18.95	−06 27 25.6	M4.0	0.151	0.5	0.18	1.2	0.50	−94.8	-1.15	-0.63	C	Y	Li, X, IRE
364	05 35 19.03	−05 46 16.3	M3.4	0.291	0.0	0.23	0.7	0.51, 0.54	−3.1	-2.63	···	W	N	Li, Na, X
365	05 35 19.10	−04 54 07.7	M4.7	0.073	0.0	0.13	1.7	...	−11.5	···	···	W	Y	Na, X, IRE
366	05 35 19.67	−05 35 35.7	M5.0	0.070	0.0	0.11	1.3	0.41	...	-1.92	···	...	Y	X
367	05 35 19.82	−05 45 40.9	M4.4	0.196	0.0	0.16	< 0.5	0.55, 0.45	−16.7	···	···	W	N	Li, Na, X
368	05 35 19.94	−05 33 53.5	M3.5	0.337	0.0	0.22	< 0.5	...	...	-2.72	···	...	N	X
369	05 35 20.21	−05 46 51.1	M2.6	0.424	0.1	0.29	0.7	0.49	−5.4	-1.93	-1.14	W	TD	Li, Na, X, IRE
370	05 35 20.28	−05 32 16.8	M6.0	0.109	0.0	0.088	< 0.5	0.17	...	-0.87	···	...	Y	X, IRE
371	05 35 20.29	−05 46 40.0	M3.5	0.255	0.0	0.21	0.8	0.47, 0.49	...	-2.62	···	...	N	Li, Na, X
372	05 35 20.36	−05 02 26.6	M4.3	0.344	0.6	0.16	< 0.5	0.29	−3.7	-2.68	···	W	N	Li, Na, X
373	05 35 20.47	−06 47 25.9	M1.2	0.278	0.0	0.40	2.0	0.60	−3.8	-2.72	···	W	N	Li
374	05 35 20.50	−06 45 40.8	M4.7	0.243	0.0	0.14	< 0.5	0.20	−11.4	···	···	W	N	Li
375	05 35 20.60	−04 46 02.4	M4.9	0.090	0.0	0.12	0.9	...	−12.9	-2.32	···	W	N	Na, X
376	05 35 20.96	−06 04 00.5	M4.5	0.066	0.0	0.14	2.2	0.40, 0.25	−75.0	-1.40	-0.94	C	TD	Li, IRE
377	05 35 21.21	−05 33 17.5	M2.0	0.119	2.4	0.37	5.5	0.24	...	-1.35	···	...	Y	IRE
378	05 35 21.77	−06 18 51.2	M4.7	0.091	0.0	0.13	1.2	0.70	−11.6	-1.74	-1.41	W	Y	Li, X, IRE
379	05 35 22.84	−04 46 41.4	M3.2	0.203	0.5	0.25	1.4	0.62	−4.3	-1.46	-0.70	W	Y	Li, Na, X, IRE
380	05 35 22.79	−05 31 37.2	M1.0	0.506	1.3	0.39	0.9	0.52	...	-1.27	-0.93	...	Y	X, IRE
381	05 35 23.30	−04 57 20.6	M2.4	0.201	0.0	0.31	1.9	0.31	−2.4	···	···	W	N	Li, Na, X
382	05 35 23.72	−04 48 16.6	M4.5	0.144	0.0	0.15	< 0.5	0.49	−94.1	-0.29	-0.28	C	Y	Li, Na, X, IRE
383	05 35 23.88	−05 51 27.9	M4.6	0.075	0.0	0.14	1.9	0.56, 0.14	−78.7	-1.12	···	C	Y	Li, Na, IRE
384	05 35 24.40	−06 11 14.7	M6.0	0.056	0.0	0.080	0.6	0.60	−14.6	-2.65	···	W	N	Li
385	05 35 24.49	−06 28 40.5	M5.0	0.117	0.0	0.12	< 0.5	0.45	−8.8	-2.78	···	W	N	X
386	05 35 25.36	−04 33 48.9	M4.7	0.119	0.0	0.14	0.6	0.21	−8.4	-1.97	-0.27	W	TD	Li, Na, X, IRE
387	05 35 25.45	−04 54 03.9	M5.2	0.077	0.0	0.11	0.9	...	−27.4	···	···	W	N	Na, X
388	05 35 25.68	−04 49 31.3	M4.7	0.175	0.1	0.14	< 0.5	0.45	−84.0	-0.86	···	C	Y	Li, Na, X, IRE
389	05 35 25.70	−05 07 03.2	M5.3	0.088	0.4	0.11	< 0.5	0.44	...	···	···	...	N	Na, X

TABLE 6 – continued

	RA	DEC		Lum	Av	Mass	Age	$EW_{\mathrm{Li}\lambda6708\mathrm{\AA}}$	$EW_{\mathrm{H}\alpha}$					
	(J2000)	(J2000)	Spt	($L_\odot$)	(mag)	($M_\odot$)	Myr	(Å)	(Å)	$\alpha_{3.6-8.0}$	$\alpha_{3.6-24}$	TTS[a]	Disk[b]	Criteria[c]
390	05 35 26.01	−06 01 39.7	M3.9	0.109	0.0	0.19	1.9	0.57	−4.3	···	···	W	N	Li, Na, X
391	05 35 26.37	−05 44 34.1	M4.5	0.072	0.0	0.14	2.1	0.51	−109.8	-1.74	-1.23	C	Y	Li, Na, X, IRE
392	05 35 26.59	−06 15 32.8	M3.6	0.136	0.1	0.22	1.7	0.30	−9.4	-2.65	···	W	N	Li
393	05 35 26.60	−06 16 28.3	M2.3	0.141	0.4	0.33	3.5	0.40	−5.8	-2.75	···	W	N	Li, Na, X
394	05 35 26.80	−06 15 34.4	M3.5	0.136	0.1	0.23	1.8	0.30, 0.17	−7.1	-2.79	···	W	N	Li
395	05 35 26.96	−06 27 13.0	M4.3	0.044	0.0	0.15	3.8	0.40	−7.6	-2.66	···	W	N	Li
396	05 35 27.07	−06 17 53.8	M6.2	0.046	0.3	0.070	0.5	...	−16.9	-2.57	···	W	N	X
397	05 35 27.93	−06 09 39.1	M3.3	0.364	0.1	0.23	0.5	1.00	−29.0	-2.62	···	W	N	Li
398	05 35 27.98	−04 50 38.8	M4.9	0.120	0.0	0.12	< 0.5	...	...	-2.70	···	...	N	Na, X
399	05 35 28.03	−05 57 43.8	M5.2	0.072	0.0	0.11	1.0	...	...	-2.49	···	...	N	Na
400	05 35 28.06	−06 21 33.2	M5.3	0.066	0.0	0.10	1.1	0.50	−17.8	-1.37	-0.98	W	Y	Li, IRE
401	05 35 28.28	−06 30 22.2	M3.6	0.089	0.8	0.22	3.0	0.23	−21.4	-1.44	-0.89	C	Y	Li, Na, IRE
402	05 35 28.40	−04 58 07.1	M5.0	0.034	0.0	0.092	3.6	...	−15.4	···	···	W	N	Na
403	05 35 28.59	−06 30 03.8	M4.6	0.067	0.0	0.13	2.1	0.50	−8.7	-1.61	···	W	Y	Li, IRE
404	05 35 28.78	−05 41 34.0	M3.4	0.100	0.1	0.24	3.0	...	−113.3	···	···	W	N	Na, X
405	05 35 28.80	−06 02 58.6	M4.8	0.029	0.2	0.10	3.9	0.50, 0.15	−8.0	···	···	W	N	Li
406	05 35 28.93	−04 49 13.9	M5.9	0.053	0.0	0.080	0.7	...	...	-2.53	···	...	N	Na, X
407	05 35 30.44	−06 05 00.8	M5.5	0.041	0.3	0.077	2.2	0.14	−50.0	-1.09	-0.82	C	Y	IRE
408	05 35 30.42	−05 34 38.6	M3.8	0.303	0.4	0.19	< 0.5	0.43	−32.9	-2.52	···	W	N	Na, X
409	05 35 30.53	−04 51 29.0	K7.0	0.551	0.0	0.66	2.2	...	...	-2.70	···	...	N	X
410	05 35 30.63	−06 50 33.6	M4.8	0.045	0.3	0.11	2.7	0.30	−11.8	-2.59	···	W	N	Li
411	05 35 31.17	−04 26 47.9	M4.5	0.081	0.0	0.14	1.7	...	−6.1	-2.72	···	W	N	Na
412	05 35 31.73	−04 49 52.6	M4.8	0.134	0.0	0.13	< 0.5	...	...	-2.52	···	...	N	Na, X
413	05 35 31.89	−06 36 25.5	M4.7	0.066	0.9	0.13	2.0	0.70	−95.3	-1.23	-0.80	C	Y	Li, IRE
414	05 35 31.94	−05 31 47.8	M9.1	0.021	0.0	0.018	< 0.5	...	...	-0.83	···	...	Y	X, IRE
415	05 35 32.02	−04 55 35.7	M4.8	0.068	0.0	0.12	1.8	...	...	···	···	...	N	Na, X
416	05 35 32.70	−06 30 18.2	M2.8	0.158	0.0	0.28	2.2	0.45	−3.7	-2.74	···	W	N	Li, Na, X
417	05 35 33.04	−06 27 29.1	M4.5	0.031	0.4	0.12	4.7	1.00	−6.7	-2.91	···	W	N	Li
418	05 35 33.46	−04 56 01.8	M5.0	0.151	0.0	0.12	< 0.5	0.18	−11.6	···	···	W	N	Li, Na, X
419	05 35 33.55	−04 24 56.6	M4.5	0.079	0.0	0.15	1.9	0.43	−5.3	-2.80	···	W	N	Li, Na
420	05 35 33.57	−06 02 20.3	M3.7	0.307	0.0	0.20	< 0.5	0.40, 0.52	−6.6	-2.75	···	W	N	Li, X
421	05 35 33.59	−04 47 32.8	M5.4	0.054	0.0	0.089	2.0	...	−23.8	···	···	W	N	Na, X
422	05 35 33.61	−05 28 50.6	M5.0	0.309	0.0	0.12	< 0.5	0.44	...	···	···	...	N	X
423	05 35 33.85	−05 38 20.7	M3.5	0.120	0.0	0.23	2.2	...	...	···	···	...	N	X
424	05 35 33.93	−06 14 32.8	M5.0	0.181	0.0	0.12	< 0.5	0.70, 0.12	−58.9	-1.06	-0.75	C	Y	Li, IRE
425	05 35 34.38	−06 05 42.7	M3.3	0.585	0.5	0.23	< 0.5	0.25	−12.1	-2.70	···	W	N	Li, Na, X
426	05 35 34.55	−04 38 05.8	M4.0	0.087	0.5	0.18	2.3	0.59	−4.1	-1.85	-1.20	W	Y	Li, Na, IRE
427	05 35 35.25	−06 48 41.9	M4.5	0.081	0.0	0.14	1.7	0.50	−8.6	-2.75	···	W	N	Li
428	05 35 35.22	−05 26 55.1	M2.5	0.379	0.8	0.30	0.9	0.57	...	···	···	...	N	X
429	05 35 35.32	−04 44 20.3	M5.4	0.055	0.0	0.090	2.0	...	−32.6	-1.68	···	C	Y	Na, IRE
430	05 35 35.54	−04 25 23.2	M4.6	0.092	0.5	0.14	1.3	...	−7.1	-1.78	-1.22	W	Y	Na, IRE
431	05 35 35.55	−05 06 58.6	M3.2	0.119	0.0	0.26	2.7	0.29	−3.7	···	···	W	N	Li, Na, X
432	05 35 35.95	−05 38 42.7	M4.0	0.166	0.0	0.18	1.0	0.40	...	-1.68	-0.85	...	Y	X, IRE
433	05 35 36.11	−05 56 53.3	M4.8	0.166	0.0	0.13	< 0.5	0.42, 0.47	−10.0	-2.73	···	W	N	Li, Na, X
434	05 35 37.23	−04 46 59.4	M5.8	0.086	0.0	0.092	< 0.5	...	...	-2.55	···	...	N	Na, X
435	05 35 37.34	−06 21 19.2	M4.7	0.127	0.0	0.14	< 0.5	0.50	−12.4	-1.26	-1.21	W	Y	Li, X, IRE
436	05 35 37.94	−04 26 08.7	M4.4	0.091	0.0	0.15	1.6	...	−5.0	-1.94	-1.29	W	TD	Na, IRE
437	05 35 38.01	−04 52 29.6	M4.4	0.113	1.4	0.15	1.1	...	−51.1	-1.36	···	C	Y	Na, IRE
438	05 35 38.03	−05 28 21.6	M3.5	0.337	0.0	0.21	< 0.5	0.42, 0.54	...	-1.71	···	...	Y	Li, X, IRE
439	05 35 38.44	−05 52 45.7	M5.8	0.033	0.0	0.066	1.5	...	−37.9	-1.29	-1.00	C	Y	Na, IRE
440	05 35 38.92	−04 41 33.8	M4.5	0.056	0.0	0.14	2.7	...	...	···	···	...	N	Na
441	05 35 39.03	−05 07 04.3	M3.7	0.241	0.0	0.20	0.7	0.23	−6.7	-2.53	···	W	N	Li, Na, X
442	05 35 39.14	−05 58 06.6	M5.3	0.071	0.0	0.10	0.8	...	−54.0	-1.59	-1.00	C	Y	Na, IRE
443	05 35 39.95	−04 21 02.2	M4.1	0.083	0.1	0.17	2.2	...	−55.7	-1.48	-1.07	C	Y	Na, IRE
444	05 35 40.46	−04 31 10.1	M5.7	0.056	0.0	0.085	0.9	...	−17.6	-2.57	···	W	N	Na
445	05 35 40.74	−04 35 30.3	M4.6	0.067	0.0	0.13	2.0	...	−5.9	···	···	W	N	Na
446	05 35 40.77	−05 11 11.9	M5.2	0.082	0.4	0.11	0.6	0.47, 0.26	−42.2	-1.27	···	C	Y	Li, Na, X, IRE
447	05 35 41.14	−05 42 51.1	M4.7	0.062	0.0	0.13	2.2	0.51	...	···	···	...	N	Li, Na, X
448	05 35 41.73	−05 03 29.1	M4.9	0.103	0.3	0.12	< 0.5	0.51	−10.8	···	···	W	N	Li, Na, X
449	05 35 41.78	−04 50 27.8	M4.7	0.110	0.0	0.14	0.7	0.52	...	-2.70	···	...	N	Li, Na, X
450	05 35 41.86	−05 52 29.6	M4.7	0.151	0.0	0.14	< 0.5	0.34	−13.6	-2.59	···	W	N	Li, Na, X
451	05 35 42.20	−06 15 14.4	M4.4	0.071	0.4	0.15	2.2	0.20, 0.34	−13.6	-2.52	···	W	N	Li, X
452	05 35 42.21	−06 11 43.8	M5.4	0.041	0.1	0.082	2.6	0.80	−18.5	-1.12	-0.44	C	TD	Li, IRE
453	05 35 42.72	−04 05 52.0	M5.3	0.058	0.0	0.095	1.5	0.44	−31.5	-2.61	···	W	N	Li, Na
454	05 35 43.06	−05 03 07.5	M4.6	0.120	0.4	0.14	0.7	0.21, 0.31	−24.1	-1.45	-0.71	C	Y	Li, Na, X, IRE
455	05 35 43.80	−05 09 58.8	M5.5	0.081	0.0	0.10	< 0.5	0.68, 0.30	−40.5	-0.77	···	C	Y	Li, Na, X, IRE
456	05 35 44.20	−05 50 04.7	M3.7	0.123	0.0	0.21	1.8	0.43	−8.3	-2.62	···	W	N	Li, Na, X
457	05 35 44.37	−04 57 16.9	M5.6	0.131	0.0	0.097	< 0.5	...	−2.7	···	···	W	N	Na, X
458	05 35 44.72	−04 30 02.0	M5.2	0.044	0.1	0.089	2.9	...	−15.6	-2.45	···	W	N	Na
459	05 35 45.31	−04 23 32.1	M4.8	0.037	0.3	0.11	3.1	...	−9.4	-2.83	···	W	N	Na
460	05 35 45.88	−06 05 38.8	M2.8	0.266	0.0	0.28	1.2	0.30, 0.50	−3.3	-2.28	···	W	N	Li
461	05 35 46.82	−04 18 32.8	M2.1	0.357	0.0	0.33	1.0	0.37	−2.7	-2.71	···	W	N	Li, Na
462	05 35 47.69	−05 58 06.1	M4.9	0.079	0.0	0.12	1.2	0.36, 0.23	−10.1	-2.61	···	W	N	Li, Na, X
463	05 35 48.28	−06 17 59.4	M2.9	0.200	0.1	0.28	1.6	0.70, 0.52	−7.0	-2.73	···	W	N	Li, X
464	05 35 48.39	−06 17 36.2	M4.2	0.149	0.0	0.17	0.9	0.50, 0.47	−10.3	-2.73	···	W	N	Li, X
465	05 35 48.44	−04 17 06.1	M4.6	0.144	0.0	0.15	< 0.5	0.41	−7.1	-2.69	···	W	N	Li, Na
466	05 35 48.60	−06 05 25.7	M4.7	0.103	0.0	0.13	0.9	0.53	−11.9	-2.01	···	W	Y	Li, Na
467	05 35 48.78	−06 09 07.2	M3.3	0.121	0.0	0.25	2.5	0.50, 0.34	−4.8	-2.75	···	W	N	Li

TABLE 6 – continued

	RA	DEC		Lum	Av	Mass	Age	$EW_{\mathrm{Li\lambda6708\AA}}$	$EW_{\mathrm{H}\alpha}$					
	(J2000)	(J2000)	Spt	($L_\odot$)	(mag)	($M_\odot$)	Myr	(Å)	(Å)	$\alpha_{3.6-8.0}$	$\alpha_{3.6-24}$	TTS[a]	Disk[b]	Criteria[c]
468	05 35 48.98	−05 01 39.4	M2.8	0.243	0.0	0.28	1.3	0.52, 0.60	−21.3	-1.45	-1.20	C	Y	Li, Na, X, IRE
469	05 35 49.03	−04 53 49.9	M4.9	0.036	0.0	0.10	3.1	...	−48.7	···	···	C	Y	Na, IRE
470	05 35 49.16	−05 56 18.3	M4.5	0.081	0.0	0.14	1.7	0.20	−10.1	-2.58	···	W	N	Na, X
471	05 35 49.24	−05 59 14.2	M4.2	0.084	0.0	0.17	2.1	0.20	−19.6	-2.04	···	W	N	Na, X
472	05 35 50.25	−06 33 35.6	M4.5	0.149	0.0	0.15	< 0.5	0.50	−9.4	-2.61	···	W	N	Li
473	05 35 50.96	−06 22 43.6	M1.1	0.246	0.0	0.42	2.6	0.42	−3.5	0.32	0.13	W	Y	Li, Na, X, IRE
474	05 35 51.32	−06 13 53.3	M4.9	0.122	0.1	0.12	< 0.5	0.46	−13.5	-1.11	-0.92	W	Y	Li, Na, X, IRE
475	05 35 52.98	−04 17 39.7	M5.1	0.064	0.0	0.11	1.4	...	−13.7	-2.59	···	W	N	Na
476	05 35 53.08	−05 59 48.0	M3.4	0.124	0.0	0.24	2.3	0.18	−6.1	-2.75	···	W	N	Li, Na, X
477	05 35 53.70	−06 30 54.7	M5.2	0.029	0.6	0.084	3.8	0.21	−20.3	-1.65	-0.62	C	TD	IRE
478	05 35 54.21	−05 05 45.5	M4.2	0.091	0.0	0.17	1.9	...	−16.3	-2.56	···	W	N	Na, X
479	05 35 54.68	−05 54 36.7	M5.2	0.083	0.0	0.11	0.6	0.56	...	···	···	...	N	Li, Na
480	05 35 55.13	−06 10 09.4	M1.7	0.290	2.0	0.35	1.5	0.23	−19.2	-2.70	···	W	N	Li, Na, X
481	05 35 55.44	−05 23 43.0	M5.0	0.116	0.0	0.12	< 0.5	...	...	···	···	...	N	X
482	05 35 56.18	−05 52 28.5	M3.1	0.208	0.0	0.25	1.4	0.28	−5.5	-2.62	···	W	N	Li, Na, X
483	05 35 56.41	−04 11 28.4	M4.4	0.111	0.0	0.16	1.2	0.17	−10.4	-2.62	···	W	N	Li, Na
484	05 35 56.45	−04 36 50.7	M4.3	0.083	0.0	0.16	2.0	0.31	−7.0	-2.28	···	W	N	Li, Na, X
485	05 35 58.33	−06 22 39.4	M5.5	0.031	0.0	0.074	3.3	0.34	−17.7	-3.02	···	W	N	X
486	05 35 58.81	−06 12 43.8	M3.9	0.075	0.0	0.19	3.0	0.40	−5.7	···	···	W	N	Li
487	05 35 58.97	−05 59 08.5	M3.0	0.166	0.0	0.27	1.9	0.57	−9.0	-2.75	···	W	N	Li, Na, X
488	05 35 59.23	−06 49 51.9	M3.1	0.174	0.4	0.26	1.7	0.50	−7.6	-2.77	···	W	N	Li
489	05 36 00.28	−06 23 47.3	M2.1	0.194	0.8	0.34	2.4	0.26, 0.51	−7.2	-2.80	···	W	N	Li, Na, X
490	05 36 01.09	−06 25 07.7	M3.7	0.159	0.0	0.20	1.4	0.40, 0.52	−10.9	-1.65	-1.13	W	TD	Li, IRE
491	05 36 01.39	−05 19 10.7	M4.9	0.124	0.0	0.12	< 0.5	0.27	−29.1	···	···	W	N	Li, Na
492	05 36 01.41	−06 44 14.6	M4.6	0.134	0.0	0.14	< 0.5	0.30	−8.0	-2.68	···	W	N	Li
493	05 36 01.66	−06 42 36.2	M5.7	0.107	0.2	0.095	< 0.5	0.40	−58.7	-1.47	-1.42	C	Y	Li, IRE
494	05 36 02.04	−04 30 43.0	M4.0	0.089	0.0	0.18	2.2	0.73	−1.6	-2.48	···	W	N	Li, Na, X
495	05 36 02.64	−05 07 36.5	K8.8	0.849	0.0	0.56	0.9	0.59	−2.6	-2.71	···	W	N	Li, X
496	05 36 02.83	−05 32 54.4	M6.0	0.071	0.0	0.088	0.5	...	−117.2	-1.72	···	C	Y	Na, IRE
497	05 36 03.24	−05 44 32.9	M6.3	0.033	0.0	0.059	0.7	...	−44.8	···	···	C	Y	Na, IRE
498	05 36 03.62	−04 14 17.8	M4.1	0.297	0.0	0.17	< 0.5	0.26	−6.8	-1.96	-1.06	W	TD	Li, Na, IRE
499	05 36 05.16	−06 25 25.4	K6.9	0.652	0.5	0.64	1.7	0.43, 0.62	−8.7	-2.65	-1.81	C	DB	Li, X, IRE
500	05 36 05.65	−05 52 13.1	M3.8	0.171	0.0	0.19	1.2	0.60	−14.5	-2.55	···	W	N	Li, Na, X
501	05 36 05.93	−05 52 54.9	M5.4	0.051	0.0	0.086	2.0	...	...	-1.98	···	...	Y	Na, IRE
502	05 36 06.59	−06 31 43.0	M3.3	0.119	0.0	0.25	2.5	0.22, 0.52	−6.6	-1.20	-0.56	W	TD	Li, Na, X, IRE
503	05 36 06.80	−05 06 15.6	M2.8	0.164	0.1	0.28	2.1	0.35	−2.7	-1.55	-1.19	W	Y	Li, Na, X, IRE
504	05 36 07.21	−04 17 00.1	M3.6	0.210	0.0	0.21	1.1	0.44	−6.9	-2.73	···	W	N	Li, Na
505	05 36 08.40	−04 28 52.6	M4.3	0.274	0.3	0.16	< 0.5	...	−11.3	-2.00	-1.36	W	TD	Na, IRE
506	05 36 08.69	−05 21 02.2	M4.0	0.307	0.0	0.18	< 0.5	0.67	...	···	···	...	N	X
507	05 36 08.87	−04 07 20.0	M3.7	0.213	0.0	0.20	1.0	...	−0.4	-2.75	···	W	N	Na
508	05 36 09.28	−04 50 00.8	M3.9	0.184	0.0	0.18	0.9	0.33	−68.0	-1.42	-1.01	C	Y	Li, Na, IRE
509	05 36 09.35	−06 17 10.8	M2.1	0.425	0.1	0.32	0.8	0.50, 0.62	−4.2	-2.68	···	W	N	Li, X
510	05 36 09.49	−06 18 36.3	M1.3	0.548	0.0	0.37	0.8	0.50, 0.55	−5.2	-2.64	···	W	N	Li, X
511	05 36 09.94	−04 26 56.7	M4.4	0.072	0.0	0.15	2.2	...	−10.0	-2.62	···	W	N	Na
512	05 36 09.98	−05 05 35.4	M5.2	0.045	0.3	0.092	2.7	...	−14.4	-2.05	···	W	N	Na, X
513	05 36 09.98	−05 57 20.2	M5.0	0.051	0.0	0.10	2.2	...	...	-2.83	···	...	N	Na
514	05 36 10.87	−06 33 47.5	M2.6	0.510	0.0	0.28	0.6	0.46	−5.0	-2.68	···	W	N	Li, Na, X
515	05 36 10.94	−04 25 37.1	M5.0	0.042	0.0	0.098	2.7	...	−10.1	-2.54	···	W	N	Na
516	05 36 11.11	−06 18 14.1	M6.0	0.032	0.2	0.061	0.9	0.80	−19.7	-2.81	···	W	N	Li
517	05 36 11.31	−06 16 56.0	M5.8	0.058	0.1	0.084	0.8	0.19	−14.8	-1.59	-0.81	W	Y	IRE
518	05 36 11.67	−06 24 58.4	M4.9	0.033	0.6	0.098	3.4	0.40, 0.18	−13.3	-1.21	0.06	W	TD	Li, IRE
519	05 36 11.80	−05 00 32.6	M3.6	0.327	0.0	0.21	< 0.5	0.44	−5.4	-2.71	···	W	N	Li, Na, X
520	05 36 12.97	−05 55 27.0	M2.8	0.155	0.0	0.29	2.4	...	−7.2	-2.50	···	W	N	Na, X
521	05 36 13.38	−05 02 23.0	M5.1	0.097	0.0	0.11	< 0.5	0.44	−136.8	-1.50	-0.88	C	TD	Li, Na, X, IRE
522	05 36 13.75	−06 02 46.0	M4.5	0.052	0.3	0.14	2.8	0.30	−9.0	-2.61	···	W	N	Li
523	05 36 14.57	−05 33 23.8	M4.8	0.067	0.0	0.12	1.8	0.60	−7.1	-2.04	···	W	N	Li, Na
524	05 36 15.42	−04 20 50.2	M5.2	0.045	0.0	0.090	2.8	...	−11.4	-2.62	···	W	N	Na
525	05 36 15.57	−06 00 50.5	M5.4	0.060	0.1	0.095	1.3	...	−56.0	-1.34	-0.86	C	Y	IRE
526	05 36 15.84	−06 14 50.7	M2.6	0.165	0.0	0.30	2.4	0.50, 0.45	−63.3	-1.51	-0.30	C	TD	Li, X, IRE
527	05 36 16.50	−05 22 41.3	M4.9	0.030	0.0	0.095	3.9	...	−23.0	···	···	W	N	Na
528	05 36 17.23	−06 17 24.5	M4.6	0.335	0.4	0.14	< 0.5	0.30, 0.50	−26.2	-1.58	-0.71	C	TD	Li, X, IRE
529	05 36 17.68	−05 44 04.9	M5.2	0.040	0.0	0.090	3.2	...	...	···	···	...	N	Na
530	05 36 18.01	−06 10 02.8	M1.9	0.118	0.7	0.38	6.0	0.39	−7.5	-2.73	···	W	N	Li, Na, X
531	05 36 18.48	−06 20 38.7	M0.5	0.401	0.3	0.45	1.6	0.50	−49.6	-1.39	-1.02	C	Y	Li, X, IRE
532	05 36 18.57	−05 54 28.5	M5.3	0.107	0.3	0.11	< 0.5	...	...	-2.85	···	...	N	Na
533	05 36 18.67	−06 31 25.6	M4.9	0.182	0.0	0.13	< 0.5	0.50, 0.54	−8.7	-2.70	···	W	N	Li
534	05 36 18.79	−05 12 18.3	M4.6	0.152	0.1	0.14	< 0.5	0.27	−7.0	-2.63	···	W	N	Li, Na, X
535	05 36 18.79	−05 10 16.6	M4.8	0.053	0.1	0.12	2.4	...	−8.7	-2.41	···	W	N	Na
536	05 36 18.99	−04 53 50.4	M5.0	0.105	0.0	0.12	< 0.5	0.72	−10.0	-2.18	···	W	Y	Li, Na
537	05 36 19.09	−06 22 50.6	M8.0	0.025	0.1	0.058	2.0	...	−24.0	···	···	W	N	X
538	05 36 19.26	−05 31 08.3	M5.1	0.041	0.0	0.092	3.1	0.49	−5.5	···	···	W	N	Li
539	05 36 19.26	−05 00 28.4	M5.5	0.077	0.1	0.098	< 0.5	0.30	−44.3	-2.63	···	W	N	Li, Na, X
540	05 36 19.35	−04 39 44.4	M5.2	0.048	0.0	0.091	2.5	...	−17.4	-1.98	···	W	Y	Na, IRE
541	05 36 19.89	−05 56 08.3	M4.5	0.096	0.0	0.15	1.4	...	...	-2.75	···	...	N	Na, X
542	05 36 20.00	−04 21 15.1	M3.9	0.126	0.0	0.19	1.6	0.24	−6.2	-2.67	···	W	N	Li, Na
543	05 36 20.50	−05 40 57.1	M5.1	0.042	0.0	0.094	2.9	...	...	-2.13	···	...	N	Na
544	05 36 21.16	−06 26 56.9	M4.5	0.035	0.2	0.13	4.1	...	−12.9	-1.47	···	W	Y	IRE
545	05 36 21.96	−06 41 42.0	M5.1	0.162	0.0	0.12	< 0.5	0.40	−12.0	-1.43	-0.95	W	Y	Li, IRE

TABLE 6 – continued

	RA	DEC		Lum	Av	Mass	Age	$EW_{\mathrm{Li}\lambda6708\mathrm{\AA}}$	$EW_{\mathrm{H}\alpha}$					
	(J2000)	(J2000)	Spt	($L_\odot$)	(mag)	($M_\odot$)	Myr	(Å)	(Å)	$\alpha_{3.6-8.0}$	$\alpha_{3.6-24}$	TTS[a]	Disk[b]	Criteria[c]
546	05 36 22.27	−05 55 47.6	M4.0	0.075	0.3	0.18	2.8	0.62	−18.2	-1.19	-1.11	C	Y	Li, Na, IRE
547	05 36 22.87	−04 18 48.5	M5.4	0.068	0.0	0.099	0.9	0.57	−13.1	-2.58	···	W	N	Li, Na
548	05 36 23.05	−05 51 54.9	M4.3	0.085	0.0	0.16	1.9	0.30	...	-2.44	···	...	N	Li, Na
549	05 36 23.26	−06 19 37.5	M3.2	0.135	0.1	0.26	2.3	0.40, 0.52	−5.1	-2.77	···	W	N	Li, X
550	05 36 23.69	−04 36 17.1	M4.8	0.048	0.0	0.11	2.5	...	...	-1.69	-0.50	...	TD	IRE
551	05 36 23.69	−04 06 15.8	K9.7	0.609	0.5	0.50	1.1	0.18	−2.9	-2.73	···	W	N	Li
552	05 36 23.76	−05 11 18.1	M5.5	0.050	0.0	0.085	1.9	...	−21.0	-2.30	···	W	N	Na
553	05 36 23.95	−06 45 23.7	M4.9	0.122	0.2	0.13	< 0.5	0.30	−15.2	-2.87	···	W	N	Li
554	05 36 24.11	−05 08 13.7	M4.3	0.086	0.0	0.16	2.0	0.31	−5.1	-2.79	···	W	N	Li, Na
555	05 36 24.14	−06 31 49.5	M3.1	0.116	0.5	0.27	3.1	0.36, 0.51	−7.3	-2.73	···	W	N	Li, Na, X
556	05 36 24.16	−05 58 26.3	M5.2	0.043	0.0	0.092	2.9	...	...	-2.75	···	...	N	Na
557	05 36 24.42	−05 06 03.0	M5.1	0.057	0.3	0.10	1.8	...	−33.2	-2.64	···	W	N	Na
558	05 36 24.72	−06 05 13.3	M1.0	0.227	1.5	0.44	3.1	0.23	−60.4	-1.55	-1.46	C	Y	Li, IRE
559	05 36 25.01	−05 23 32.2	M3.0	0.193	2.8	0.27	1.6	...	−19.6	-2.75	···	W	N	Na
560	05 36 25.28	−06 23 07.2	M7.0	0.027	0.0	0.048	0.6	0.90, 0.25	−13.7	···	···	W	N	Li, X
561	05 36 25.41	−06 24 31.2	M5.7	0.061	0.3	0.089	0.8	0.60	−14.8	-2.54	···	W	N	Li, X
562	05 36 25.55	−06 51 28.3	M4.9	0.093	0.2	0.13	0.8	0.43	−11.9	-2.61	···	W	N	Li, Na
563	05 36 25.57	−05 18 42.0	M5.3	0.111	0.0	0.11	< 0.5	0.27	−20.3	···	···	W	N	Li, Na
564	05 36 25.64	−04 21 58.6	M4.4	0.221	0.0	0.16	< 0.5	0.47	−3.8	-2.62	···	W	N	Li, Na
565	05 36 26.35	−06 48 43.6	M5.8	0.087	0.2	0.093	< 0.5	0.30	−12.5	-2.37	···	W	N	Li
566	05 36 26.47	−06 06 16.3	M4.5	0.082	0.3	0.14	1.7	0.30	−14.8	-2.89	···	W	N	Li
567	05 36 27.89	−06 25 36.0	M4.3	0.159	0.0	0.16	0.6	0.30	−15.6	-1.91	-0.37	W	TD	Li, X, IRE
568	05 36 27.90	−04 58 06.8	M4.4	0.071	0.0	0.15	2.2	0.69	−8.1	···	···	W	N	Li, Na
569	05 36 28.74	−05 42 26.3	M5.0	0.167	0.6	0.12	< 0.5	0.13	−11.5	-2.80	···	W	N	Li, Na
570	05 36 29.28	−04 53 51.0	M3.7	0.216	0.1	0.20	0.9	0.35	−8.3	-2.13	-1.65	W	Y	Li, Na, IRE
571	05 36 29.30	−04 43 59.9	M4.6	0.085	0.0	0.14	1.5	...	−8.6	-2.05	-0.72	W	TD	Na, IRE
572	05 36 29.40	−06 15 44.8	M4.4	0.119	0.0	0.15	1.1	0.20	−4.6	-2.71	···	W	N	Li, X
573	05 36 29.81	−06 14 19.7	M5.5	0.065	0.0	0.096	0.9	0.50	−10.0	-2.76	···	W	N	Li, X
574	05 36 29.90	−06 38 22.3	M1.3	0.281	0.0	0.39	1.9	0.37	−3.5	-2.84	···	W	N	Li, Na, X
575	05 36 30.17	−05 53 09.9	M4.9	0.158	0.0	0.12	< 0.5	0.56	...	-2.70	···	...	N	Li, Na
576	05 36 30.48	−06 30 06.9	M4.4	0.045	0.0	0.14	3.5	0.40	−5.8	-2.68	···	W	N	Li
577	05 36 30.50	−06 23 56.6	M4.5	0.030	1.2	0.12	4.8	...	−36.1	-1.70	···	C	Y	X, IRE
578	05 36 30.52	−06 42 03.2	M6.0	0.019	0.0	0.056	4.0	0.60	−21.1	-3.01	···	W	N	Li
579	05 36 31.02	−05 01 02.7	M4.2	0.090	0.0	0.17	1.9	...	−9.4	···	···	W	N	Na
580	05 36 31.84	−06 23 23.1	M5.3	0.026	0.3	0.079	4.0	...	−64.2	-1.33	-0.75	C	Y	IRE
581	05 36 32.42	−06 40 43.0	M4.9	0.103	0.0	0.12	< 0.5	0.66	−43.1	-1.25	-0.89	C	Y	Li, Na, IRE
582	05 36 32.86	−06 00 50.2	M4.5	0.058	0.3	0.14	2.5	0.50	−13.1	-2.65	···	W	N	Li
583	05 36 32.87	−06 12 37.5	M1.7	0.444	0.0	0.34	0.9	0.44	−4.5	-2.70	···	W	N	Li, Na, X
584	05 36 32.99	−06 02 29.8	M3.4	0.114	0.2	0.24	2.5	0.40	−9.9	-2.58	···	W	N	Li
585	05 36 33.01	−06 00 16.6	M4.9	0.088	0.0	0.12	1.1	...	...	-2.29	···	...	N	Na
586	05 36 33.36	−05 45 35.5	M4.9	0.060	0.0	0.11	2.0	...	−14.6	-2.55	···	W	N	Na
587	05 36 33.81	−06 19 27.0	M2.4	0.157	1.4	0.31	2.7	0.40, 0.43	−12.4	-2.76	···	W	N	Li, Na, X
588	05 36 33.81	−04 24 03.7	M3.5	0.132	0.0	0.23	2.0	0.34	−4.9	-2.69	···	W	N	Li, Na
589	05 36 34.37	−05 40 54.8	M5.8	0.119	0.3	0.093	< 0.5	...	−17.3	-2.66	···	W	N	Na
590	05 36 35.23	−06 50 12.2	M6.0	0.042	0.0	0.069	0.7	0.50	−5.1	-2.64	···	W	N	Li
591	05 36 35.42	−06 17 36.5	M4.4	0.042	0.1	0.14	3.8	1.20, 0.39	−5.7	-2.62	···	W	N	Li
592	05 36 37.35	−05 24 43.5	M4.1	0.130	0.0	0.17	1.3	0.40	−5.3	-2.17	···	W	N	Li, Na
593	05 36 37.39	−05 10 22.1	M5.0	0.106	0.0	0.12	< 0.5	0.44	−24.5	-2.54	···	W	N	Li, Na
594	05 36 37.49	−06 16 07.7	M5.7	0.035	0.2	0.069	1.7	0.13	−19.9	-2.69	···	W	N	X
595	05 36 37.51	−06 27 17.3	M2.1	0.132	1.7	0.35	4.2	0.26, 0.32	−7.8	-1.82	-1.59	W	Y	Li, Na, IRE
596	05 36 37.61	−05 31 19.0	M5.1	0.061	0.0	0.10	1.5	...	...	···	···	...	N	Na
597	05 36 37.99	−04 22 17.9	M4.9	0.052	0.0	0.11	2.3	0.25	−7.4	-2.67	···	W	N	Li, Na
598	05 36 38.03	−06 24 25.2	M4.1	0.073	0.0	0.18	2.7	0.48, 0.47	−5.6	-2.66	···	W	N	Li, Na, X
599	05 36 39.58	−04 38 01.5	M5.4	0.040	0.0	0.082	2.9	0.52	−14.4	···	···	W	N	Li, Na
600	05 36 40.18	−05 07 29.2	M5.3	0.070	0.0	0.10	1.0	0.32	−15.4	-2.98	···	W	N	Li, Na
601	05 36 40.69	−06 52 04.5	M1.0	0.374	0.6	0.41	1.4	0.41	−6.0	-2.72	···	W	N	Li, Na, X
602	05 36 40.78	−04 21 20.2	M3.3	0.285	0.0	0.24	0.9	0.44	−4.9	-2.70	···	W	N	Li, Na
603	05 36 40.94	−04 20 44.3	M3.3	0.170	0.0	0.24	1.6	0.26	−2.9	-2.71	···	W	N	Li, Na
604	05 36 41.67	−06 11 46.5	M4.6	0.088	0.0	0.14	1.4	0.40	−10.0	-2.74	···	W	N	Li, X
605	05 36 42.04	−06 07 06.1	M3.3	0.339	0.3	0.23	0.6	0.50	−5.8	-2.61	···	W	N	Li
606	05 36 42.80	−05 27 34.4	M4.2	0.119	0.0	0.17	1.4	0.23	...	···	···	...	N	Li, Na
607	05 36 43.17	−06 16 57.2	M5.4	0.020	0.6	0.073	4.6	0.60	−27.2	-3.06	···	W	N	Li
608	05 36 43.98	−05 58 31.8	M3.8	0.407	0.0	0.20	< 0.5	0.47	...	-2.68	···	...	N	Li, Na
609	05 36 44.56	−06 02 09.1	M4.8	0.102	0.1	0.13	0.7	0.50	−13.7	-2.86	···	W	N	Li
610	05 36 44.94	−06 16 04.6	M4.5	0.063	0.2	0.14	2.3	0.60	−12.4	-2.43	···	W	N	Li, X
611	05 36 44.95	−06 04 35.3	M4.3	0.075	0.0	0.16	2.2	0.40	−6.6	-2.80	···	W	N	Li
612	05 36 45.21	−06 28 09.6	M3.4	0.375	0.3	0.23	< 0.5	0.45, 0.55	−19.1	-2.68	···	W	N	Li, Na, X
613	05 36 46.69	−06 07 22.3	M2.2	0.419	0.0	0.31	0.8	0.50	−3.4	-2.64	···	W	N	Li
614	05 36 47.27	−05 57 31.0	M3.2	0.176	0.0	0.25	1.7	0.25	...	-2.38	···	...	N	Li, Na
615	05 36 47.54	−06 08 20.3	M1.8	0.173	0.3	0.37	3.2	0.25	−13.7	-2.77	-0.47	C	TD	Li, Na, IRE
616	05 36 48.16	−05 40 52.9	M4.5	0.149	0.0	0.15	< 0.5	0.51	...	-2.62	···	...	N	Li, Na
617	05 36 48.36	−04 35 45.8	M5.0	0.053	0.0	0.10	2.1	...	−6.6	-2.58	···	W	N	Na
618	05 36 48.37	−05 14 16.6	M4.8	0.146	0.0	0.13	< 0.5	0.28	−11.9	-2.66	···	W	N	Li, Na
619	05 36 49.33	−05 33 20.6	M4.6	0.037	0.2	0.12	3.6	...	−12.4	-1.53	···	W	Y	Na, IRE
620	05 36 50.23	−06 48 58.2	M3.3	0.245	0.4	0.23	1.0	0.26	−8.8	-2.67	···	W	N	Li, Na, X
621	05 36 50.73	−05 37 47.3	M4.5	0.211	0.0	0.15	< 0.5	0.28	−5.5	-2.88	···	W	N	Li, Na
622	05 36 50.90	−06 10 55.2	M5.5	0.037	0.0	0.076	2.7	0.40	−16.6	-2.68	···	W	N	Li
623	05 36 50.94	−05 33 04.4	M3.8	0.300	0.0	0.19	< 0.5	0.44	...	-2.74	···	...	N	Li, Na

TABLE 6 – continued

	RA	DEC		Lum	Av	Mass	Age	$EW_{\mathrm{Li\lambda6708\AA}}$	$EW_{\mathrm{H}\alpha}$					
	(J2000)	(J2000)	Spt	($L_\odot$)	(mag)	($M_\odot$)	Myr	(Å)	(Å)	$\alpha_{3.6-8.0}$	$\alpha_{3.6-24}$	TTS[a]	Disk[b]	Criteria[c]
624	05 36 52.66	−05 59 18.0	M4.6	0.069	0.0	0.14	2.1	0.31	...	-2.72	···	...	N	Li, Na
625	05 36 52.67	−05 46 06.4	M5.3	0.035	0.0	0.084	3.3	0.54	−19.3	-1.45	···	C	Y	Li, Na, IRE
626	05 36 53.03	−05 56 43.4	M4.4	0.116	0.0	0.16	1.2	0.49	...	-2.82	···	...	N	Li, Na
627	05 36 53.26	−06 35 00.4	M3.4	0.126	0.6	0.24	2.2	0.40	−9.4	-2.56	···	W	N	Li, Na, X
628	05 36 53.84	−06 20 53.7	M3.5	0.117	0.2	0.23	2.2	0.50, 0.53	−5.8	-2.54	···	W	N	Li, X
629	05 36 54.29	−06 19 45.6	M1.9	0.237	0.4	0.35	1.9	0.39	−8.3	-2.64	···	W	N	Li, Na, X
630	05 36 54.37	−06 07 21.9	M4.0	0.096	0.1	0.18	2.0	0.50	−6.9	-2.60	···	W	N	Li
631	05 36 55.22	−06 20 25.8	M2.2	0.177	0.2	0.33	2.5	0.43	−20.9	-1.40	-0.26	C	TD	Li, Na, IRE
632	05 36 57.35	−06 18 45.2	M5.0	0.130	0.0	0.12	< 0.5	0.20	−8.0	-2.77	···	W	N	Li, X
633	05 36 57.57	−05 04 25.9	M5.4	0.069	0.0	0.100	0.8	...	−15.2	-2.39	···	W	N	Na
634	05 36 58.98	−06 29 04.9	M3.4	0.260	0.6	0.22	0.9	0.26	−10.1	-2.32	-0.64	W	TD	Li, Na, IRE
635	05 36 59.38	−05 40 55.8	M5.3	0.066	0.0	0.10	1.2	...	−13.7	-2.37	···	W	N	Na
636	05 36 59.97	−06 11 45.4	M2.1	0.169	0.8	0.34	2.8	0.29	−10.5	-2.65	···	W	N	Li, X
637	05 37 00.68	−05 25 01.1	M4.4	0.312	0.0	0.16	< 0.5	0.42	−8.1	-2.84	···	W	N	Li, Na
638	05 37 00.69	−04 41 09.8	M4.1	0.064	0.0	0.17	3.0	...	−1.0	-2.49	···	W	N	Na
639	05 37 01.43	−04 19 09.7	M2.4	0.199	0.0	0.30	1.9	0.42	−3.5	-2.80	···	W	N	Li, Na
640	05 37 03.05	−05 51 56.1	M4.8	0.050	0.0	0.12	2.5	...	...	-2.31	···	...	N	Na
641	05 37 03.32	−05 09 17.1	M4.5	0.045	0.0	0.13	3.2	...	−10.5	-2.49	···	W	N	Na
642	05 37 04.72	−06 04 55.5	M5.0	0.093	0.0	0.12	< 0.5	0.31	...	-3.12	···	...	N	Li, Na
643	05 37 04.91	−05 37 12.7	M4.9	0.338	0.0	0.13	< 0.5	0.34	−13.2	-2.72	···	W	N	Li, Na
644	05 37 05.31	−04 43 06.1	M5.3	0.058	0.0	0.097	1.6	0.50	−9.8	-2.80	···	W	N	Li, Na
645	05 37 05.78	−06 27 16.5	M3.5	0.261	0.0	0.22	0.8	0.19	−7.7	-2.70	···	W	N	Li, Na, X
646	05 37 05.90	−06 47 14.9	M3.4	0.267	0.1	0.23	0.9	...	...	-2.70	···	...	N	X
647	05 37 05.94	−05 40 55.5	M4.8	0.065	0.5	0.12	1.9	...	−20.6	-1.73	-1.05	C	TD	Na, IRE
648	05 37 06.12	−05 37 25.2	M3.2	0.172	0.0	0.25	1.6	...	...	-2.60	···	...	N	Na
649	05 37 06.50	−05 53 57.3	M4.3	0.096	0.0	0.16	1.7	0.36	...	-3.06	···	...	N	Li, Na
650	05 37 07.06	−05 11 20.9	M3.7	0.101	0.0	0.21	2.4	...	−2.5	-2.62	···	W	N	Na
651	05 37 07.31	−05 24 01.8	M2.1	0.223	0.0	0.33	1.9	0.40	−2.7	-2.75	···	W	N	Li, Na
652	05 37 07.44	−05 53 29.1	M5.2	0.087	0.0	0.11	< 0.5	...	...	-2.75	···	...	N	Na
653	05 37 07.71	−06 42 18.6	M5.7	0.041	0.1	0.074	1.0	...	−13.2	-2.63	···	W	N	X
654	05 37 08.71	−04 38 23.8	M4.1	0.132	0.0	0.17	1.2	0.30	−6.8	-2.82	···	W	N	Li, Na
655	05 37 09.93	−06 45 46.5	M2.8	0.171	0.0	0.28	2.0	0.30	−10.5	-2.74	···	W	N	Li
656	05 37 10.13	−05 17 58.7	M5.2	0.062	0.0	0.10	1.4	0.41	−9.3	-2.24	···	W	N	Li, Na
657	05 37 10.68	−06 47 12.0	M4.6	0.058	0.0	0.13	2.3	0.32	−6.3	-2.47	···	W	N	Li, Na, X
658	05 37 10.85	−06 30 15.2	M5.5	0.153	0.0	0.099	< 0.5	0.38	−19.4	-2.71	···	W	N	Li, Na, X
659	05 37 11.57	−06 06 45.2	M5.2	0.055	0.0	0.095	2.0	0.78	...	-2.15	···	...	N	Li, Na
660	05 37 13.99	−05 13 26.3	M3.0	0.182	0.0	0.27	1.7	...	−0.2	-2.67	···	W	N	Na
661	05 37 14.73	−06 35 15.8	M4.8	0.095	0.0	0.13	0.9	0.35	−11.6	-2.86	···	W	N	Li, Na, X
662	05 37 14.81	−06 01 41.8	M4.8	0.040	0.0	0.11	3.0	0.71	...	-1.98	-0.77	...	TD	Li, Na, IRE
663	05 37 16.37	−05 26 04.1	M4.9	0.025	0.0	0.093	4.6	...	−6.2	-1.63	···	W	Y	Na, IRE
664	05 37 16.87	−06 47 50.7	M5.5	0.045	0.7	0.080	1.8	...	−13.3	-2.69	···	W	N	X
665	05 37 18.25	−05 49 20.7	M4.4	0.197	0.5	0.16	< 0.5	0.31	−44.2	-1.36	-1.19	C	Y	Li, Na, IRE
666	05 37 18.87	−06 09 41.2	K9.9	0.431	0.1	0.51	1.8	0.38	−6.1	-2.15	-1.59	W	Y	Li, IRE
667	05 37 18.89	−06 47 04.0	M5.1	0.063	0.1	0.11	1.5	0.20	−15.3	-2.70	···	W	N	Li, X
668	05 37 22.17	−06 54 45.4	M5.4	0.131	0.0	0.10	< 0.5	0.30	−16.3	-0.90	-0.24	W	Y	Li, X, IRE
669	05 37 22.86	−06 44 46.6	M1.5	0.272	0.3	0.37	1.8	0.38	−17.0	-1.79	-1.33	C	Y	Li, Na, X, IRE
670	05 37 22.94	−06 03 21.1	M3.7	0.161	0.0	0.20	1.4	0.43	...	-2.70	···	...	N	Li, Na
671	05 37 24.40	−05 46 40.0	M5.0	0.060	0.0	0.11	1.8	...	...	-2.77	···	...	N	Na
672	05 37 24.91	−06 02 42.3	M5.2	0.064	0.0	0.10	1.3	...	...	-2.50	···	...	N	Na
673	05 37 30.18	−05 49 38.1	M5.2	0.061	0.0	0.10	1.4	...	...	-2.75	···	...	N	Na
674	05 37 32.72	−05 35 08.0	M4.8	0.034	0.0	0.11	3.5	...	...	-1.76	···	...	Y	Na, IRE
675	05 37 34.00	−05 59 35.8	M5.0	0.078	0.0	0.12	1.1	...	...	-2.61	···	...	N	Na
676	05 37 34.07	−06 44 02.3	M4.6	0.095	0.0	0.14	1.3	0.43	−11.3	-2.82	···	W	N	Li, Na, X
677	05 37 35.24	−06 28 21.7	M2.9	0.136	0.3	0.29	2.8	...	−7.0	-2.78	···	W	N	Na, X
678	05 37 38.98	−06 45 15.4	M3.6	0.371	0.0	0.21	< 0.5	...	−4.7	-2.59	···	W	N	Na, X
679	05 37 49.35	−06 51 37.3	M3.5	0.238	1.1	0.22	1.0	0.50	−13.1	-1.97	-0.45	W	TD	Li, X, IRE
680	05 37 50.24	−04 26 16.8	M1.9	0.398	0.6	0.33	0.9	0.25	−21.4	···	···	C	Y	Li, X, IRE
681	05 37 51.58	−06 41 29.1	M3.8	0.147	0.5	0.20	1.4	0.41	−11.4	-2.66	···	W	N	Li, Na, X
682	05 37 53.08	−06 35 55.4	M5.2	0.098	0.1	0.11	< 0.5	0.50	−40.3	-1.22	-0.98	C	Y	Li, X, IRE
683	05 37 55.03	−06 44 59.1	M3.3	0.243	0.0	0.24	1.1	0.40	−6.5	-2.68	···	W	N	Li, X
684	05 37 55.15	−06 57 40.7	M5.7	0.114	0.6	0.095	< 0.5	0.70	−17.3	-2.56	···	W	N	Li
685	05 37 55.22	−06 57 35.8	M4.4	0.254	0.9	0.16	< 0.5	0.30	−8.0	-1.87	-1.48	W	Y	Li, IRE
686	05 37 58.90	−06 43 30.9	M5.6	0.157	0.0	0.097	< 0.5	...	−26.8	···	···	C	Y	IRE
687	05 37 59.81	−06 42 05.6	M4.0	0.195	0.0	0.18	0.7	0.40	−4.5	-2.62	···	W	N	Li, X
688	05 38 02.49	−06 40 56.9	M5.0	0.049	0.0	0.10	2.2	...	−14.3	-2.59	···	W	N	X
689	05 38 02.85	−05 02 36.4	K9.9	0.304	0.0	0.54	3.3	0.62	−2.4	···	···	W	N	Li
690	05 38 10.63	−06 22 08.6	K8.9	0.690	1.1	0.56	1.2	0.47	−14.3	···	···	C	Y	Li, IRE
691	05 39 07.96	−06 29 10.3	K8.5	0.823	0.1	0.57	0.9	0.62	...	···	···	...	N	Li